Fundamental Insights into the Structure and Dynamics of Confined Substrates inside Silica Nanostructures, using a combination of Molecular Dynamics and Grand Canonical Monte Carlo Simulations

by

Nilesh Varadan Orupattur

A thesis submitted in partial fulfillment of the requirements for the degree of

Master of Science

in

CHEMICAL ENGINEERING

Department of Chemical and Materials Engineering
University of Alberta

Abstract

Condensed phase reactions in the presence of heterogeneous catalysts are widely performed for the conversion of biomass into useful intermediates and value-added products. Specifically, nanoporous catalysts have garnered interest for liquid-phase oxidation, hydrogenation, dehydrogenation and/or isomerization reactions in the production of bio-based chemicals. Properties of molecules confined in such nanoporous materials are substantially different from those present in the bulk substrate. This is attributed to size and geometry of the confinement, and alteration in substrate-substrate interactions and substrate-surface interactions within the porous media. Changes in properties and molecular interactions can also significantly modify the reaction kinetics and thermodynamics of the confined reactants, thereby leading to an alteration in the conversion and selectivity of the heterogeneous catalytic reactions within the nanopore. Recently, Pulse-Field Gradient Nuclear Magnetic Resonance (PFG-NMR) experiments have played a crucial role in measuring intrapore diffusivities of organic substrates. In these experiments, the ratio of self-diffusivities in bulk to self-diffusivities inside the pore, also called as PFG interaction parameter, was used for the comparison of mobility between functionalized compounds like alcohols, polyols and carbonyl compounds. Polyols were specifically included due to the presence of multiple hydroxyl groups with an ability to interact well with the metal oxide surface. Interestingly, polyols showed an enhanced rate of self-diffusion within the nanostructures, whereas alcohols and carbonyl compounds showed reduced diffusivities. Anomalous behaviour of polyols was hypothesized to arise from the breakage of substrate-substrate Hydrogen bonds within the confinement, although the molecular-level explanation for disruption of Hydrogen bonding network was unaddressed.

Inspired by the knowledge gap on the effect of confinement on the dynamics of functionalized molecules inside heterogeneous catalysts, in the present work, a combination of molecular dynamics (MD) and grand canonical Monte Carlo (GCMC) simulation method was used to study the effect of confinement on mobility of nano-confined substrates within nanoporous Silica catalysts (which is commonly used as a support in the valorization of bio-based chemicals). We have considered water, glycerol, acetone, and heptane as our substrates, as representatives of different functional groups and varying molecular sizes. These substrates were confined inside Silica nanostructures of one dimension (Slit pore of 4 nm) and two dimensions (Cylindrical pores of 2, 4, and 6 nm). Repulsive beads technique was used to create the silica nanostructures, GCMC was used to obtain intrapore density of substrates, and MD was used to calculate the structural, dynamic and thermodynamic properties of the confined substrates. In this study, Heptane was used as a benchmark, due to lack of functional groups resulting in weak interactions with porous media and with other heptane molecules. Intrapore diffusivities of the substrate molecules were calculated for all the confinements to compare with the PFG-NMR experimental results. Heptane and water showed negligible impact of confinement size and geometry on the diffusivities. We observed a reduction in diffusivities of acetone with the reduction in the size of the confinement. Glycerol showed relatively enhanced diffusivities inside slit-pore of 4 nm and cylindrical pores of 6 and 4 nm, whereas it showed reduced diffusivities in the cylindrical pore of 2 nm due to stronger interactions with the pore surface. Furthermore, to attain mechanistic and thermodynamic insights into the confinement effects imposed by the silica nanostructures of varying geometry and size on the dynamics of the substrate molecules, H-bonding structure, intermolecular interactions, density profiles, and change in entropy and potential energy were analyzed. The effective pore volumes available for glycerol and water were higher than acetone and heptane, leading to an enhancement

in the diffusivities of the hydroxyl-containing compounds. Reduction in the total number of hydrogen bonds was observed for glycerol inside all the confinements, confirming the experimental hypothesis of the disruption of Hydrogen bonding network of polyols inside nanoporous structures. Acetone intermolecular interactions and local densities near the center were observed to increase with the reduction in confinement size, leading to reduction in the diffusivities. In addition to intermolecular interactions, the geometry and size of the confinement and change in entropies and potential energies of substrate molecules played a crucial role in alteration of dynamics within the nanopores. Understanding these confinement effects on the intrapore dynamics of substrate molecules could aid in studying the modification of intrinsic reaction kinetics and thermodynamics of heterogeneous catalytic reactions inside nanopores.

Keywords: diffusion, confinement effects, molecular dynamics, hydrogen bonding, density profiles, heterogeneous catalysis, condensed phase

Preface

This thesis is an original work by Nilesh Varadan Orupattur. The simulations, data analysis, conclusive analysis in chapter 3, chapter 4, and chapter 5 respectively, along with the literature review in chapter 2 are originally my work under the supervision of Dr. Samir H. Mushrif, University of Alberta. A portion of my research data from chapter 4 was presented at the Future Energy Systems Digital Research Showcase 2020 and the AIChE Annual Proceedings 2020.

Dedicated to my Amma, Appa and Nikki…

Acknowledgments

At the outset, I would like to express immense gratitude to my supervisor, Dr. Samir H. Mushrif for his guidance and encouragement throughout my graduate studies. I thank the CME Department for providing me with this opportunity and a great research environment. Furthermore, I would like to thank the University of Alberta Faculty of Engineering, NSERC and Future Energy Systems for the funding received during the course of my graduate studies, and Compute Canada for providing excellent computational support.

I would like to further extend my thanks and appreciation to my research group members – Arul, Sagar, Jose, Ojus, Shang, Seth, Katherine and Xuebin for their continuous motivation during the course of my degree. It has been an absolute delight to work with you guys. Your timely inputs and constant encouragement have served as one of the driving forces in my research and my life in Edmonton.

I am extremely appreciative of the family I built here. Faraz, Yashas, Ananthan, Sanjula, Yash, Bansod, Oghuzan, Kanishk, Anuja, Mani, Arun, Pai, Khyati, Hemanth, Ankit, Suyash, Raviraj, Saad, Aadil and many more treasured friends at DICE. I would like to thank Shweta for her unending motivation, patience, and support; looking forward to more fruitful business idea discussions.

I would also like to thank my friends back home in India, particularly Srinidhi and Rampalliwar, for lending an ear and giving me the push whenever I need it the most; Shantanu, Nipun, Veer, Mantri and Awate for their encouragement via regular FaceTime sessions; Neil, Dupare, Anish, Nikitesh, Varun, Pawan and Dhapodkar for making my life easier during this pandemic and keeping me connected to the world of sports; Rahul, KNS and many more for being part of my adventure for nearly a decade.

Most importantly, I would like to thank my parents and sister for believing in me throughout this journey. Appa, for being a role model; Amma, for her love, patience and care; and Nikki for her encouragement and for being an inspiration.

Best regards,
Nilesh

Table of Contents

List of Tables

List of Figures

1 Introduction

The conventional fossil fuels derived from non-renewable resources such as coal, petroleum, and natural gas are currently the main sources for the production of important commodity chemicals and fuels. However, these fossil resources contribute highly towards the effects of global warming on society.[1–3] Furthermore, their rapid depletion causes a significant increase in the prices of petrochemical products. Apropos, the quest for alternative renewable resources and the development of new processes to produce fine chemicals and fuels take precedence. One such alternative resource is biomass, which is renewable and less detrimental to the environment in comparison to fossil fuels.[4] Being an abundant and natural carbon resource, biomass may be viewed as a promising alternative to fossil fuels; furthermore, it may be further transformed into various value-added products, clean solvents, and highly energy-dense fuels.[5,6] To this end, heterogeneous catalysis, a process wherein the catalysts and reactants exist in different phases (usually solids, and liquids or gases, respectively), offers a platform for the use of several chemical processes such as fast pyrolysis, hydro-processing, oxidation, dehydration, hydrolysis, (trans)esterification, and isomerization of bio-derived chemicals.

Heterogeneous catalysis operates at the intersection of chemical engineering, chemistry and materials science. It includes the development and investigation of catalysts– materials that can alter the rate of a reaction by lowering the activation energy barrier and/or by modifying the selectivity of reactants in a chemical reaction.[7] In addition, it is a multifaceted process containing numerous areas of interest, such as catalyst compositions, geometric effects, entropic effects and substrate-surface chemistry.[8] Catalysts are used in the production of at least 60% of industrial chemicals[9], notably in the areas of renewable energy[10,11], sustainable fuel production[12], pollution mitigation[13,14] and pharmaceuticals.[15] The valorization of bio-derivatives in particular is challenging owing to the low volatility of the constituent molecules. Therefore, it is imperative that the catalysts chosen to enhance reactions involving such compounds be able to perform well at moderately elevated temperatures, as well as in aqueous and organic solvent media, or mixtures of both. It has been noted that heterogeneous catalysts interact with solvents to a significant degree, exhibiting major, and possibly irreversible, changes in their structure, selectivity, as well as catalytic activity, due to surface solvent adsorption and/or reaction with the

solvent media.[16–18] Therefore, it is important to discern, understand, and control the relationships between the catalytic structure and the active sites that come into contact with the solution, in order to design a catalyst suitable to the proposed reaction.[19] Such an assessment has been deemed increasingly significant in the case of inorganic catalysts such as zeolites and metal oxide-supported nanoparticles, which were first developed for upgradation of petroleum and biomass valorization, in which they are made suitable for reuse under liquid-phase operating conditions.[20–26]

The effectiveness of a catalyst in promoting a certain chemical reaction needs to be evaluated by considering the effect of confinement on the kinetic and thermodynamic properties.[27] Molecules confined inside nanoporous catalysts have properties substantially different from that of the bulk liquid. This is attributed to physical restrictions imposed by the pore wall, and alterations in substrate−substrate and substrate−surface interactions. These interactions may therefore dramatically affect the dynamic properties of molecular fluids, further affecting the intrinsic catalytic reaction kinetics and thermodynamics. Diffusion is an eminent dynamic property, and its understanding might present us with information on the structural properties of the porous catalyst.[28] Numerous experimental and computational studies have been carried out in this regard, to study the effect of confinement on the dynamics and intermolecular interactions of nano-confined substrates. One such ground-breaking study was established by C. D'Agostino and coworkers, wherein a pulsed-field gradient nuclear magnetic resonance (PFG-NMR) technique was used to study the diffusion of substrate molecules within SiO_2, TiO_2 and Al_2O_3 mesoporous materials.[29] This was done to understand the effect of functional groups on the self-diffusivity of reactant molecules within the nanopores. The different functional group properties showed a significant difference in the PFG interaction parameter, which is defined as the ratio of diffusivity inside the pore to the diffusivity in the bulk liquid. This helped establish that physical interactions within the pores play a crucial role in the modification of intrapore diffusion, in addition to the physical structure of the pore itself. Molecules with carbonyl groups (such as acetone), had the highest PFG interaction values, resulting in reduced self-diffusivity within the pores as compared to alkanes. Polyols (like glycerol) on the other hand showed an anomaly of enhanced self-diffusivity (lower values of PFG interaction parameters as compared to alkanes) inside the porous medium, even with the presence of hydroxyl groups with an ability to interact well with the metal

oxide surface. Enhancement in the diffusivities could lead to change in adsorption and intrinsic reaction kinetics of polyols.[30] This bolstered their hypothesis that the perturbation in the translational molecular motion was due to hydrogen bonds of the liquid being disrupted (refer Figure 1.1) by solid substrate topology, leading to enhanced diffusion of polyols in the porous structure of mesoporous materials; but the mechanism behind this phenomena needs a molecular-level understanding.

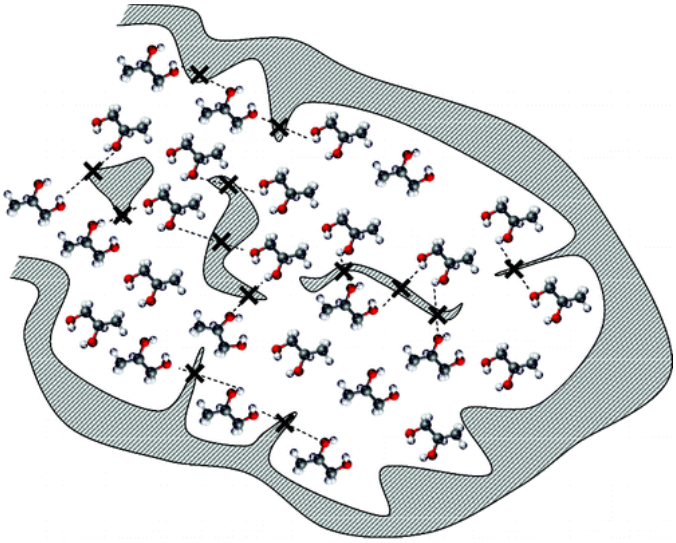

Figure 1.1: Disruption of Hydrogen bonding network of substrate molecules confined inside a nanostructure. Reproduced with permission from ref.[29].

Although the restricted space inside a confinement potentially provides an advantage of shape/size selectivity of the reactants and products, it is counteracted by sluggish reaction kinetics as a result of diffusion limitations.[31–34] It was observed that the confinement effects play a crucial role in the alteration of overall chemical reaction kinetics of the oxidation reactions of polyols like 1,3-propanediol and 1,4-butanediol and glycerol, suggesting a need to understand the dynamic properties as well as the molecular interactions within the confinement, in comparison to the bulk substrates. In contrast, it has been observed that nanoporous catalysts, such as zeolites, solvate reactants within the nanopores, and thus exhibit atypical entropy-driven behavior that is not characteristic of bulk liquids. In the case of acid-catalyzed dehydration of cyclohexanol, such behavior gives rise to a higher association between the substrate and hydronium ions which, combined with inherently higher rate constants for the dehydration reaction, leads to an overall enhanced reaction process. It is reported that when the dehydration reaction is catalyzed by

hydronium ions inside the zeolite pores, the resulting turnover frequencies are approximately two orders of magnitude greater than those observed in the liquid phase.[28,35]

Understanding the origin of the deviations of reactant molecules inside a nanostructure from a typical bulk-liquid behavior is crucial in many industrial applications. Specifically, heterogeneous catalysis of bio-based polyols like glycerol have garnered widespread interest due to its multi-functionality in cosmetics, pharmaceuticals and food industries.[36] At present, this insight is obtained preferentially through in situ spectroscopic techniques in conjunction with modeling studies. To combat the issue arising due to the inability of the experiments to capture molecular-level understanding of the phenomenon behind the aforementioned confinement effects, researchers have developed molecular modeling techniques for the design of catalysts and to understand their reaction chemistry, and develop structure-property relationships. In this regard, computer simulation techniques, including Quantum mechanics, Monte Carlo and Molecular Dynamics methods, have played a crucial role in studying these effects at a molecular scale and also to explain previously reported experimental observations.[37] A notable study was recently conducted to understand the anomalous behavior of glycerol molecules inside a slit-shaped alumina catalyst, using a combination of PFG-NMR technique and Molecular Dynamics simulations. In their work, the authors reported that the overall self-diffusion rate is higher inside the slit-pore than in the pure bulk liquid under certain conditions of slit-pore size, and pore saturation. They attributed this finding to the competition between the strong structural order at the interface of the liquid and catalyst surface, and the breakage in the hydrogen bonds far away from the interface.[38] Milischuk and coworkers conducted Molecular Dynamics simulations of a water-solvated silica nanopore of diameter 4 nm and found that the density of the water exhibited changes as a function of the interfacial distance, as well as the reduction in translational motion of water molecules due to strong hydrogen bonds at the silica-water interface.[39] These aforementioned works have acknowledged a few crucial knowledge gaps pertaining to experimental observations such as the effect of different confinement sizes on the intermolecular interactions (Hydrogen bonding), dynamic properties (change in the diffusivities) and intrapore densities profiles of reactants like glycerol and water. However, a molecular-level understanding of the confinement effects imposed by nanostructures of different geometries (slit and cylindrical pores) and sizes on the modification of (a) the intrapore diffusivity, density and intermolecular

interactions; (b) the thermodynamic properties like potential energy and entropy; (c) intrinsic reaction kinetics and thermodynamics of the confined functionalized substrates (alcohols, polyols, carbonyl compounds) is still unclear. Detailed understanding of the structural, dynamic and thermodynamic properties of confined substrates could aid us to explain the phenomenon behind change in intrinsic reaction kinetics and thermodynamics of the heterogeneous catalytic reactions within porous media.

In the present work, we study the alteration in structural and dynamic properties of water, acetone, glycerol and heptane molecules confined inside silica nanostructures (one-dimensional slit pore and two-dimensional cylindrical pores as shown in Figure 1.2), arising due to (a) geometry and size of the nanostructure, (b) change in the substrate-substrate interactions, and (c) substrate-surface interactions.

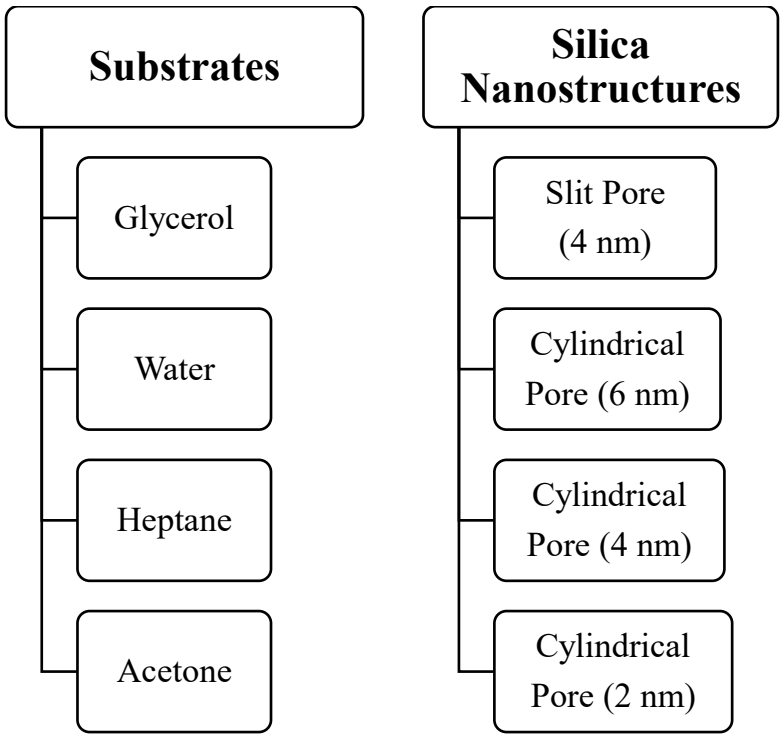

Figure 1.2: Silica nanostructures and substrate molecules studied in the present work.

A combination of Grand Canonical Monte Carlo (GCMC) and force-field based Molecular Dynamics (MD) was used in this study. The intrapore densities of these substrates were obtained using GCMC, and MD was used to study the physical (diffusivities and intermolecular

interactions) and change in thermodynamic (potential energy and entropy) properties of the nano-confined substrates. We have taken heptane (alkane) as the reference molecule, due to its lack of chemical functionalities resulting in negligible intermolecular interactions and interactions with the pore surface. Hydrogen bonding network and local densities of the substrates across the porous structure were also investigated. Based on these calculations, we validate the experimental hypothesis on the disruption of hydrogen bonding network of the hydroxyl-containing molecules, and further provide mechanistic (intermolecular interactions, molecular orientation and density profiles) and thermodynamic (change in entropy and potential energy) insights into the alteration of the dynamics of the substrate molecules inside the confined space of varying geometry and sizes.

The remainder of the thesis is organized as follows: In Section 2, we provide a detailed overview of the experimental and computational findings on confinement effects on condensed phase heterogeneous catalytic reactions and emphasize noteworthy knowledge gaps pertaining to this field of study. In Section 3, we delineate the computational methods used for performing the molecular simulations. We also provide a basic workflow of the simulations used for conducting the research. Section 4 includes the results obtained on the dynamics and intermolecular interactions of the substrate molecules. The thesis is concluded in Section 5, where we summarize the findings based on mechanistic and thermodynamic results reported in Section 4.

2 Literature survey

The development of active, selective, and energy-efficient heterogeneous catalytic processes is of great importance in forging a sustainable future, as heterogeneous catalysis is central to a host of processes in the chemical and energy industries.[40] Catalytic processes are integral to the synthesis of several chemical products which account for nearly 25% of industrial energy usage,[41] the most energy-intensive of which depend on heterogeneous catalysis. To this end, developing efficient processes, and subsequently testing them, using inferences from fundamental studies could yield significant benefits in decreasing energy consumption, as well as environmental impact.[42] The sustainable conversion of biomass into major chemical compounds is an area that benefits greatly from the development of new and more efficient catalysis methods. Being a renewable, and, thus, sustainable carbon source, biomass is the preferential feedstock to produce liquid fuels and other chemicals. Furthermore, the oxygen-rich nature of biomass feedstock, as well as its multifunctional nature, point to the possibility of synthesizing oxygenates through more cost-efficient and direct means, as compared to other oxygen-lean hydrocarbon feedstocks. The design of highly active and selective catalysts is largely dependent on the fundamental understanding of key parameters (called descriptors) of the materials that determine the surface-mediated bond activation and formation of reactants and intermediates.[43] Therefore, establishing the structure-activity relations using model and platform chemicals, such as bio-based alcohols and polyols, is a vital step. Additionally, a molecular-level understanding of catalytic processes has also been used to optimize catalysts and process operating conditions for biomass valorization.[40,42–44]

Henceforth, we begin with the introduction of condensed phase catalytic conversion of bio-derived products (with an emphasis on glycerol) in Section 2.1. In Section 2.2, we delineated the effect of confinement of the nanoporous catalysts on the dynamic properties and intrinsic reaction kinetics and thermodynamics of reactant and solvent molecules. Finally, in Section 2.3, we provided the summary of current knowledge gaps in the study of confinement effects discussed in Section 2.2 and outline the objectives and scope of this thesis.

2.1 Condensed Phase Catalytic reactions for biomass processing

Heterogeneous catalysts comprising metal nanoparticles supported on oxides have found widespread use in reactions like selective oxidation and hydrogenation of bio-derivatives such as glycerol, which is a by-product of the transesterification of vegetable oil to biodiesel (BD), in aqueous and organic solvent media.[45,46] The expanding need for environmentally harmless BD has consequently led to an abundance of glycerol that is ought to be used to increase BD profitability. Glycerol's efficient conversion into several value-added products transpires in increased production and utilization of this alternative bio-renewable fuel resource. Thus, for the increased biodiesel production in the future, probing into new technological avenues for the utilization of glycerol will prove beneficial.[47] Glycerol has the versatility to be selectively transformed via a range of processes, such as dehydration, hydrogenation, hydrogenolysis, esterification, etherification, and oxidation to attain several potential products.[48–56] Glycerol may be transformed to chemical and fuel products through a variety of processes, one of which is catalytic hydrogenolysis, or hydrodeoxygenation. This process provides an effective method for the production of valued diols; for instance, the transformation of glycerol through hydrogenolysis results in the formation of 1,3-propanediol, which is a more desirable derivative commercially than 1,2-propanediol, owing to its use as a monomer for a number of polymers, such as poly-trimethylene terephthalate (PTT).[64—70] Additionally, the production of acrolein and acrylic acid using metal nanoparticles, which are important industrial liaises for the chemical and polymer industries is by far one of the alluring avenues for glycerol valorization in the proximate future.[49] Due to its low volatility, biomass and bio-derived product (like glycerol) conversion is often conducted in liquid-phase media; this makes the investigation of catalytic processes under functional conditions a challenging task. In addition to this, the presence of solvents in most biomass conversion and upgradation processes further complicates the study of surface-mediated reaction mechanisms in the liquid phase.[43,46,64] Solvents may affect a significant change in reactivity as well as product selectivity in catalytic reactions; in some cases, the properties and/or structures of the catalytic sites are found to vary in the presence of solvents. Recent literature points to findings that show that significant control may be achieved on the reactivity of catalytic reactions on biomass by appropriately selecting and tuning the composition of aqueous solvents and/or solvent mixtures. Since catalytic structure-activity relations may vary greatly in the presence of solvents, characterizing the catalytic sites in such conditions is a critical step.[37] A

detailed report on the applications and challenges of metal oxide supported nanoparticles for condensed phase glycerol valorization reactions is presented in Section A1.3 of the appendix. In conclusion, better comprehension and understanding of the interactions of the metal active sites with the substrates, solvents and products will result in the development of superior catalysts and improved control of activity/selectivity parameters.

In earlier literature, the emphasis was largely centered around the tuning of electronic and geometric properties of metal catalysts by adding a second metal, or through confining the particles in carrier materials with tailored porosity.[65] The downside of using such methods is that the catalyst architecture and composition so obtained were increasingly complex. In more recent years, renewed efforts in catalyst design have been focused on more efficient use of the active metal phase through precise size control. Using the classical ideas of structure sensitivity of reactions, the dimensions of the nanoparticles have been adjusted to enrich the surface with catalytic sites in order to boost the yield and/or selectivity of the desired product(s).[66] As mentioned in Section 1, the transport properties of confined substrate particles are significantly different from those of bulk phase molecules, possibly due to the pore structure, and modified substrate-surface and substrate-substrate interactions due to confinement. However, a detailed understanding of the intrapore dynamics of solvent/reactant molecules arising from confinement effects, as well as intrinsic reaction kinetics and thermodynamics in the condensed phase conversion of bio-derivatives such as glycerol, propanediols and butanediols, is still not completely addressed in the literature, despite the knowledge of confinement effects on catalytic activity and selectivity.[30,34,67,68]

2.2 Confinement effects in heterogeneous catalysis

Recently, confined environments in heterogeneous catalysts have been recognized as equally important as catalytically active sites.[69] These confinement effects in porous materials have been found to affect diffusion, and phase transformations in heterogeneous catalytic reactions, thus altering the intrinsic kinetics and thermodynamics as well.[70–75] Therefore, the confined environment results in changes in certain reactions due to adsorption, geometrical constraints, selective absorption, and changes to the potential energy surface, and subsequently influences the

reaction's selectivity and activity.[27,69,76–83] In this subsection, we highlight recent examples that illustrate the influence of confinement effects on the dynamic properties of the substrate molecules (Section 2.2.1), which in turn govern the activity and selectivity of heterogeneous catalytic reactions (Section 2.2.2). Finally, we delineate the current findings and knowledge gaps on the effect of confinement on the structural, dynamic and thermodynamic properties investigated using spectroscopy and molecular modeling methods in Section 2.2.3.

2.2.1 Confinement effects on intrapore dynamics of reactant and solvent molecules

Experimental findings and the knowledge gaps on effect of confinement on the intrapore diffusivities of functionalized reactants and solvents have been reported in this subsection. In their recent publication, Mantle, et al.[84] have reported an interesting phenomenon that occurs during the diffusion of alcohols, particularly diols, in metal oxide-supported catalysts. In this study, they examined the self-diffusion behavior of 1-octanol, 2-octanol, 3-octanol, 1,2-butanediol, and 1,4-butanediol in a number of heterogeneous gold catalysts with metal oxide supports. The authors found that, for 2-octanol, the competitive adsorption of the ketone product resulted in the inhibition effect that is observed in traditionally performed catalytic activity studies. Furthermore, they also discovered that the self-diffusivity of butanediols was significantly higher than expected, and closer to their free liquid values, as compared to octanols and n-octane. This phenomenon of enhanced self-diffusion rates in porous materials was previously reported in the literature for water in a partially-filled porous glass, with a low degree of volume filling, by F. Dorazio and coworkers, as well as for n-hexane in partially filled porous media. The authors reasoned that this enhancement was the result of a molecular exchange between the liquid and vapor phases within the pores.[85,86]

A pioneering work in the direction of pure substrates was reported by C. D'Agostino's group; in this work, the authors studied the self-diffusion rates for substrate molecules using liquid-saturated porous materials.[29] They focused on the measurement of self-diffusion coefficients of hydrocarbons, alcohols, polyols, and carbonyl compounds within TiO_2, γ-Al_2O_3, and SiO_2 support pellets using the PFG-NMR technique. The PFG-NMR technique is a tool that may be used to assess the diffusion properties of molecules in a variety of forms such as ionic liquids, molecular sieves, and heterogeneous catalysts.[87–90] The measurement of transport properties in porous

media is perhaps a rare field that fully exploits the usefulness of NMR techniques in investigating diffusion in complex systems in a non-invasive and chemically selective manner, by monitoring molecular displacements over a wide spectrum of length scales. Liquid alkanes were considered the optimal choice to conduct studies to procure structural information (tortuosity) on pore network connectivity of the porous media, due to their lack of functional groups, thus minimizing physical interactions with the porous matrix, in addition to intermolecular interactions. It is expected that the diffusion of such alkanes is dependent only on the geometrical and structural properties of the porous medium. It is, indeed, found that for materials such as the liquid alkanes chosen, the ratio between self-diffusivity of free bulk liquid to that of the liquid within the porous support, termed as the PFG interaction parameter, does not depend on the molecular weight, molecular structure, or the carbon chain length. In contrast, when compounds containing functional groups were chosen for the same study, the PFG interaction parameter values were found to vary significantly, illustrating the effect of interactions of the compounds within the porous media, as well as the physical pore structure. In this sense, it is observed that compounds containing carbonyls, such as acetone, show the highest PFG interaction parameter values owing to which their self-diffusivity within the pore space is much lesser than that of alkanes. On the other hand, polyols like glycerol and butane-diols show enhanced self-diffusivity within the pore structure compared to that of alkanes. Interestingly, glycerol possesses significant enhanced self-diffusivity properties in all support media, with its value within γ-Al_2O_3 even larger than its free bulk liquid self-diffusivity. The authors address this enhancement in diffusivity by hypothesizing that the translational molecular motion experiences perturbations due to disruptions in the hydrogen bond network of the polyol compounds that occur as a result of topological defects in the solid substrate medium. Furthermore, abnormally high self-diffusivity has been observed in the case of alkanes and water in partially-filled porous materials; it is reasoned that this is observed due to a fast interphase exchange between condensed and vapor phases within the confining volume.[91] The critical point for the coexistence of vapor and liquid phases in simple fluids, such as alkanes, is found to be lower in confined environments due to the decrease in van der Waals attraction with a decrease in the number of neighboring molecules. Therefore, at lower temperatures, the liquid-vapor region disappears, resulting in a lower critical temperature.[92,93]; however, this reasoning does not hold for polyol's high mobility within the pore structure, since its vapor pressure is negligible for the temperatures studied.[38] In similar lines, Liu and coworkers found that the confined diffusion of

p-xylene was enhanced by the 3D intersecting channels in SCM-15 zeolite. The preferential diffusion of p-xylene is found to be affected by the loading; at low loading, it is found to diffuse along the Z direction due to the presence of strong adsorption sites and intersections, providing a space for molecular rotation. In contrast, at high loading, p-xylene is found to diffuse along the X direction due to the presence of continuum intersections, which are channels resulting from fused cavities, that reduce the diffusion barriers and maintain the large diffusion coefficient of the compound. This reliance of diffusion behavior of the compounds on the loading was attributed to the presence of continuum intersections in zeolite materials characterized by weak adsorption, low diffusion barrier, and large space.[94]

Looking at the aforementioned observations collectively, we can state that the study of intrapore diffusivities of organic reactants inside nanoporous catalysts is important, and the knowledge gaps pertaining to this field of study needs molecular-level understanding. As mentioned earlier, the anomalous enhanced diffusivities of polyols like glycerol in comparison to alkanes, alcohols and carbonyl compounds inside nanoporous catalysts is still unclear. Additionally, the effect of pore size and geometry on the intrapore diffusivities, structural properties and intermolecular interactions of functionalized compounds like alcohols, polyols and carbonyl compounds needs fundamental understanding in order to further study its effects on the intrinsic reaction kinetics and thermodynamics of the catalytic reactions.

2.2.2 Confinement effects on condensed phase catalytic reactions

In this subsection, we delineate the experimental findings and knowledge gaps pertaining to the effect of confinement on intrinsic reaction kinetics and thermodynamics of condensed phase catalytic reactions inside nanoporous catalysts. In the case of condensed phase heterogeneous catalytic reaction studies, NMR diffusion, and relaxation studies have been conducted to examine the effect of a solvent (such as water) on the catalytic oxidation of 1,4-butane-diol in methanol over Au/TiO_2 medium. The longitudinal and transverse relaxation times of substrate molecules within a catalyst, denoted by T_1 and T_2 respectively, can be measured using the NMR relaxation technique. The adsorption strength of the catalyst of the chosen substrate may be inferred from the ratio T_1/ T_2.[34,68,95,96] It has been observed that adding water to the dry catalytic system prompted a decrease in both conversion as well as selectivity towards dimethyl succinate. In

particular, it was observed that adding water to the pure methanol solvent diluted the system, yet decreased the effective rate of diffusion of reactant into catalyst pores. The authors provided two possible explanations for this phenomenon: (a) adding water to the pure solvent system was observed to inhibit the adsorption of the reactant, thus leading to a lower conversion; (b) introducing a second species (here, water) into a pure solvent (here, methanol) disintegrates the original liquid's hydrogen bonds to form a new hydrogen-bonded polyol/water network that is characterized by enhanced dynamics (diffusion) compared to that of the original bulk structure.[68,97] Similar studies were carried out to assess the effect of a solvent on the aerobic catalytic oxidation of 1,3-propanediol and its two methyl-substituted homologues, 2-methyl-1,3-propanediol and 2,2-dimethyl-1,3-propanediol, over an Au/TiO_2 medium. As in the case of 1,4-butanediol, the same conclusions were made for the changes observed in reaction rates and selectivity of the propanediols inside confined environments.[95] In their recent work, Varghese and coworkers conducted NMR relaxometry studies combined with MD and DFT calculations and proposed that the condensed phase conversion of glycerol to propanediols was promoted by the addition of H_2SO_4 due to an increased concentration of glycerol within the catalyst pores, and the enhanced reaction between glycerol and ReOx-Ir catalyst.[98] It may, thus, be summarized that the diffusivity inside the catalysts, and therefore, the internal mass transfer within nanoporous substances is dependent on the intra-porous hydrogen bond networks between the reactant and the solvent confined inside nanoporous materials. The change in the diffusivities of confined reactants lead to a modification in the overall kinetics and thermodynamics of the catalytic reactions. When the hydrogen bond network of the reactant is disturbed due to the interface or the presence of the solvent, the diffusivity is found to increase which, in turn, increases the possibility of the occurrence of higher reaction rates. As a result of such bond disruptions, polyols in nanoporous catalysts display higher diffusivity at the catalyst interface than in the bulk phase. Therefore, the solvation free energy change occurring due to solvent manipulation with metal nanoporous catalysts may be used to enhance the reaction rate.[37]

In contrast, it has been reported that the rate of dehydration reactions by hydronium ions are enhanced when carried out in zeolite pores, which are found to exhibit confinement effects like those observed in enzyme catalysis. When the dehydration of cyclohexanol is carried out in the pores of zeolite HBEA material, it was found that the pores promoted substrate-hydronium ion

association to a degree five times higher than that observed in the homogeneous acidic aqueous medium.[91] This higher level of association is suggested to be due to a decreased entropy loss during association, as confined substrates in the pores exhibit a comparatively lower entropy than in the bulk phase, and thus, a lower loss in entropy during association. While the enthalpies of activation are of similar magnitude for the dehydration process within the zeolite pores as well as in the bulk phase, it is found that the entropy gain is higher in the former case as compared to the latter, leading to a higher intrinsic rate constant for dehydration. This increase in the rate constant, coupled with the higher association of the hydronium ions with the substrate, lead to an enhanced catalytic performance of the hydronium ions within the zeolite pores. Through rigorous kinetics and mechanistic studies conducted on the dehydration of numerous methyl-substituted cyclohexanols in H-ZSM-5,[99] it was concluded that the dehydration mechanism was not altered due to the confinement of hydronium ions within the zeolite pores, as compared to the reaction in the bulk liquid phase. The mechanism was found to rely purely on the positional and geometric features of the substituent groups in the cyclohexanol molecule. However, the turnover frequencies of the hydronium ion-catalyzed dehydration process carried out within zeolite pores were observed to be two orders of magnitude greater than observed in the liquid phase. In conclusion, it was found that the entropy-driven behavior of solvated reactants inside nanoporous catalysts differs from that in bulk liquids. In the case of acid-catalyzed dehydration, this difference leads to higher association between the substrate and hydronium ions. When this effect is coupled with intrinsically high rate constants for dehydration, the overall process is enhanced.[37] Additionally, it was posited that the unique nano-environment resulting from confined zeolite spaces enhances the interaction between reactants, such as alcohols, and hydronium ions, in comparison with the same interactions in a homogeneous phase. In the latter case, the molecular association between the reactant and the ion is much weaker, resulting in lower reactivity (for instance, dehydration). Therefore, the intrinsic catalytic activity can be influenced by tailoring the steric constraints and thereby reorganizing the local solvent-substrate interaction. In the case of dehydration within zeolite confined spaces, it was found that the activity decreases as the pore size increases.[100]

To study the effects of pore size and shape on the catalytic chemistry of biomass conversion reactions, zeolites of varying pore sizes and shapes (small pore ZK-5, SAPO-34, medium pore Ferrierite, ZSM-23, MCM-22, SSZ-20, ZSM-11, ZSM-5, IM-5, TNU-9, and large pore SSZ-55,

Beta zeolite, Y zeolite) were tested in a pyroprobe reactor for the conversion of glucose to aromatics. It was observed that the yield of aromatic product was a function of the zeolite pore size; small pore zeolites did not yield any aromatics with oxygenated products such as CO, CO_2, and coke, upon pyrolyzing glucose, while medium pore zeolites (5.2 – 5.9 Å) yielded a large amount of aromatics. In the case of large pore zeolites, high coke yield was found, with low yields of aromatics and oxygenated products. Apart from pore size, it was observed that internal pore space, as well as steric hindrances, determined aromatic yield. In this regard, medium pore zeolites with moderate internal pore space and steric hindrance (ZSM-5 and ZSM-11) were found to yield the highest amount of aromatic product with the least amount of coke.[100] In their recent work, Shetty and coworkers reported that the positive effect of zeolite confinements results from the stabilization of the transition state due to confinement, and its intermolecular interaction with alkanols which is dependent on both the confinement size as well as alkanol structure within the pore. The higher rate of dehydration of secondary alkanols, 3-heptanol, and 2-methyl-3-hexanol observed in the case of zeolite MFI comprising smaller pores than zeolite BEA was attributed to lower activation enthalpy in the tighter confinement spaces of the zeolite MFI which offsets a less positive activation entropy. In the case of dehydration of a tertiary alkanol such as 2-methyl-2-hexanol, the higher activity observed in zeolite BEA compared to that in zeolite MFI was primarily seen as a result of reduction of activation enthalpy resulting from the stabilization of intraporous interactions.[94]

Based on the aforementioned results on the effect of confinement on intrapore catalytic activity and selectivity of the condensed phase reactions, the following knowledge gaps need molecular level understanding: (i) effect of pore size and geometry on the reaction kinetics and thermodynamics of condensed phase reactions, (ii) the change in intrapore entropies and enthalpies of nanoconfined reactants and solvents, (iii) effect of change in intermolecular interactions on the dynamics and intrinsic reaction kinetics and thermodynamics of the confined reactants. To tackle these knowledge gaps, researchers have employed computational modeling methods like MD, GCMC and density functional theory (DFT) to study the confinement effects, which is discussed in detail in the following subsection.

2.2.3 Computational findings on the effect of confinement

The aforementioned studies (Sections 2.2.1 and 2.2.2) offer an overview of the significance of examining confinement effects of mesoporous materials on the dynamics, intermolecular interactions, entropy of the substrate molecules, and their relation to conversion and selectivity in heterogeneous catalytic reactions. In an attempt to discern the phenomena observed in experimental studies, molecular simulation techniques have been applied to understand the fundamental relation between confinement effects of metal oxides and diffusion, as well as the structural properties of nanoconfined substrates.[38,101–103] Specifically in the case of substrate-surface interfaces, inherent inhomogeneity exists in the system due to spatially dependent intermolecular interactions, leading to a density variation perpendicular to the interface. It is vital to understand the interface dynamics in contrast to bulk fluid behavior in order to apply and improve technologies like heterogeneous catalysis. In this context, theories such as statistical mechanics, DFT and MD techniques, in conjunction with computer simulation techniques, such as Monte Carlo (MC) methods are significant components of the studies. Most theoretical models of confined fluids, density function methods aside, do not explicitly describe spatial inhomogeneity and instead treat the phenomenon as a phase equilibrium problem between two macroscopically distinct phases that have unique densities, as in Travalloni's model and the quasi-two dimensional fluid approach. In particle-based simulations, however, the spatial distribution of the fluid within the confining media is explicitly described, thus enabling the study of the relationship between the molecular structure and mobility. While substantial research has been reported on computer simulation studies of associating liquids (such as water) in confining environments such as slit-shaped nanopores and nanotubes, such studies are lesser available for organic substrates in mesoporous materials, which receive significant interest in condensed matter physics.[104–109] In this regard, glycerol has received widespread interest over the last few decades owing to its ability to form highly directional intra- and inter-molecular hydrogen bonds. In its liquid state, the complex hydrogen bonding network gives rise to an intermediate-range order; this is atypical in molecular fluids that exhibit purely dispersive interactions.

Through previous simulation studies conducted for glycerol in fully saturated cylindrical channels of hydroxylated silica, it was shown that confinement leads to classical effects such as structural heterogeneities, as well as significantly lowered relaxation dynamics. In order to investigate both

dynamical and static parameters with a molecular level spatial resolution, a semi-rigid cylindrical silica nanopore model containing glycerol molecules was used, possessing the same density as the bulk liquid. It was found that, within the confined space, the translational self-diffusion slowed down by a factor of 8 compared to the same in the bulk phase at the same density. Furthermore, a 10% reduction in the glycerol-glycerol H-bonds was reported inside the confined space.[102] In contrast, Campos-Villalobos and coworkers performed a combination of PFG-NMR experiments and MD simulations, and observed enhanced diffusivity for glycerol inside slit pores of 2 nm, 4 nm, and 6 nm, for different pore saturations, keeping density similar to that of bulk phase. They attributed the overall increase in self-diffusion to the competition between the strong structural order at the solid-liquid interface, and the H-bond disruption near the center of the confinement. [38] The contrasting results might be arising due to different sizes and shapes of the confinements and errors in pore creation (such as the use of semi-rigid model for silica) and assumption of equal bulk and intrapore densities of glycerol. Similarly, it was reported that the reduction in the diffusivities of acetone inside nanoporous silica catalysts was a result of increased acetone-acetone interactions and local densities near the center of the confinement.[110]

The majority of computational studies reported in this subsection have investigated the effect of confinement on structural properties and intermolecular interactions of the substrate molecules, whereas based on the observations reported in Section 2.2.2 it is clear that the change in thermodynamics properties such as entropy and enthalpy plays a crucial role in the modifications of dynamics and intrinsic reaction kinetics and thermodynamics of the catalytic reactions. Therefore, in our study, we have cumulatively analyze the change in thermodynamic properties in addition to physical properties (structural properties and intermolecular interactions) of the confined reactant and solvents inside nanoporous silica catalysts of different sizes and geometries. In the following section, we provide the objectives and scope of the research conducted in this thesis for understanding the effect of confinement on mechanistic and thermodynamic properties of glycerol, water, heptane and acetone molecules inside silica nanostructures of varying sizes and shapes (slit and cylindrical pores).

2.3 Objectives and scope of the thesis

Based on the experimental and computational observations reported in Section 2.2, it could be stated that a molecular-level understanding of the confinement effects imposed by nanostructures of different shapes (slit and cylindrical pores) and sizes on the change in (a) diffusivity, (b) density, (c) molecular orientation, (d) intermolecular interactions and (e) entropy and potential energy; of the confined functionalized reactants (alcohols, polyols, carbonyl compounds) is still unclear. Specifically, the enhancement in the diffusivities of the nanoconfined polyols like glycerol in comparison to alkanes, alcohols and carbonyl compounds was attributed to change in the structural properties and intermolecular interactions (hydrogen bonding network disruption), although the effect of pore size and geometry on the change in thermodynamic properties like entropy and potential energy is still unaddressed. As mentioned earlier in section 2.2.2, the modifications in diffusivity, intermolecular interactions (like dipole-dipole and hydrogen bonding), and molecular orientations of the confined substrates could cause a significant change in the selectivity and conversion of the catalytic chemical reactions. Detailed understanding of the role of (i) geometry, size and chemical nature of the nanostructures, (ii) change in the intermolecular interactions and molecular structure, (iii) intrapore dynamic properties; could be applied further in the study of intrinsic reaction kinetics and thermodynamics of the catalytic reactions of the substrate molecules inside a confined space.

The objective of this thesis is to study the effect of confinements of varying sizes (2, 4 and 6 nm) and geometries (slit and cylindrical pores) on the (a) intrapore densities of the confined water, acetone, glycerol and heptane molecules: (b) relative change in the diffusivities of the substrate molecules in comparison to the bulk liquid; (c) change in the entropy and potential energy of the substrates; (d) modifications in the number and strength of intermolecular interactions between the substrate-substrate and substrate-surface molecules; (e) radial density profiles of the confined substrates. We are considering water, glycerol, acetone, and heptane as our substrates, due to the presence of different types of functional groups and varying molecular sizes.

The scope of this thesis is to provide a molecular-level explanation for the experimental observations discussed in Section 2.2.1 on the anomalous enhancement in diffusivities of polyols like glycerol inside the nanopores in comparison to acetone (reduction in the diffusivities) and

heptane (negligible change in the diffusivities). Change in intermolecular interactions of substrate molecules inside the confinements was investigated to verify the experimental hypothesis of disruption of hydrogen bonding network of polyols like glycerol. We have additionally investigated change in the thermodynamic properties (like entropy and potential energy) of water, acetone, glycerol and heptane molecules inside silica nanostructures of varying geometry and size to provide an explanation for the results obtained on the change in structural (like intermolecular interactions, molecular orientations, density profiles across the confinement) and dynamic properties. Finally, we provide a detailed explanation for the effect of confinement of different sizes and geometries on the intrapore dynamics of the substrate molecules, by studying and comparing the change in physical (intermolecular interactions, molecular orientations, density profiles) and thermodynamic properties (entropy and potential energy per molecule) of the substrate molecules within the nanopores. We have limited the scope of this analysis to only physical interactions of the substrates inside the nanopores, and chemical reaction studies for the confined reactant-solvent systems are beyond the scope of our research. As mentioned earlier in Section 2.2.2, understanding the change in structural, dynamic and thermodynamic properties of confined substrates allows us to further study the change in the intrinsic kinetics and thermodynamics of the catalytic reactions inside the nanopores. In addition, we limit the pore size to 6 nm due to the increased computational cost associated with the bigger confinement sizes (10-20 nm) which were used in the PFG-NMR experiments explained in Section 2.2.1. In the following section, we have detailed the methodology used to perform the MD and GCMC simulations for the calculation of structural, dynamic and thermodynamics properties of nanoconfined substrate molecules.

3 Methodology

In this section, we begin with the workflow for molecular simulation methods used in the thesis, along with the detailed description of the simulation procedure used for performing the molecular modeling methods in Section 3.1. Furthermore, we represent the methodology followed for analysis of the simulations pertaining to the study of confinement effects of the silica nanostructures imposed on the dynamics of the substrate molecules is explained in detail in Section 3.2.

3.1 Molecular Modeling Methods

An accurate prediction of the kinetics and thermodynamics of condensed phase chemistry can be attained only when the simulation models used to contain the explicit substrate molecules that represent the condensed phase environment at the relevant densities. To this end, implicit solvation was not used as it is unable to capture intermolecular interactions, such as hydrogen bonding.[37] Since substrate molecules in a condensed phase environment can exhibit numerous configurations, extensive sampling is a requirement; this need promotes the use of molecular dynamics simulations in the study of condensed phase phenomena. *Ab initio* molecular dynamics, abbreviated as AIMD, compute atomic forces based on electronic structure calculations computed while the simulation is ongoing.[111,112] While this technique is ideal for the investigation of equilibrium thermodynamic properties, reaction studies as well as dynamic properties of condensed phase systems, the electronic structure calculations involved are computationally expensive. Therefore, the systems studied through AIMD are typically limited to the order of a few hundred atoms. In the present study outlined, the systems chosen are much larger, of the order of thousands of atoms (more than 20,000 atoms for 6 nm cylindrical pores), making it impractical to carry out these molecular simulations using *ab initio* methods. In addition, we have restricted the scope of this study to only physical interactions, and modeling methods like MD and GCMC have proven to be reliable and less computationally expensive techniques for studying these interactions.[101]

When atomic force, and subsequently, potential energy calculations are performed using empirical parameters rather than first principles, the computational cost associated with MD simulations is

notably lower. The interatomic potential is computed using the force field (collection of empirical equations and numerous parameters); since the force fields of liquids and organic molecules are readily available, this technique is used to examine the properties of pure substrates as well as mixtures.[113–115] Additionally, GCMC simulations have been reported as a computationally inexpensive method to calculate the intrapore densities of liquid molecules, by equating the chemical potential of the molecules inside the confinement to that of the bulk liquid.[116–119] GCMC simulations were used to obtain the initial simulation system (with accurate intrapore densities of the substrates) for the MD analysis. Therefore in the context of this thesis, we will be only focussing on force-field based MD and GCMC simulations. The physics behind MD and GCMC simulations are discussed in detail in Section A2 of the appendix. In this study, we have used a combination of MD and GCMC methods for performing the bulk and intrapore simulations. Figure 3.1 shows a basic workflow for the methodology followed in this thesis.

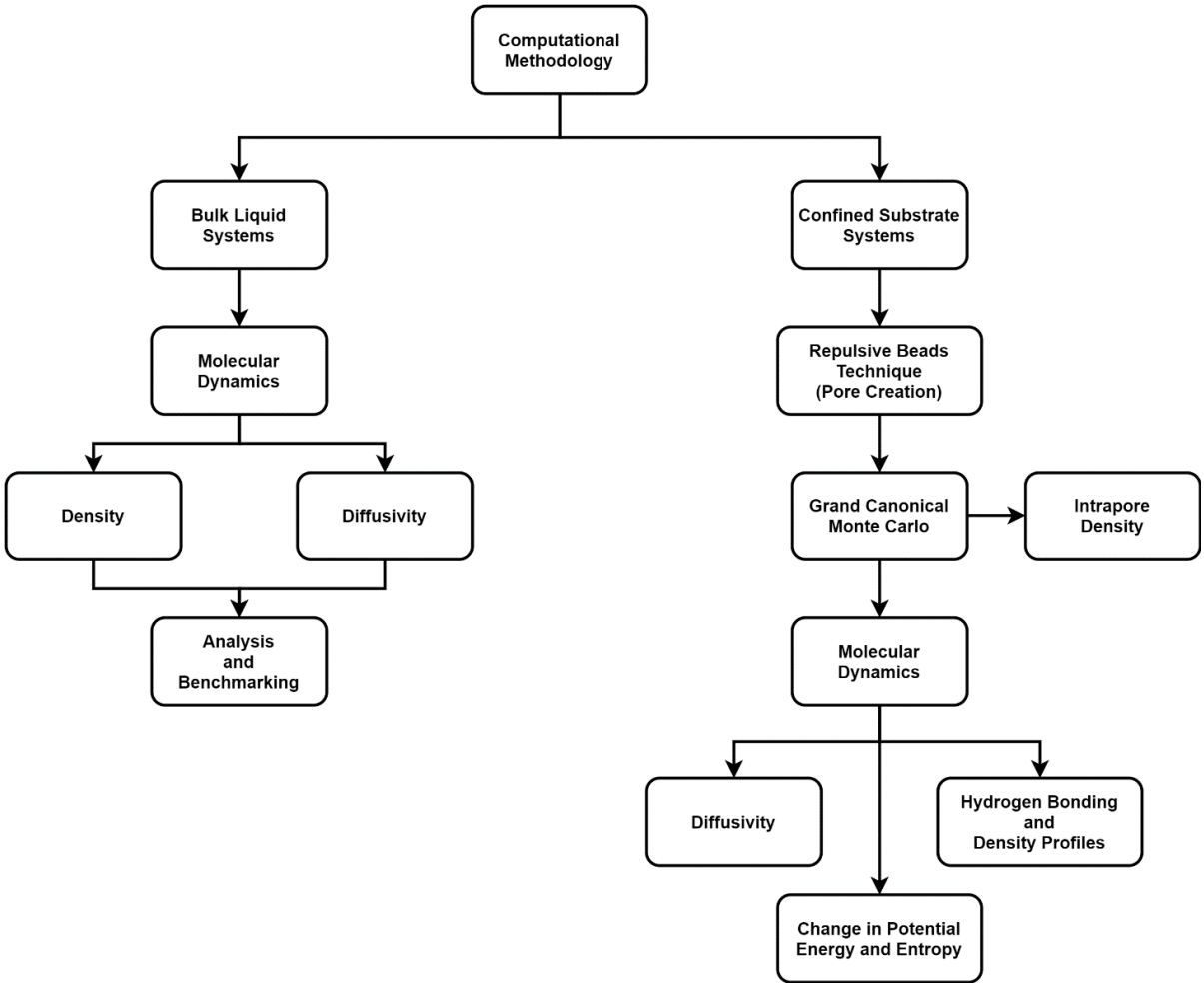

Figure 3.1: Workflow used for performing the molecular simulations in this thesis.

For this study, we are considering water, glycerol, acetone, and heptane as our substrates, due to the presence of different types of functional groups and varying molecular sizes. These substrates are confined inside silica nanostructures of one dimension (Slit pore of 4 nm) and two dimensions (Cylindrical pores of 2, 4 and 6 nm). We are considering water for benchmarking the simulation methods used in this work, as there is extensive data available for the intrapore dynamics of water inside Silica nanopore.[101,120,121] GCMC simulations were performed using TOWHEE version 6.2.11, to calculate the intrapore densities of the substrate molecules. MD was performed using GROMACS 2018.7, to study the dynamic, structural and thermodynamic properties of the bulk liquid and nanoconfined substrate molecules. Table 3.1 shows the respective partial charges and forcefield parameters used for the execution of MD and GCMC simulations for the species considered. For the organic liquid molecules, we have used the OPLS/AA forcefield, and the bulk densities were benchmarked against published experimental data (reported in Chapter A3 of the Appendix).[110,122,123] The OPLS/AA forcefield has proven to be an optimal choice for organic liquids in the condensed phase due to very low average errors (2-3%) in the calculation of densities and potential energies, making it ideal for our simulations.[124,125] For water, we have used the simple point charge/extended (SPC/E) model, which is widely used to accurately compute densities, diffusivities and intermolecular interactions.[126] For silica, we used the LJ parameters developed by Bródka and Zerda[110] and the partial charges given by Gulmen and Thompson.[127]

For the bulk substrate systems of pure water, glycerol, acetone and heptane, we have performed MD simulation to obtain the bulk densities and diffusivities. For the confined systems: firstly, we created silica nanostructures of different sizes and shapes using the repulsive beads technique suggested by Gulmen and Thompson.[127] Secondly, we prepared samples of silica nanostructures in equilibrium with the bulk substrate, by using GCMC simulations. Finally, we performed MD simulations for nanoconfined substrates to compute the intrapore diffusivities, intermolecular interactions, density profiles and change in potential energy and entropy. A detailed description of the aforementioned simulation procedure used in this study is explained in the following subsections.

Table 3.1: Forcefield parameters (ε and σ) and atomic partial charges (Q) for water, silica, acetone, glycerol and heptane implemented in this study.

Molecule	*Atom*	*Q (e)*	*ε/k_B (K)*	*σ (nm)*
Silica	O	−0.64	230	0.27
	Si	1.28	291.9	0.42
Water	O	−0.8476	78	0.3166
	H	0.4238	…..	…..
Acetone	C (central)	0.734	52.87	0.375
	O	-0.566	105.75	0.296
	C (terminal)	-0.507	80.57	0.391
	H	0.141	….	….
Glycerol	C (central)	0.055	55.09	0.3816
	C (terminal)	0.182	55.09	0.3816
	O	-0.6048	105.74	0.3442
	H (aliphatic)	0.026	7.9058	0.2774
	H (hydroxyl)	0.4158	25.077	0.1425
	H (centre carbon)	0.044	7.9058	0.2774
Heptane	C (terminal $C_{1,7}$)	-0.331	33.23	0.35
	C (backbone $C_{2,6}$)	0.174	33.23	0.35
	C (backbone $C_{3,5}$)	0.071	33.23	0.35
	C (central C_4)	-0.14	33.23	0.35
	H (terminal $C_{1,7}$)	0.075	15.1	0.25
	H (backbone $C_{2,6}$)	-0.027	15.1	0.25
	H (backbone $C_{3,5}$)	-0.015	15.1	0.25
	H (central C_4)	0.015	15.1	0.25

3.1.1 Bulk Substrate Systems

We begin with the bulk liquid systems for the four substrates. Figure 3.2 shows a basic representation of the bulk system used for analysis and benchmarking the properties of the substrate molecules. GROMACS version 2018.7 was used to perform MD simulations. The OPLS/AA (optimized potential for liquid simulations – all atom) forcefield is used in this study.

Firstly, geometry optimization was performed for the pure substrates in a cubic box of 5 nm using Steepest Descent Algorithm.[128] The system was equilibrated for 500 ps. Further, NPT simulations were performed to calculate the densities of the substrates. Finally, a production run was performed for 2 ns using Nosé-Hoover thermostat[129] with a temperature relaxation constant of 50 fs. The electrostatic (Particle-Mesh-Ewald) and vdW (Lennard Jones interaction) cut-offs were set at 1.0 nm for all the simulations. Velocity-verlet integration algorithm was used to perform the MD simulations. Bulk substrates were benchmarked against the density and diffusivities measured in experiments (Detailed benchmarking is reported in Section A3). The bulk diffusivities of the pure substrates were calculated using the Mean Square Displacement (MSD) method (discussed in detail in Section 3.3.1).

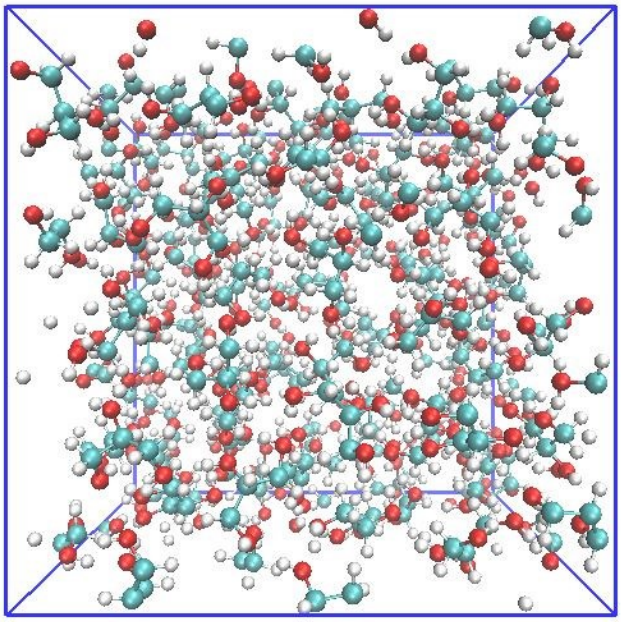

Figure 3.2: Pure substrate system inside a cubic box. Oxygen, carbon, and hydrogen atoms are represented by red, blue and white colored spheres respectively.

3.1.2 Substrate systems confined inside silica nanopores

It is important to note that for our simulations we are considering two types of confinements: a) Slit pore of 1D and b) cylindrical pores of 2D. The underlying rationale behind taking different confinement sizes and dimensions is to get an improved understanding of the confinement effects with varying surface area to volume ratios. We begin with the simple slit pore structure of 4 nm, where the substrate molecules are confined within two slabs of Silica molecules. In this type of

confinement, the molecules have restricted motion parallel to the X-axis as shown in Figure 3.3(a). The presence of previously published computational studies for 1D silica confinements makes it ideal for further benchmarking our methods. For the 2D confinements, we consider cylindrical pores of 2, 4 and 6 nm. In this case, the substrate molecules are confined within a cylindrical pore with a restricted motion parallel to the X and Y axes as seen in Figure 3.3(b).

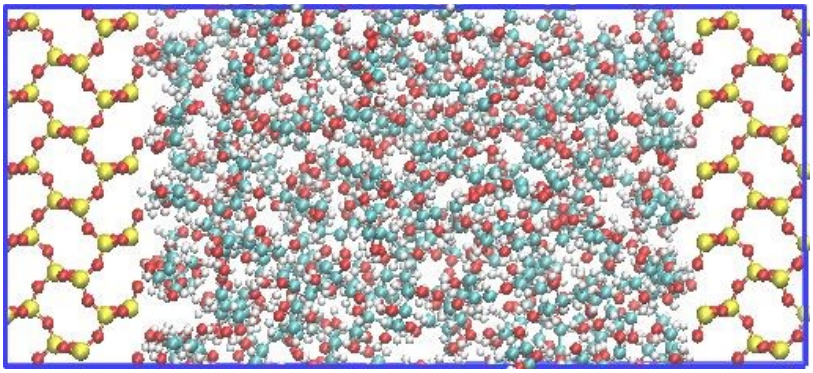

(a)

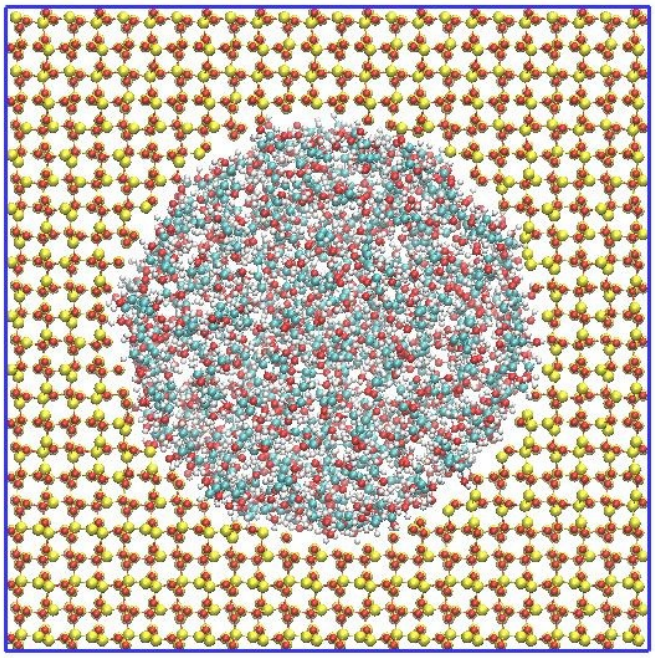

(b)

Figure 3.3: (a) One-dimensional silica confinement (Slit pore of 4 nm) with confined substrate molecules. (b) Two-dimensional silica confinement (Cylindrical pore of 4 nm) with confined substrate molecules. Oxygen, carbon, silica and hydrogen atoms are represented by red, blue, yellow and white coloured spheres respectively.

3.1.2.1 Creation of silica nanostructures

For the creation of pores, we start with a crystal structure of Silica and remove silica molecules inside a cylindrical portion of the required diameter. Once this structure is generated, we introduce hypothetical atoms called repulsive beads (with zero charges) at a distance from the silica surface as shown in Figure 3.4. This method is referred to as repulsive beads technique, which was proposed by Gulmen and Thompson.[127] To generate the cylindrical pore, we inserted repulsive beads (BE) into the center of the SiO_2 simulation cell. These particles interacted with the Si and O atoms through a purely repulsive potential,

$$V = C_{12}/r^{12} \tag{3.1}$$

where $C_{12} = 1.38 \times 10^8\ eV\ Å^{12}$, with both Silicon and oxygen atom. This method is applied to obtain a rigid silica nanostructure for our analysis.

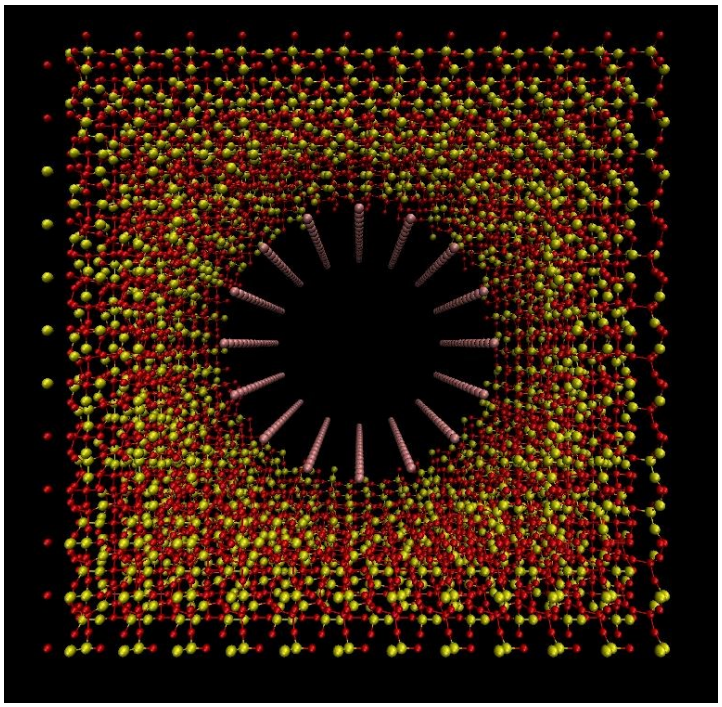

Figure 3.4: Cylindrical silica pore (Silicon and oxygen atoms are represented by yellow and red colored spheres respectively) with repulsive beads (pink spheres near the center).

For each pore size, a given number of repulsive beads are aligned in a cylindrical arrangement to keep the silica particles intact during the MD simulations. An NVT run was performed at 8000 K

(annealing silica pore), and the temperature was reduced to 300 K with 100 K increments. The final structure acquired (without the repulsive beads) was further used for GCMC simulations in order to calculate the density of reactants inside the pores. A similar procedure is followed for 1D confinement, where the repulsive beads are placed in form of sheets at a distance from the silica surface. The parameters used in this method are reported in Table 3.2.

Table 3.2: Parameters used for Silica nanostructures creation using the repulsive beads.
(SP = Slit pore and CP = Cylindrical pore).

System	*# SiO_2*	*N_{BE}*	*N_{BE} = (z)×(xy)*	*r_{BE} (nm)*
SP of 4 nm	250	64	8×8	1.3
CP of 2 nm	576	56	7×8	0.3
CP of 4 nm	2276	256	16×16	1.3
CP of 6 nm	4528	462	21×22	2.3

3.1.2.2 Densities of the organic liquids

After the silica nanopores have been constructed, we need to prepare a sample of silica nanostructures at equilibrium with the substrate molecules. In order to determine the density of substrate molecules inside respective silica nano-confinements, we performed grand canonical Monte Carlo (MC) simulations using the simulation package TOWHEE version 6.2.11. Two-box Gibbs ensemble MC simulations were conducted. The first box was initially an empty silica pore fixed in space and the second contained the substrate molecules, at T = 298 K. MC insertion and deletion moves, together with rotational and translational moves, were carried out until we observed a plateau in the number of water molecules inside the pore. The chemical potential of the bulk liquid using VMG Symmetry, with the use of Non-random two-liquid (NRTL) equation of state, and was given as an input for the GCMC simulations. We also observed that chemical potential in both equilibrated boxes was of the same magnitude. The coupled-decoupled configurational bias MC algorithm was used for insertion and deletion moves. In this method, the molecule is "grown" one atom at a time into the pore to increase the efficiency of insertion moves. The output structure (as represented in Figure 3.4 (b)) from the GCMC simulations was used for further MD analysis.

3.1.2.3 Molecular Dynamics simulations

A sample of catalyst pore in equilibrium with the reactant (with the calculated density) is created. Molecular dynamics simulations were carried out for this sample to analyze the trajectory to obtain information on the properties of the confined substrate. MD simulations were carried out in NVT ensemble with Nosé-Hoover thermostat with temperature relaxation constant of 50 fs and a timestep of 2 fs, reported in Table 3.3.

Table 3.3: Simulation systems of substrate molecules (water, glycerol, acetone and heptane) confined inside silica nanostructures of varying size and dimensions used in this study.
(SP = Slit pore and CP = Cylindrical pore).

System	*# Heptane*	*# Acetone*	*# Water*	*# Glycerol*
SP of 4 nm	106	210	864	211
CP of 6 nm	649	1287	5540	1246
CP of 4 nm	195	409	1685	379
CP of 2 nm	28	67	280	63

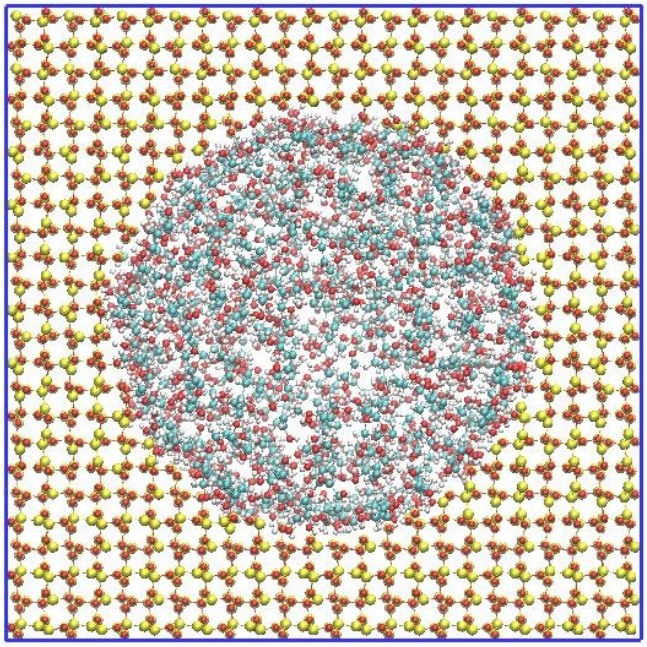

Figure 3.5: Two-dimensional silica confinement (Cylindrical pore of 4 nm) with confined glycerol molecules, obtained as the output of MD simulations. Oxygen, carbon, silica and hydrogen atoms are represented by red, blue, yellow and white colored spheres respectively.

After equilibration runs, the production runs of at least 5 ns for each nanopore were carried out. The electrostatic (Particle-Mesh-Ewald) and vdW (Lennard Jones interaction) cut-offs were set at 1.0 nm for all the simulations. Velocity-verlet integration algorithm was used to perform the MD simulations. A snapshot of the cross-section of the 4 nm cylindrical pore at full hydration is shown in Figure 3.5.

3.2 Analysis of the MD simulations

Upon completion of the aforementioned molecular simulations, analysis of the results is crucial to the interpretation of the simulations. The usual outputs from an MD simulation are the positions of all particles at each time t, and the quantities calculated may only depend on the time evolution of position variable and time. The trajectory of the system at each time step was used to calculate the structural and dynamic properties of the substrate molecules, which is important to compare with the experimental results. In this section, we will outline the primary quantities calculated in this thesis and their relation to quantities measured in previously published experimental results. A general workflow for the analysis scheme used in the thesis is depicted in Figure 3.6.

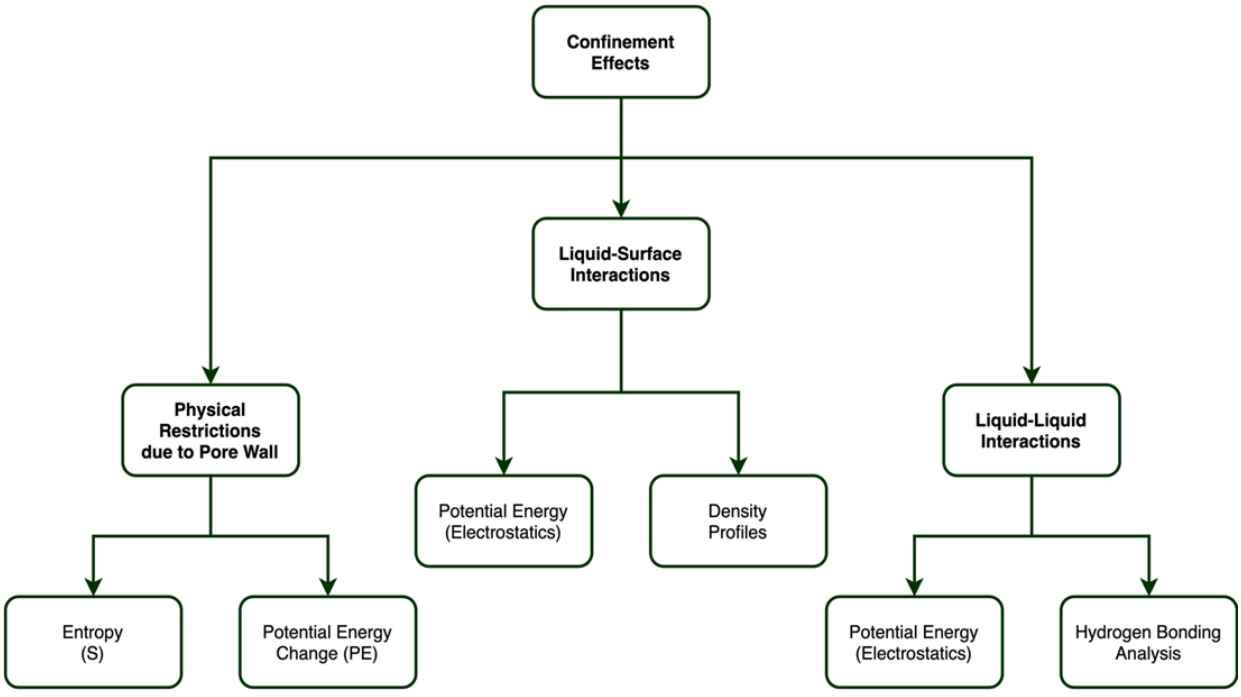

Figure 3.6: Basic scheme of methodology for MD analysis

3.2.1 Diffusivities calculations

Of fundamental importance to the analysis of the dynamics of a liquid is the mean squared displacement (MSD),

$$\langle \delta r^2 \rangle = \langle \frac{1}{N} \sum_{i=1}^{N} (r_i(t) - r_i(0))^2 \rangle \quad (3.2)$$

In this equation, the $\langle\ \rangle$ represents an ensemble average and $r_i(t)$ is the position at time t. At short times, particles undergo ballistic motion and $\langle \delta r^2 \rangle \propto t^2$. We have performed an additional NVE run after the production run for all the substrates for the diffusivity calculations, due to the influence of temperature coupling present due to the thermostat is bound to cause an error in the diffusivities (introduced due to fluctuations in the temperature of the system). Diffusivities of substrate molecules in bulk were used for benchmarking with the experimental observations, and the benchmarking report has been provided in Section A3.

3.2.2 Change in Potential energy and Entropy calculations

In this section, we explain the methodology used for the calculation of the change in the thermodynamic properties of the nanoconfined substrate molecules, namely Entropy (S) and Potential Energy (PE), corresponding to the effect of confinement imposed by various silica nanostructures.

Starting with the physical restrictions imposed by the silica wall, the thermodynamic properties are bound to change inside the confinement due to change in the intermolecular interactions and also the restrictions possessed on the mobility of the molecules due to the confinement. The mobility of molecules inside a nanostructure is affected by the restrictions caused due to the pore structure. For various nanostructures, the mobility is restricted in (a) X direction in 1D confinement; (b) X and Y directions in 2D confinement. This would lead to a relative change in S and PE of the substrate molecules. Schlitter's formula was used for the configurational entropy calculation, which yields an upper bound to the true entropy. It is computed by evaluating the covariance matrix of Cartesian positional coordinates obtained from the MD simulation output.[130] We calculate the change in the S and PE of the substrate molecules as it goes from

the bulk liquid to inside any confinement. The change in S and PE were calculated using the following equations,

$$\Delta PE = \frac{PE\ of\ substrate\ in\ pore - PE\ of\ empty\ pore}{No.\ of\ substrate\ molecules\ inside\ the\ confinement} - \frac{PE\ of\ substrate\ in\ bulk}{Total\ no.\ of\ molecules} \quad (3.3)$$

$$\Delta S = \frac{S\ of\ substrate\ in\ pore}{No.\ of\ molecules\ inside\ the\ confinement} - \frac{S\ of\ substrate\ in\ bulk}{Total\ no.\ of\ molecules} \quad (3.4)$$

Furthermore, we normalize the value of Potential energy change with respect to the number of molecules interacting with the surface in order to compare across different confinements. For normalizing with respect to the surface, we calculate the no. of molecules reacting with the pore to the total number of molecules inside the confinement. We devise a factor for normalization (F) using the following equation,

$$F = \frac{Surface\ area \times K}{Volume\ of\ the\ pore} \approx \frac{No.\ of\ molecules\ interacting\ with\ the\ surface}{Total\ no.\ of\ molecules\ inside\ the\ pore} \quad (3.5)$$

where factor K is the length of the first layer of the substrate molecules around the silica surface. This is calculated from the first peak (first solvation shell) of the radial distribution functions between the oxygen atom of the silica atom (reference atom) and the center atom of the respective molecules. Figure 3.7 shows the pictorial representation of the measure used to calculate the factor K for different types of confinements.

Once the value of K was determined, F was calculated for all the substrates inside various types of silica nanostructures using the following equations,

$$Slab:\ F = \frac{2 \times L^2 \times K}{(L)^2 \times D} \approx \frac{2K}{D} \quad (3.6)$$

$$Pore:\ F = \frac{\pi \times D \times L \times K}{\pi \times (\frac{D}{2})^2 \times L} \approx \frac{4K}{D} \quad (3.7)$$

where D is the diameter of the cylindrical pore or the length between the silica surfaces in the case of slit pore, L is the height of the cylindrical pore or the length and depth of the silica slit pore, as shown in figure 3.12. The values of F and K for all the systems are reported in section A2.3 in the Appendix.

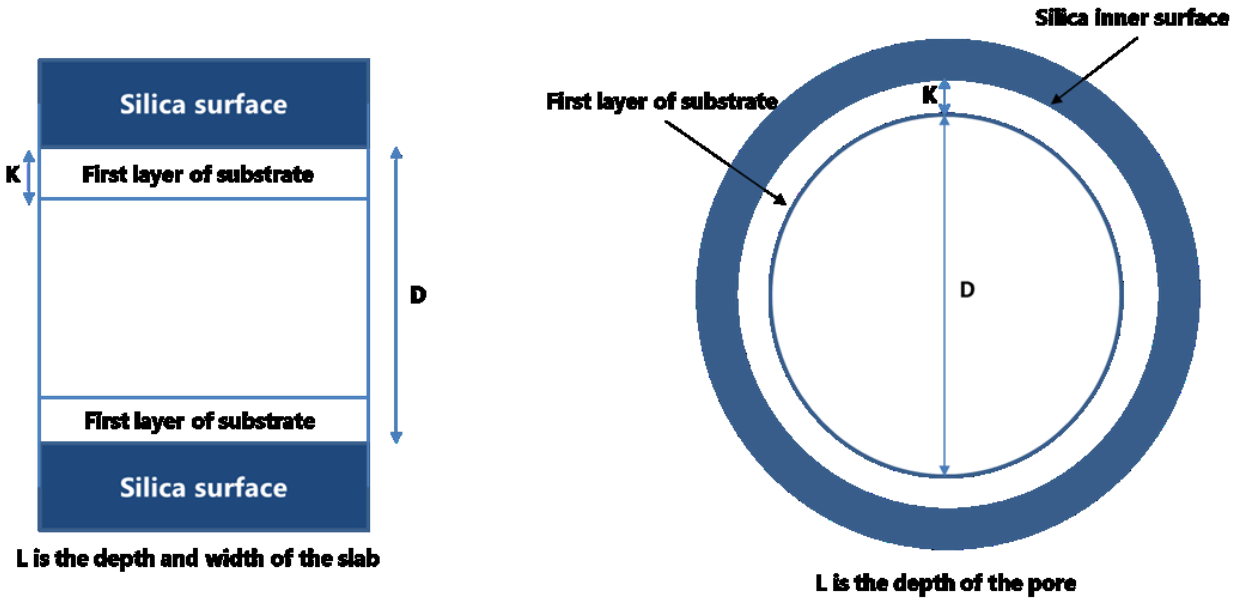

Figure 3.7: Pictorial depiction of the 1D Slit-pore (left) and 2D Cylindrical-pore (right).

Using the value of F, we can calculate the normalized PE change using the equation,

$$Normalized\ PE\ change\ (\Delta NPE) = \frac{\Delta PE}{F} \tag{3.8}$$

The values of NPE for various substrates were used to compare different confinements to analyze the influence of varying confinement sizes and shapes on the dynamic properties of the substrate molecules. To further study the effect due to surface interactions, it is necessary to obtain the change in PE explicitly due to a change in intermolecular interactions. The following section examines the methodology used to obtain PE change due to the substrate-surface interactions.

3.2.3 Intermolecular Interactions (Electrostatics)

In this section, we will analyze the change in potential energy as the charges on the silica atoms are switched on and off. The introduction of electrostatics to the silica surface will lead to

substrate-surface interactions. By doing so, the effect due to physical restrictions of the pore wall can be compromised to a major extent resulting in an amplified change in PE due to intermolecular interactions.

In this method, two silica nanostructures with confined liquids are considered: (a) without charges on silica atoms (PE_1); (b) with charges on silica atoms (PE_2). Further, silica nanostructure without liquid molecules is taken as a reference, where we separate the electrostatics component of the PE (PE_{Elec}) from the GROMACS output. The following equation was used to calculate the PE change per molecule of the substrate, due to the introduction of electrostatics on the silica atoms:

$$\Delta PE_{Elec} = \frac{PE_1 - PE_2 - PE_{Elec}}{Total\ number\ of\ substrate\ molecules\ inside\ the\ confinement} \quad (3.9)$$

In this case, high values of ΔPE_{Elec} (more positive) suggests better surface-substrate interactions. For comparison across various confinements, we further normalize ΔPE_{Elec} with respect to the surface area to volume ratio, thus yielding the effective change in the intermolecular interactions.

$$Normalized\ PE\ change\ due\ to\ electrostatics\ (\Delta NPE_{Elec}) = \frac{\Delta PE_{Elec}}{F} \quad (3.10)$$

The ΔNPE_{Elec} data provide us additional information about the change in substrate-surface and substrate-substrate interactions due to the silica confinement. ΔPE_{Elec} and ΔNPE_{Elec} was used to study the effect of alteration in intermolecular interactions on the dynamics of the nanoconfined substrates.

4 Results and discussion

In this section, we provide the results and detailed analysis on the effect of confinement on the dynamics of the substrate molecules obtained from the molecular simulations performed using the methodology in section 3.2. Firstly, we look into the calculated intrapore densities of the substrates confined inside the silica nanostructures in Section 4.1. Secondly, we report the calculated values of diffusivities of the bulk and nanoconfined substrates, and further, compare them with the experimental observations in Section 4.2. Finally, in subsection 4.3, we have reported the results obtained from the molecular simulations on the effect of confinement on the intermolecular interactions of heptane, acetone, water and glycerol separately and provide a summary for the influence of change in intermolecular interactions, and geometry and size effects of the confinement on the change in the diffusivities of the nanoconfined substrates containing different functional groups. In addition, we analyzed the experimental hypothesis[29] on disruption of hydrogen bonds for nanoconfined glycerol and provided an additional explanation for the anomalous behavior (enhanced diffusivities) of glycerol in comparison to acetone, heptane and water.

4.1 Intrapore densities of the nanoconfined Substrates

In this subsection, we present the calculated values of densities of water, heptane, glycerol and acetone molecules in bulk and inside the silica nanostructures, computed using the methodology discussed in section 3.2.2. Figure 4.1 shows the computed densities for water, glycerol, acetone and heptane molecules in bulk, slit pore of 4 nm, and cylindrical pores of 2, 4 and 6 nm; at T = 298 K. The computed bulk densities are in complete agreement with the experimental observations and a report on benchmarking is provided in Section A3 of the Appendix. For water, the computed densities vary with the change in the size as well as the geometry of the confinement. As we go from bulk to a slit of 4 nm, we see that the density increases by a small magnitude of 17 kg/m^3. The density value further increases till the cylindrical pore size of 6 nm where we see a spike of 7 kg/m^3 (from slit pore of 4 nm to cylindrical pore of 6 nm) in the intrapore density. We observed a drop in the density of water within smaller pores of 4 and 2 nm, which is approximately equal to the bulk liquid (1% lower than the bulk). Our results are in agreement with experimental results of

water density in Silica nanopore under ambient conditions and also with previously published MD results for silica pores with confined water molecules, where they have reported a loss in densities (6-10%) as compared to bulk for the pore sizes of 4 and 2 nm.[131,132] Neutron scattering was used by Mancinelli et al.[133]in order to study the structure of water inside MCM-41 nanopores. Two distinct populations of pore water each comprising a layer a plug of water forming in the center of the pore and a layer of 0.5 nm thickness around the pore walls are reported at ambient temperature. The density of the monolayer of water surrounding the silica nanopores, as reported by Rother and coworkers, was found to be around 70% of the bulk fluid. The density of the water molecules near the centre of the pores, on the other hand, was observed to be equal to bulk.[134] As revealed by the MD simulations on the study of properties of confined water in cylindrical silica nanopores of 4 nm, while only 12% of hydrophobic atoms of the nanotube are said to have a water oxygen atom within a 3.5 Å distance, about 97% of hydrophilic oxygen atoms of the nanotube have a water oxygen atom within the same distance. Due to the presence of small unfilled cavities near the pore walls, a lower density of water was observed (11% lower than the bulk) in the adsorbed layer of water.[135]

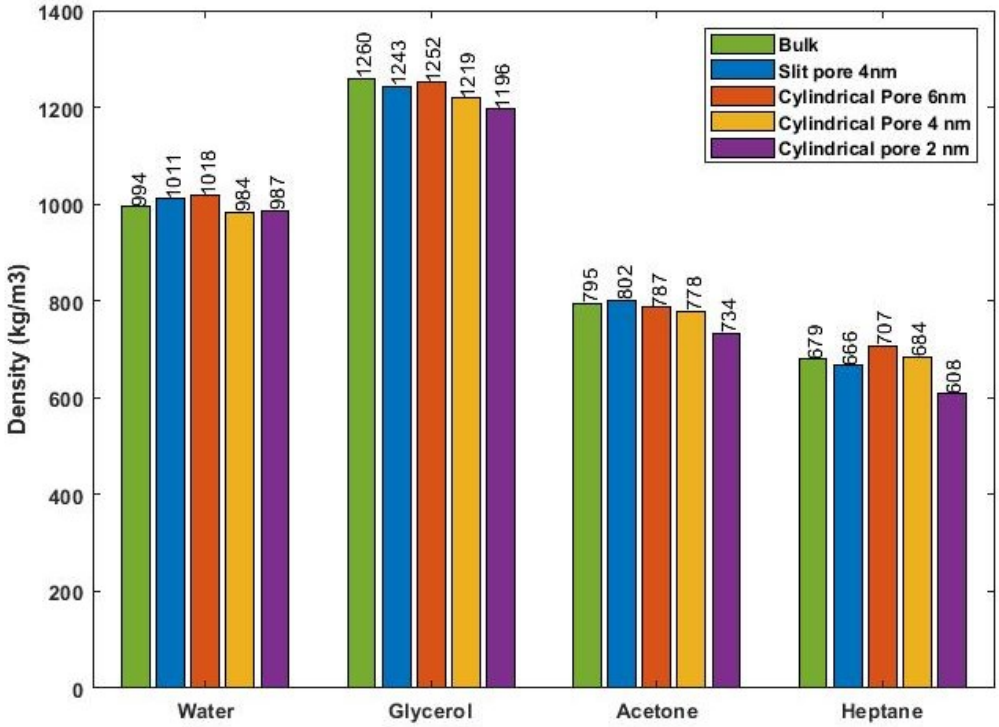

Figure 4.1: Computed densities of water, glycerol, acetone and heptane in bulk and inside various silica nano-confinements.

For a more complex substrate like glycerol, we see a minor drop in the density values as we go from the bulk liquid to slit pore of 4 nm. Within the 2D cylindrical pores, we observe that the density drops further with the reduction in the size of the confinement, especially for the case of a 2 nm cylindrical pore. A very similar trend is followed by acetone, where the drop in the density values is recorded with the increase in the dimension of the confinement (Slit to cylindrical pore) and with the decrease in the size of the confinement. For a bigger molecule like heptane, the density values remain similar to the bulk for slit pore of 4 nm and cylindrical pores of 4 and 6 nm. Whereas, we see a drastic drop (11% reduction) in the value of density with the decrease in the size of the cylindrical pore from 4 to 2 nm. The drop in the densities of the bigger molecules like acetone, glycerol and heptane could be due to the relative size of the molecules in comparison to the size of the pore. Recent computational studies on the study of dynamic properties of glycerol inside nanopores have made an assumption of equal bulk and intrapore densities of glycerol molecules.[38,102] However, based on the aforementioned results, it is fair to state that the negation of the intrapore density calculations could possibly lead to errors in the prediction of structural and dynamic properties of the confined substrates.

Looking at the data collectively, we observed that the density of comparatively larger molecules like acetone, glycerol and heptane drops with the reduction in the size of the confinement, whereas for smaller molecules like water it remained almost equal to bulk (±2%). Specifically, for the cylindrical pore of 2 nm, we see a drop in densities of 1%, 5%, 7% and 10.4% for water, glycerol, acetone and heptane respectively. Based on these results, we believe that the extent of the drop in the densities could be attributed to the size and shape of the glycerol, acetone and heptane molecules in comparison to the confinement sizes of 6, 4 and 2 nm.

4.2 Diffusivities of the Nano-confined substrates

The bulk and intrapore diffusivity of the substrate molecules inside various silica confinements computed using MSDs (refer to section 3.3.1) are reported in this section. The bulk diffusivity values are in accordance with the experimental results and a detailed benchmarking report is provided in Section A3 of the appendix. We calculated the PFG interaction parameters for water, heptane, glycerol and acetone molecules inside the four silica confinements. PFG interaction

parameter is the ratio of diffusivity of molecules in bulk to the diffusivity inside porous structures, as shown below.

$$PFG\ interaction\ parameter = \frac{Diffusivity\ in\ Bulk}{Diffusivity\ in\ Pore} \quad (4.1)$$

A high value of PFG interaction parameter suggests low intrapore diffusivity. Figure 4.2 shows the computed values of the PFG interaction parameters obtained from the output of the MD simulations using the methodology discussed in Section 3.2.4.1. The reported values of the PFG interaction parameters are within the error margin of 0.02-0.06.

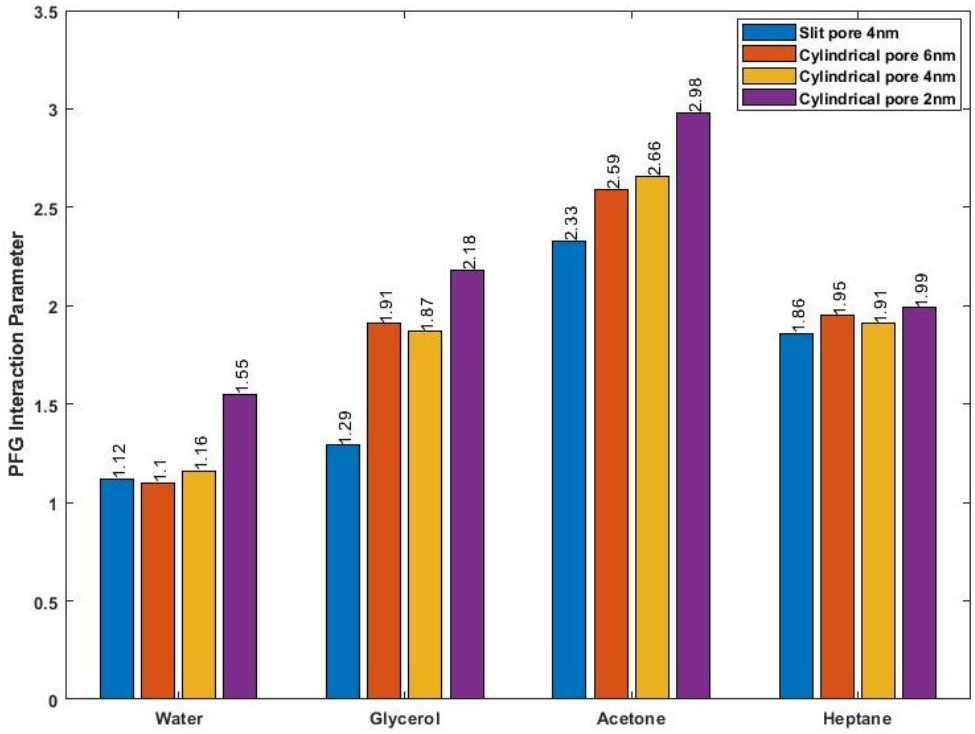

Figure 4.2: Computed PFG interaction parameters of water, glycerol, acetone and heptane inside various silica nanostructures.

The PFG interaction parameters are observed to be >1 irrespective of the substrate or the confinement, signifying that the diffusivities of all the molecules are lower inside the confinements in comparison to the bulk liquid. This was attributed to physical restrictions imposed by the silica nanostructure (irrespective of its size and/or chemical nature) on the motion of the confined molecules in comparison to the bulk liquid.[29] In the case of heptane, we see negligible impact

of confinement as the PFG interaction parameters remain the same inside all the nanostructures. As we go from a slit pore of 4 nm to cylindrical pore of 6 nm (1D to 2D confinement), we see a small spike of 0.09 in the computed PFG interaction factors, but within cylindrical pores of different sizes the diffusivities remain unchanged with the reduction in the size of the confinement. The negligible change in the intrapore diffusivities of heptane with the change in the geometry or size of the confinement was attributed to lack of functional groups with an ability to interact with the silica surface.[29] For acetone, the PFG parameters are seen to be increasing with both decrease in size and increase in the dimension of the confinement. As we go from a slit pore of 4 nm to a cylindrical pore of 6 nm, we see a spike in the PFG interaction parameter with the change in dimension of the confinement from slit pore (4 nm) to cylindrical pore (6, 4 and 2 nm). Within the cylindrical pores, the PFG parameters increase gradually with a decrease in the size of the cylindrical pore from 6 to 4 nm, but increases more significantly (12% increase) between 4 to 2 nm. It was reported in literature that the group of molecules with carbonyl functional groups tend to have the highest values of the PFG interaction parameter (1.7-2.2), which can also be noted in the computed diffusivities.[29] For a primitive molecule like water, the values of PFG interaction parameters remain constant (around 1-1.2) for slit pore of 4 nm and cylindrical pores of 4 and 6 nm, suggesting a near bulk-like behavior. But with further reduction in the pore size to 2 nm, we see a huge spike of 0.39 in the value of PFG parameter, resulting due to a reduced diffusivity inside the cylindrical pore. Our results of the reduction in the intrapore diffusivities of water molecules with the decrease in the size of the cylindrical confinements are in complete agreement with the experimental and simulation results.[101,131,132,136–138] Specifically, MD simulations on the intrapore dynamics of water in silica nanopores reported a similar decrease in the diffusivities with the reduction of the pore size from 4 to 2 nm (PFG interactions parameters increases from 1.1 to 1.4).[39] This decrease in the diffusivities was reported as a result of reduced translational mobility of water molecules around the silica surface as opposed to the center of the pore.[39] Finally, for glycerol, we see a drastic increase in the PFG interaction parameters as the dimension of the confinement increases (from slit pore to cylindrical pore). It remains constant across the cylindrical pores of 6 nm and 4 nm. But with reduction in size to 2 nm, we see a spike of 0.31 in the PFG factors resulting in a drop in the intrapore diffusivity. Campos-Villalobos and coworkers showed similar results for an increase in the PFG interaction parameters (approximately 1.5 to 3) for glycerol molecules with a reduction in the size of slit-pores of Alumina catalyst (from 6 to 2

nm).[38] With an assumption that the intrapore density was equal to the bulk liquid, they reported that in fully saturated pores, the dynamics of glycerol was mainly affected by the mobility reduction at the solid-liquid interface, which was in turn the result of a structural order and higher density in the contact layer than in the bulk liquid and the presence of hydrogen bonds between molecules in the hydroxyl groups and contact layer at the surface.

Furthermore, we compared the computed PFG interaction parameters with the experimental results published in the literature, measured using the PFG-NMR experiments. As previously explained in Section 2.2, it was reported that the PFG interaction parameters followed a particular trend based on the functional group present. This result was obtained using a factor defined as normalized PFG interaction parameters (using alkanes as a reference due to the lack of functional groups).

$$Normalized\ PFG\ interaction\ parameter = \frac{PFG_{Substrate}}{PFG_{Alkane}} \tag{4.2}$$

Where $PFG_{Substrates}$ denotes the PFG interaction parameter of the substrate taken into consideration and PFG_{Alkane} is the PFG interaction parameter of the reference alkane molecules (as the value of PFG interaction parameter was constant for all the alkanes irrespective of the chemical nature of the confinement). A detailed explanation of the theory behind the NMR and PFG-NMR experiments is reported in Section A1 of the Appendix. The trend provided in the literature for the normalized PFG interaction parameters is as follows, $Carbonyl\ compunds > Alkanes > Polyols$.[29] This trend was observed for all the substrates systems, irrespective of the type or size of mesoporous catalyst (SiO_2, TiO_2 and Al_2O_3). The average size of these cylindrical pores was around 15 nm. Polyols like glycerol showed an anomalous enhanced diffusivity (as compared to alkanes) within different porous materials as opposed to carbonyl compounds like acetone (high PFG interaction parameters). It was hypothesized that the enhanced diffusivity of the polyols is due to the disruption of the hydrogen bond network of the polyol molecules inside the nanostructures.[29] For our study, we limit the pore size to 6 nm due to the increased computational cost associated with the bigger confinement sizes like 15 nm, as used in the experiments. In addition to slit-pore configurations used in previously published computational results used to evaluate the influence of intermolecular interactions on the dynamic properties, we

also consider two-dimensional confinements (cylindrical pores) of varying sizes to address the knowledge gaps on the effect of confinement size and geometry on the diffusivities of nanoconfined substrates. Figure 4.3 shows the computed values of the normalized PFG parameters for all the systems. Our results are in qualitative agreement with the experimental PFG parameters, which could be a result of the difference in the pore sizes between experiments (around 15 nm) and simulations (2-6 nm). It was noted that for the slit pore of 4 nm and cylindrical pores of 4 and 6 nm, the trend of the normalized PFG interaction parameters is in accordance with the experimental results (qualitatively), i.e. $Acetone > Heptane > Glycerol$.[29] Whereas, between 4 to 2 nm, there is a drastic change in the diffusivities and the aforementioned trend is not obeyed. Inside the 2 nm cylindrical pore, both acetone and glycerol show reduced diffusivities in comparison to heptane and the anomaly of enhancement in the diffusivities of polyols inside nanoconfinement is not observed. This unique result suggests that the change in diffusivities is a function of both dimension as well as the size of the confinement and a general statement on the trend of diffusivities (PFG interaction parameters of Acetone>Heptane>Glycerol) cannot be made.

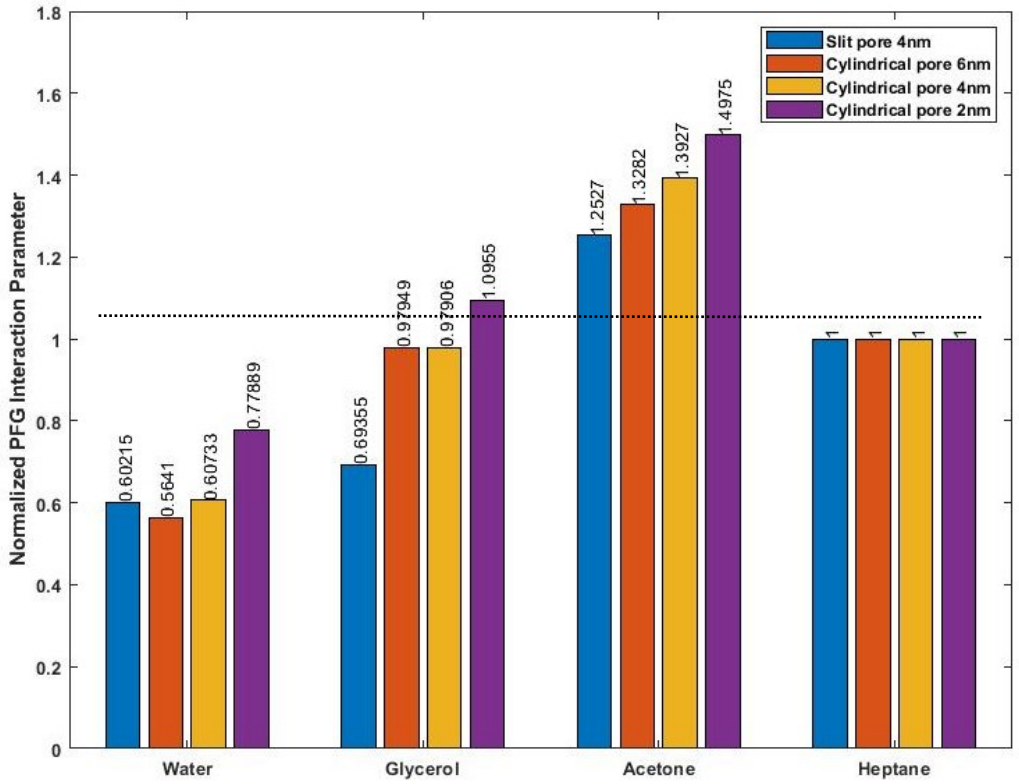

Figure 4.3: Normalized PFG interaction parameters computed using Molecular Dynamics simulations.

Based on the aforementioned results obtained from our simulations, it is clear that the change in the diffusivities of functionalized compounds is attributed to the shape and size of the confinement, and intermolecular interactions between the substrate-surface and substrate-substrate molecules. Therefore, the effect of size and geometry of the confinement on the intrapore dynamics and intermolecular interactions of the substrate molecules needs to be studied at a molecular level in order to provide a detailed explanation for the results obtained on the diffusivities of confined substrates. As reported in Section 2.2, molecules like cyclohexanol have been observed to lose entropy inside confinements like zeolites.[91] The loss in entropy could be compensated by a loss in the enthalpy of the confined substrates to minimize the free energy. This would result in a change in the intermolecular interactions of the confined molecules, leading to a change in the potential energy. So, to further understand the reason behind this phenomenon, we look into the effect of size and geometry of the confinement on the entropy, potential energy and intermolecular interactions of the substrate molecules inside nanostructures.

4.3 Confinement effects on thermodynamic properties and intermolecular interactions of confined substrates

In this section, we report the results obtained from the MD simulations on the change in entropy and potential energy of the confined substrates using the methodology provided in section 3.3.2, followed by the analysis of intermolecular interactions of the substrate molecules (using methodology provided in Section 3.3.3), namely substrate-substrate and substrate-surface interactions, due to the confinement effects imposed by the silica nanostructures. We analyze the thermodynamic (Entropy and potential energy) and structural properties (Intermolecular interactions and density profiles) of the substrates molecules and provide a summary on the effect of silica confinements on the structure and dynamics (intrapore diffusivities) of water, acetone, glycerol and heptane molecules, based on the aforementioned results.

4.3.1 Heptane

Starting with basic substrate heptane, used as our reference system due to the lack of functional groups, which results in weak intermolecular interactions with the porous medium as well as heptane-heptane interactions. In addition, the PFG interaction parameters of alkanes were observed

to remain constant irrespective of the size or chemical nature of the confinement, suggesting a minimal effect of the confinement on the diffusivities of alkane molecules like heptane.[29] To explain the trend of diffusivities (negligible change in the diffusivities with the change in geometry and size of nanostructures) for heptane, we have provided results on the change in thermodynamic properties like potential energy and entropy, and analyzed the density profiles in the following sections.

4.3.1.1 Potential Energy and Entropy of Nanoconfined Heptane

In this subsection, we presented the results on the change in entropy and potential energy as the heptane molecules bulk liquid to inside any confinement using the methodology given in Section 3.3.2. The computed values of the change in the entropy (ΔS) for heptane molecules inside the four nanostructures are reported in Figure 4.4. For these molecules, entropy is lost inside the confinement irrespective of the size or dimension. The computed loss of entropy increases as we go from slit pore of 1D to cylindrical pore of 2D. We see a further drop with the decrease in size of the pore, with a significantly higher loss in entropy with the reduction in the size from 4 to 2 nm.

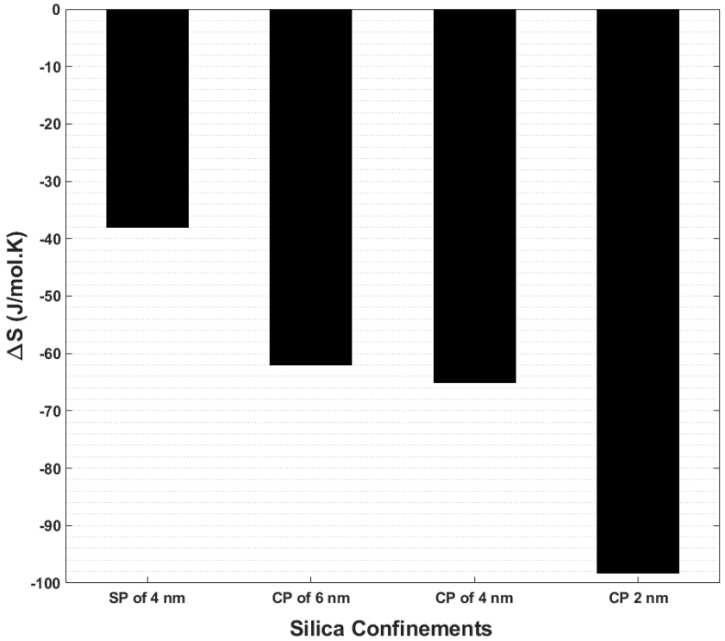

Figure 4.4: Computed values of change in entropy (ΔS) of Heptane between the bulk substrate and confined substrates (Confinement – Bulk) inside various silica nanostructures (CP is cylindrical pore and SP is slit pore).

In the context of entropic effects in heterogeneous catalysis, it has been reported in literature that porous catalysts, such as zeolites, solvate reactants within the nanopores, and thus exhibit atypical entropy-driven behavior that is not characteristic of bulk liquids. In the case of acid-catalyzed dehydration of cyclohexanol, lower entropy of reactants inside zeolite structures gives rise to higher association between the reactant and hydronium ions which, combined with inherently higher rate constants for the dehydration reaction, leads to an overall enhanced reaction process.[91] In another work, competitive adsorption studies were performed for liquid alkanes like methane, ethane, propane, butane and methane-ethane mixtures. It was observed that the bigger liquid alkanes had a comparatively lower entropy inside the Silicalite catalyst. Also, for the methane-ethane mixtures, at high pressures, methane is preferentially adsorbed due to entropic effects inside the porous structures, due to higher entropy of methane-filled zeolites at high pressures.[139–141] The confinement effect in alkane mixtures was experimentally proven through the behavior of a hexadecane-heptadecane binary system in bulk phase, as well as in nanopores of porous glass materials, using differential scanning calorimetry (DSC) and temperature-dependent powder X-ray diffraction (XRD). Through these experiments, it was observed that the alkane mixtures showed reduced ordering of molecular orientations inside small nanopores.[142–144] Given the size of the heptane molecule (seven carbon chain), it could be possible that the reduction in the entropies with the decrease in the size of the confinements is due to constraints imposed by the silica nanostructures on the reorientation (or alignment) of the heptane molecules within smaller pore sizes. Since we observed negligible change in the translational motion (refer to Figure 4.2) of heptane molecules inside the nanopores of different sizes and geometries, we could state that the loss of entropy inside the confinements is due to the restrictions in the rotational motion of the heptane molecule.

In order to overcome the loss in entropy, the molecules attempt to reorganize inside the nano-confinement, which could cause a corresponding loss in the potential energy with respect to the bulk liquid. The alteration in the molecular orientations can be caused by a change in the intermolecular interactions (van der Waals and Columbic interactions) of the confined heptane molecules, leading to a change in the potential energy. To validate this hypothesis, we calculate the change in potential energy (ΔPE) reported in Figure 4.5. In this figure, a positive value of ΔPE

suggests less favorable intermolecular interactions of the substrate molecules inside the pore compared to the bulk liquid (refer equation 3.3).

The computed values of ΔPE for heptane increases with the increase in the dimension of the confinement (from slit pore to cylindrical pores). Within the 2D cylindrical pores of varying size, the ΔPE increases with the reduction in the pore size from 6 to 4 nm, but it remains the same with a further reduction to 2 nm. This could be a result of different alignments of heptane molecules inside the slit-pore in comparison to cylindrical pore. Referring to Figure 4.4, we observe a drastic increase in the entropy change with the reduction of the size of cylindrical pore from 4 to 2 nm, which is not reflected in the ΔPE suggesting a change in the intermolecular interactions.

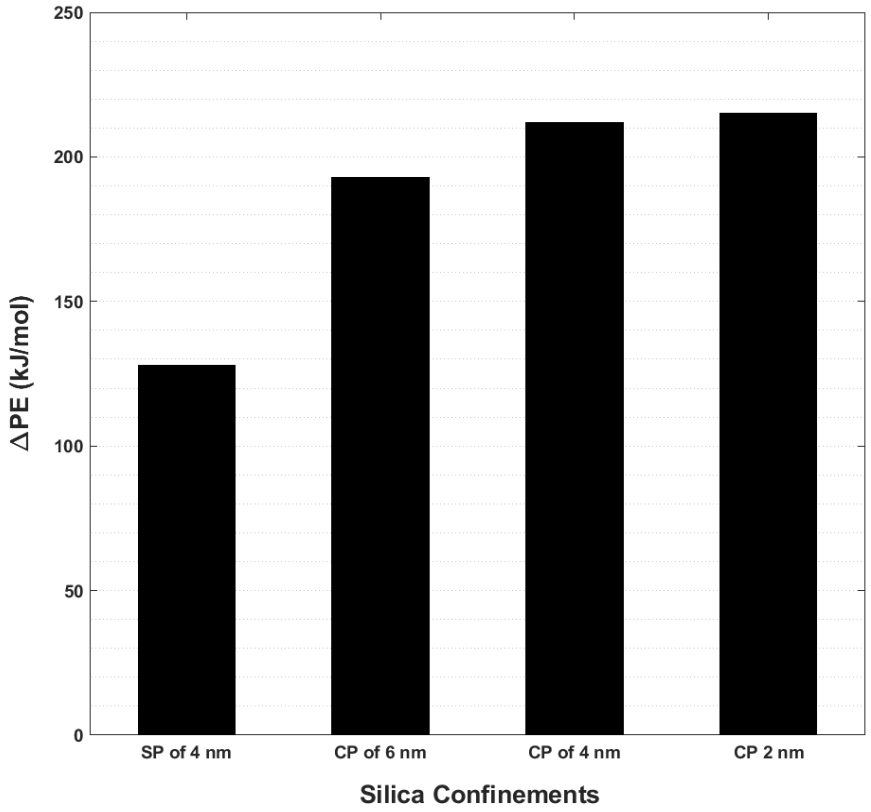

Figure 4.5: Computed values of change in potential energy (ΔPE) of Heptane between the bulk substrate and confined substrates (Confinement – Bulk) inside various silica nanostructures. (CP is cylindrical pore and SP is slit pore).

An interesting observation from the entropy and PE calculations collectively is that the entropy of the heptane molecules are lowered inside the confinement, but the molecules do not attempt to

lower their PE to minimize the free energy. On the contrary, we observed a gain in the PE change for the heptane molecules inside the confinements, suggesting that the intermolecular interactions are getting weaker with the reduction in the size of the confinement. Specifically, in the case of the 2 nm cylindrical pore, we see a drastic drop in the entropy, whereas the ΔPE remains constant. This could be due to the weakening of intermolecular interactions of heptane inside the cylindrical pore. Based on these results, a combined effect of entropy loss (causing a decrease in the mobility) and weaker intermolecular interactions (causing an increase in the mobility) could potentially lead to negligible change in the diffusivities of the confined heptane molecules (refer to Figure 4.2).

Alkanes like heptane can form intermolecular interactions like van der Waals (vdW) and electrostatic interactions. It was observed that the van der Waals interaction component contribution towards the adsorption energy of alkanes like octane was more dominant than the columbic interactions inside porous materials. The alkane-surface interactions were stronger than the alkane-alkane interactions.[142,143,145] In the following subsection, we study the intermolecular interactions between heptane-heptane and heptane-surface in order to validate the aforementioned result and also to study the role of change in the intermolecular interactions on the intrapore mobilities of heptane molecules.

4.3.1.2 Intermolecular interactions between heptane and Silica molecules

Intermolecular interactions of the nanoconfined heptane substrate molecules with themselves and with the silica surface is discussed in this section. Applying the methodology reported in section 3.2.4.3, we reported the change in potential energy (ΔPE_{Elec}) of the heptane molecules, as the electrostatics of the silica atoms are switched on (vdW and Electrostatic interactions) and off (only vdW interactions). Introduction of electrostatics on the silica atoms leads to alteration to the intermolecular interactions between heptane and silica atoms, due to the ability of heptane molecule to interact weakly with the surface atoms. By doing so, we have eliminated the effects due to the physical structure of the pore wall and van der Waals forces between heptane-heptane and heptane-silica atoms (as the vdW interactions are canceled out upon calculating the PE change between the two systems); and the change in the PE observed here is purely for the electrostatic interactions between the heptane-silica molecules. Figure 4.6 shows the computed values of

ΔPE_{Elec} for heptane molecules confined inside four different silica nanostructures. In this figure, a positive value of ΔPE_{Elec} represents favorable interactions (refer to equation 3.9).

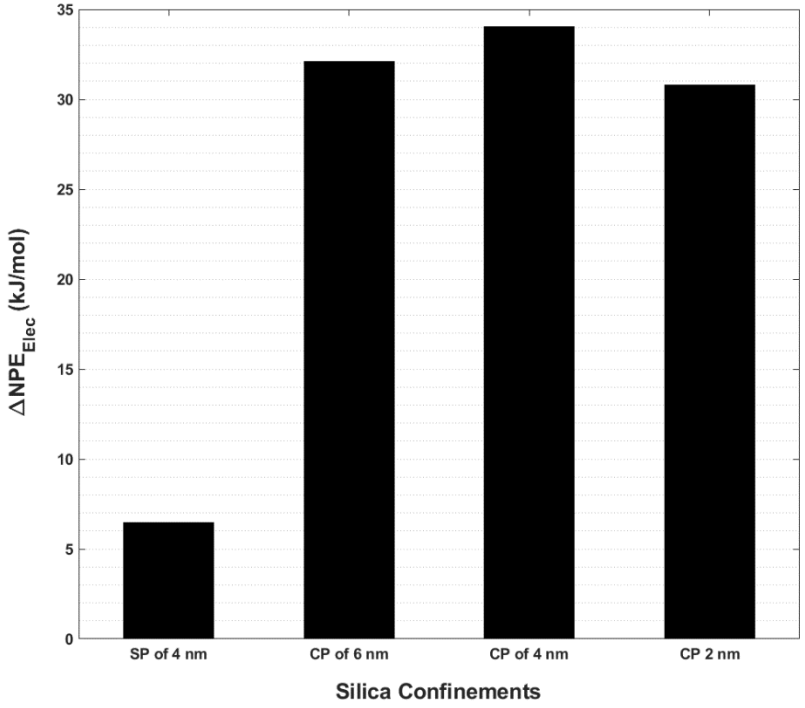

Figure 4.6: Computed values of change in potential energy (ΔPE_{Elec}) of Heptane molecules with and without the charges assigned on the silica atoms (without – with charges). In this plot, SP is slit pore and CP is cylindrical pore.

From this plot, we observed that the ΔPE_{Elec} increases drastically with the change in the dimension of the confinement (slit to cylindrical pore). This increase is a result of a higher surface area to volume ratio available for the molecules interacting with the silica surface. However, for cylindrical pores of different sizes such an argument is not valid as the computed ΔPE remains constant with the decrease in the size of the confinement from 6 to 2 nm. To further understand this, we normalized this potential energy with respect to the surface area to volume ratio, as suggested previously in Section 3.2.4.2. Additionally, an interesting observation obtained from this analysis is that the PE change due to only electrostatics (ΔPE_{Elec}) is in the range of 5-35 kJ/mol per molecule of heptane, whereas the combined contribution of vdW and electrostatic interactions in the previously calculated ΔPE was observed to be in the range of 100-250 kJ/mol. Our results are in agreement with the computational results published on the dominance of vdW forces over

electrostatics in the case of n-alkanes like octane.[142,143,145] Although heptane molecules don't interact well with the silica surface, we observed high ΔPE_{Elec} values for the cylindrical pores because of the large number of hydrogen molecules present in the heptane molecule.

Upon normalizing the ΔPE_{Elec} with respect to the factor F (refer to Section 3.2.4.2), the substrate-surface interactions per number of molecules interacting with the surface yield information about the varying strength of interaction across different nanostructures, as after normalization the heptane molecules are exposed to equal surface area of the pore wall. Figure 4.7 shows the computed values of normalized PE change (ΔNPE_{Elec}) associated with the heptane-silica interactions inside different silica confinements.

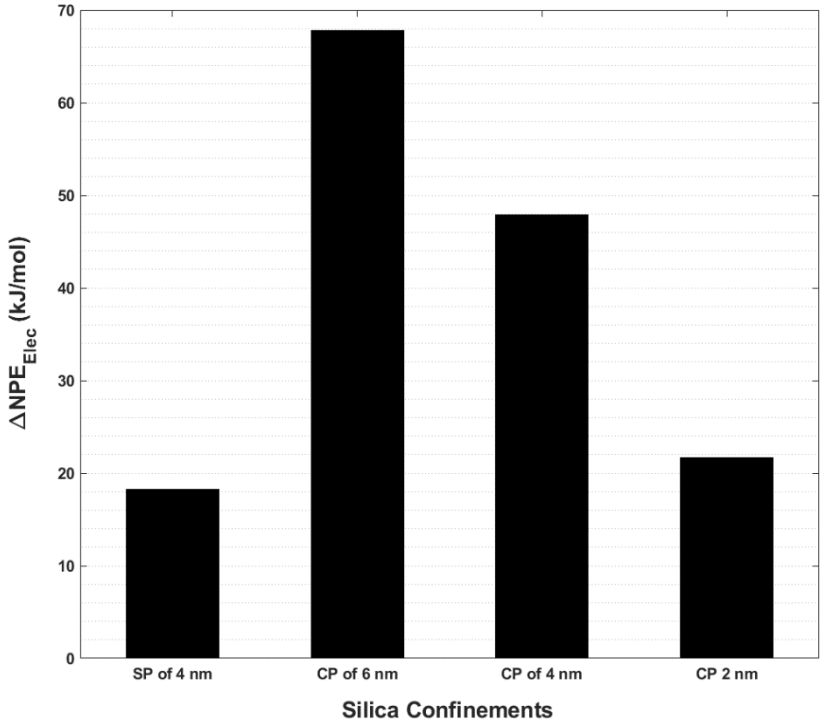

Figure 4.7: Computed values of change in potential energy (ΔNPE_{Elec}) of Heptane without and with of charges on silica atoms (without – with charges).

We see that the ΔNPE_{Elec} of substrate-surface interactions due to the inclusion of charges on the silica atoms increases significantly with the change in the dimension (Slit pore to cylindrical pores), suggesting that the heptane-surface interactions are much stronger function with the

increase in the surface area to volume ratio. But within the cylindrical pores, we see that the ΔNPE_{Elec} is getting lower with the decrease in the size of the confinement, suggesting that the interactions are getting weaker with the reduction in the size.

The heptane-surface interactions are getting weaker with the reduction in the size of the cylindrical pore due to lesser space available for the mobility or the systematic reorganization of large molecules like heptane inside the nanopores. This could lead to a perturbation in the alignment (restrictions in the molecular orientation) of heptane molecules around the silica surface in the case of 2 nm cylindrical pore, which was also reported previously in the literature.[142–144] In addition, the drop in the ΔNPE_{Elec} with the reduction of cylindrical pore sizes from 6 to 2 nm was much higher in comparison to the change in ΔPE_{Elec}. This suggests that the formation of heptane-surface interactions with the inclusion of charges on silica atoms has consequently lead to reduction in the heptane-heptane electrostatic interactions giving rise to a further drop in the ΔNPE_{Elec} values.

Looking at the data collectively, the negligible change in the intrapore diffusivities of heptane molecules with the reduction of size of the confinements could be attributed to the change in the entropy and intermolecular interactions of confined heptane. The increase in the loss of entropy of heptane molecules with the reduction in the size of the nanostructure leads to a reduction in the diffusivities. However, this reduction in the diffusivities is countered by the weakening of intermolecular interactions of heptane molecules (causing an enhancement in the diffusivities). A combined effect of the entropy loss and subsequent change in the intermolecular interactions of heptane molecules lead to constant diffusivities of heptane molecules inside all the nanoconfinements.

In addition to the calculations of thermodynamic properties of the confined heptane molecules, we calculated the density profiles of the heptane molecules across the silica confinements to study the radial density and effective pore volumes available for the movement of the substrate molecules. This result helps in understanding the change in the density profile of heptane molecules across the nanoconfinement and could provide an additional insight into the change in the diffusivities of nanoconfined heptane.

4.3.1.3 Density Profile and Effective Pore Volume

In this subsection, we studied the local densities of the heptane molecules across the silica nanostructures by calculating the percentage of molecules residing in the first shell next to the silica surface. Figure 4.8 shows the snapshots of the MD simulations of the two systems mentioned above.

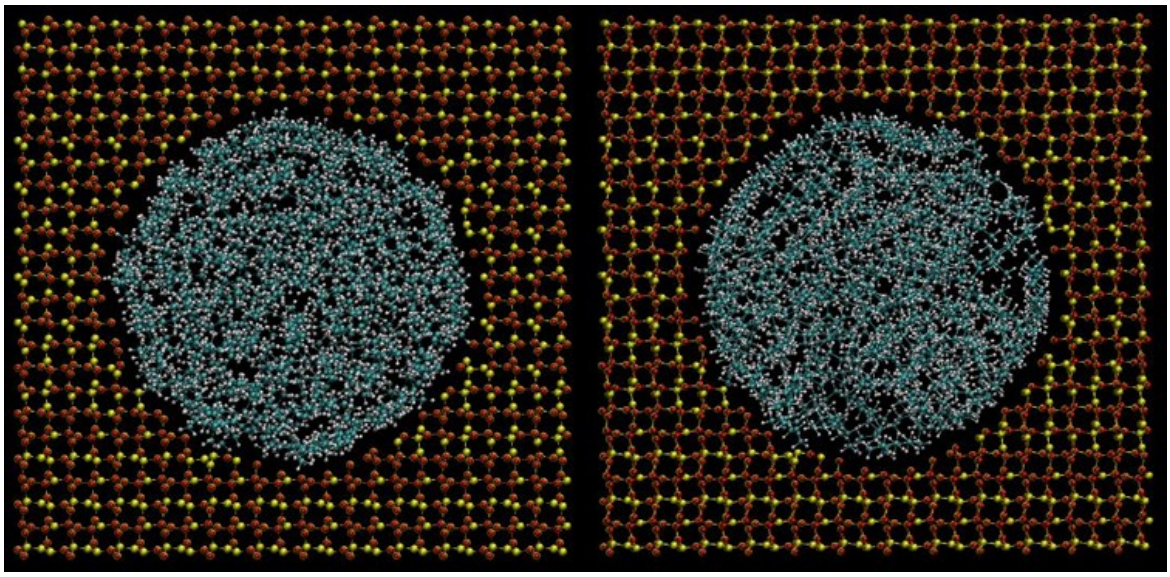

Figure 4.8: MD trajectory snapshots of the nanoconfined heptane molecules inside the cylindrical silica nanopore of 4 nm with (right) and without (left) charges assigned on the silica atoms.

The systems with zero charges on silica molecules are hypothetical, however, it was used for the qualitative comparison of the substrate-surface distance between the substrate molecules. Looking at the effective pore volumes, the available volume for the molecules remains roughly constant with the inclusion of charges on the silica atoms, suggesting minimal effect of the charges on the silica atoms.

Table 4.1 shows the computed values of percentage of molecules of heptane present in the first solvation shell (obtained using the RDF between the oxygen of the silica and central carbon atom of the heptane molecule) around the surface of the silica catalyst. We observed that the percentage of heptane molecules in the first shell is fairly low (<10%) in contrast to remainder of the molecules inside the confined space (refer to Table 4.1). This result suggests higher local density near the center as opposed to near the surface. The local density values (percentage) increase with the

increase in dimension of the confinement (from slit pore of 4 nm to cylindrical pore of 4 nm). And within the cylindrical pores, the value increases with the reduction in the size of the porous structure.

Table 4.1: Percentage of heptane molecules present near the silica surface as compared to the total number of substrate molecules confined inside the nanostructure.

Confinement	***Percentage of molecules in the first shell near the silica surface***
Slit pore 4 nm	4.7%
Cylindrical pore 6 nm	4.2%
Cylindrical pore 4 nm	7.0%
Cylindrical pore 2 nm	10.8%

Based on these results, it is clear that the density profiles of heptane near the silica surface for all the confinements remain almost constant, which could lead to negligible change in the intrapore diffusivities, as observed in Figure 4.2. Although, these results did not provide sufficient information on the alteration in the diffusivities of heptane molecules, it could be used as a reference for further analysis on the change in the local densities and effective pore volumes of the other substrate molecules (Acetone, glycerol and water) across the confinement.

4.3.1.4 Summary for Heptane

Confinement effects on the intrapore dynamics of Heptane was studied using a combination of MD and GCMC simulations. The above results obtained for heptane are summarized in this subsection to provide an overview on the change in intrapore dynamics of heptane molecules inside a silica catalyst. Intrapore densities remain constant with the change in both the size and dimension of the silica nanostructure, except for 2 nm cylindrical pore where we observed a much lower density. From diffusivity calculations, we observed negligible impact of confinement on the PFG interaction parameters. Nanoconfined heptane molecules had lower entropy values in comparison to the bulk. Specifically, 2 nm cylindrical pore showed a dramatic loss in the entropy in comparison to other confinements. This is due to the molecular size of heptane, restricting

molecular reorientation of heptane molecules near the silica surface. This result is in line with the published result on the perturbation of the molecular alignment of long chain alkanes inside small nanopores.[142–144] Significant change in the entropy for 2 nm cylindrical pore is not reflected in the change in the PE of the nanoconfined heptane molecules with respect to the bulk. This is attributed to the alteration in the intermolecular interactions of the heptane molecules inside the nanostructures. Heptane-heptane interactions are weak in general due to the absence of functional groups. Lower magnitude of ΔPE_{Elec} (accounts for electrostatic interactions) in comparison to ΔPE suggests that the vdW interactions are more dominant in comparison to the electrostatic interactions. This was also observed in the case of long chain alkanes confined inside graphite nanopores.[142,143,145] Based on ΔNPE_{Elec} calculations, as we go from slit pore to cylindrical pores, the strength of heptane-surface interactions increases due to better surface area to volume ratios. But with the reduction in size of the cylindrical pores, heptane-surface interactions become weaker, suggesting a slight enhancement in the diffusivity. Due to weakening of heptane-surface interactions with reduction in the size, and minimal alterations in the vdW forces, ΔPE change remains almost constant across cylindrical pores. Heptane showed constant effective pore volume with the inclusion of charges on the surface silica atoms, and marginally higher local density near the centre of confinements. In conclusion, a combination of entropy loss (leading to reduced diffusivities) and subsequent weakening of the intermolecular interactions of heptane molecules (slight enhancement in diffusivities) lead to negligible change in the diffusivities of heptane molecules with change in the size and geometry of nanoconfinements. Effect of confinement on the heptane dynamics was minimal, which makes it ideal for benchmarking other substrates.

4.3.2 Acetone

Acetone is a polar molecule and has the ability to interact well with the silica surface. We have considered acetone molecules for this study due to the presence of carbonyl groups, which reflects the effect of physical interactions of guest molecules within the porous media, besides the effect due to physical structure of the pore space. Another reason backing the consideration would be the availability of experimental results for the dynamics of nanoconfined acetone inside metal oxide catalysts.[29] As reported figure 4.2, acetone showed a systematic increase in the PFG interaction parameters (reduction in the diffusivities) with the change in the geometry from slit-pore to cylindrical pore, and also with the reduction in the size of cylindrical confinement from 6 to 2 nm.

Although it is a polar molecule like glycerol, it followed a different trend in the diffusivities (reduction) in comparison to glycerol (enhancement) inside all the nano-confinements. To explain the trend of diffusivities for acetone, we have provided results on the change in thermodynamic properties (potential energy and entropy) and analyzed the density profiles in the following sections.

4.3.2.1 Potential Energy and Entropy Calculations

In this subsection, we calculated the change in entropy and potential energy as the acetone molecules go from bulk liquid to inside any confinement using the methodology given in Section 3.2.4.2. The computed values of the change in the entropy (ΔS) for acetone molecules inside the four nanostructures is reported in Figure 4.9.

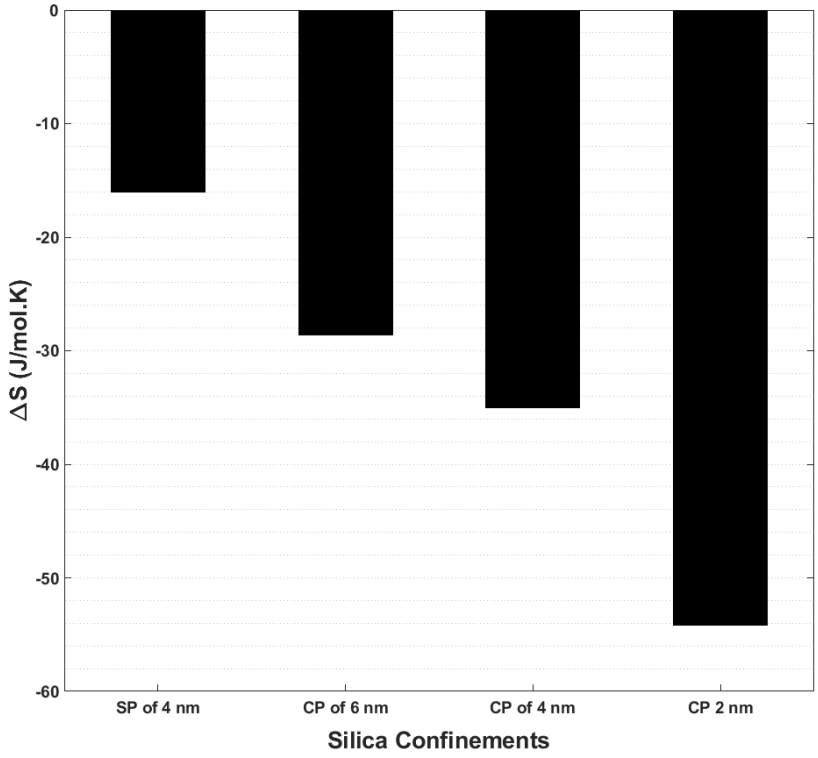

Figure 4.9: Computed values of change in entropy (ΔS) of acetone between the bulk substrate and confined substrates (Confinement – Bulk) inside various silica nanostructures (CP is cylindrical pore and SP is slit pore).

For these molecules, entropy is lost inside the confinement irrespective of the size or dimension. The computed loss in entropy increases as we go from slit pore of 1D to cylindrical pore of 2D. We see a further drop with the decrease in size of the pore, with a significantly higher loss in entropy with the reduction in the size from 4 to 2 nm. This trend in the entropy change is similar to the results obtained for heptane molecules in Section 4.3.1.1, and it could be due to change in the molecular orientations of acetone molecules inside the nanopores. A possible explanation for the entropy loss of acetone molecules in 2 nm cylindrical pore could be a result of severe restrictions imposed by the porous structure on the reorientation of the acetone molecules. As mentioned in Section 4.2, acetone shows an increase in the PFG interactions with reduction in size of the confinement of the cylindrical pores, which suggests a reduction in the translational motion. For instance, Dhiman and coworkers published results on the role of molecular shape of confined acetone, acetaldehyde, acetonitrile and propane molecules (inside ZSM-5 catalyst) on the alteration of the intrapore translational and rotational dynamics. They reported that the narrow channels of ZSM-5 put a severe restriction on the rotational motion of all the guest molecules that results in restricted motion within the nanopore.[146] Similarly, Brodka and Zerda carried out molecular dynamics studies on acetone, under relatively relaxed confinement in variable diameter (1.5 nm to 3.0 nm) cylindrical pores of silica. They observed that both rotational and translation motion of the confined acetone molecules is observed to be hindered.[110,147]

In order to overcome the loss in entropy, the molecules attempt to reorganize inside the nano-confinement, which could cause a corresponding loss in the potential energy per molecule of acetone with respect to the bulk liquid. The alteration in the molecular orientations can be caused by a change in the intermolecular interactions (van der Waals and Columbic interactions) of the confined acetone molecules, leading to a change in the potential energy. To validate this hypothesis, we calculate the change in potential energy (ΔPE) reported in Figure 4.10. In this figure, a positive value of ΔPE suggests less favourable intermolecular interactions of the substrate molecules inside the pore compared to the bulk liquid (refer equation 3.3).

The computed values of ΔPE for acetone does not vary with respect to the change in the dimension of the confinement (Slit to cylindrical pores). Within the 2D pores of varying size, the ΔPE increases gradually with the reduction in the pore size from 6 to 2 nm, which could be a result of

change in acetone-surface and acetone-acetone interactions with the change in confinement size. Referring to Figure 4.9, we observe a drastic drop in the entropy change, which is not reflected in the ΔPE values, suggesting a change in the intermolecular interactions. In comparison to heptane, we do not observe a significant increase in the ΔPE as we go from slit pore of 4 nm to cylindrical pore of 6 nm. This could be due to much favourable interactions (negative PE) of acetone and silica surface in comparison to the heptane molecules, lowering the overall ΔPE for the acetone molecules inside the confinements. This reduction in ΔPE due to favourable surface-substrate interactions are more dominant in the case of cylindrical pores than the slit pore due to better surface area to volume ratio available for the interacting acetone molecules.

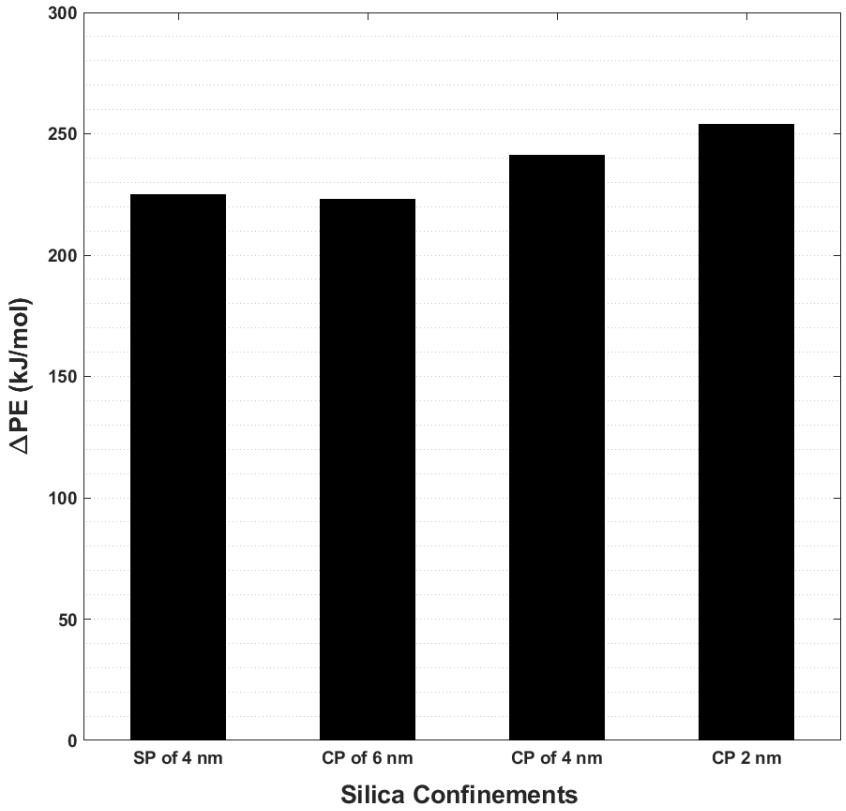

Figure 4.10: Computed values of change in potential energy (ΔPE) of between the bulk substrate and confined substrates (Confinement – Bulk) inside various silica nanostructures (CP is cylindrical pore and SP is slit pore).

Acetone can exhibit intermolecular interactions like van der Waals (vdW) and dipole-dipole. It was reported that the vdW interactions between molecules and silica are weak. Dipole–dipole

interactions between acetone molecules additionally restrict their motion, and when these forces are removed, one observes an increase of the diffusion coefficient for the surface molecules.[110] To validate this result, we analyzed the acetone-acetone and acetone-silica interactions in this following subsection to provide a conclusion on the PE change observed above.

4.3.2.2 Intermolecular interactions between Acetone-acetone and Acetone-silica molecules

Intermolecular interactions of the substrate molecules with themselves and with the silica surface would affect the dynamics of the nanoconfined substrates. Applying the methodology given in section 3.2.4.3, we reported the change in potential energy (ΔPE_{Elec}), as the electrostatics of the silica atoms are switched on (vdW and Electrostatic interactions) and off (only vdW interactions). Introduction of electrostatics on the silica atoms leads to alteration to the intermolecular interactions between acetone and silica atoms, due to the ability of acetone molecules to interact weakly with the surface atoms. By doing so, we have negated the effects due physical structure of the pore wall and van der Waals forces between acetone-acetone and acetone-silica atoms by a great margin; and the change in the PE observed here is purely for the electrostatic interactions between the acetone-silica molecules.

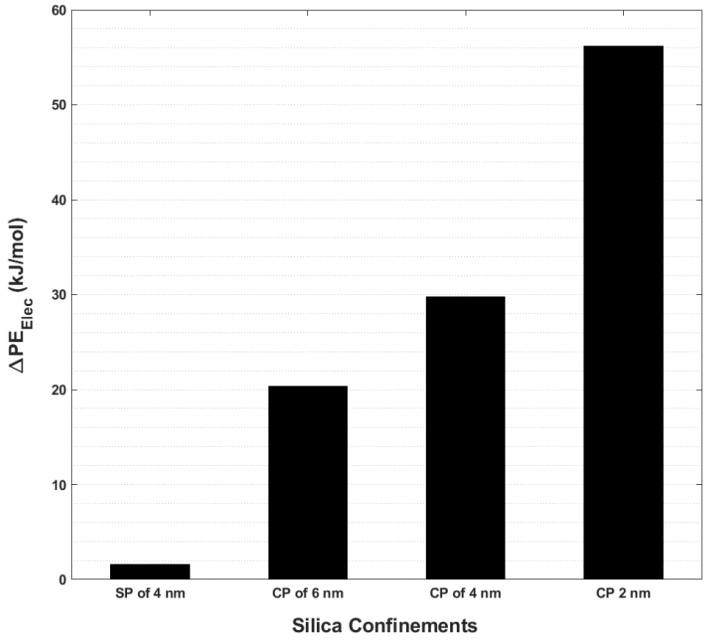

Figure 4.11: Computed values of change in potential energy (ΔPE_{Elec}) of Acetone with the introduction of charges on silica atoms. (PE change: without – with charges assigned on the silica atoms).

Figure 4.11 shows the computed values of ΔPE_{Elec} for acetone molecules inside four different silica nanostructures. In this figure, a positive value of ΔPE_{Elec} represents favourable interactions (refer equation 3.9). From this plot, we observed that the ΔPE_{Elec} increases drastically with the change in the dimension of the confinement (slit to cylindrical pore). This increase is a result of better surface area to volume ratio available for the molecules interacting with the silica surface. Within cylindrical pores of different sizes, the computed ΔPE_{Elec} increases with the reduction in the size of the confinement from 6 to 4 nm, and increases significantly with further decrease in the size to 2 nm. The change in PE was witnessed to be a function of the surface area to volume ratio. The trend in ΔPE_{Elec} is much different in comparison to heptane (refer Figure 4.6), which could be due to much stronger interactions of acetone molecules with the silica surface in comparison to heptane-silica interactions, with the increase in surface area to volume ratio of the confinement. Our results are in accordance with the simulation studies on the strength of acetone-silica interactions, where they have reported that acetone-silica interactions becomes stronger with the decrease in the size of the silica nanostructure.[110] Combining the results obtained for ΔPE_{Elec} and ΔPE, we collectively observed that the electrostatic interactions between acetone-silica molecules improves with decrease in the size of the confinement, whereas the vdW interactions was observed to get weaker between acetone and silica. This was also reported in literature that the vdW interactions between acetone-silica atoms are relatively weaker than the electrostatic attraction between the same molecules.[110,148]

To further understand this, we will normalize this potential energy with respect to the surface area to volume ratio, as suggested previously in Section 3.2.4.2. Upon normalizing the ΔPE_{Elec} with respect to the factor F (refer Section 3.2.4.2), the substrate-surface interactions per number of molecules interacting with the surface yields information about the varying strength of interaction across different nanostructures, as after normalization the acetone molecules are exposed to equal surface area of the pore wall.

Figure 4.12 shows the computed values of normalized PE change (ΔNPE_{Elec}) for acetone-silica interactions inside different silica confinements. We see that the ΔNPE_{Elec} of substrate-surface interactions due to the inclusion of charges on the silica atoms increases significantly with the change in the (Slit pore to cylindrical pores), suggesting that the acetone-surface interactions are

much stronger with the increase in the surface area to volume ratio. But within the pores, we see that the ΔNPE_{Elec} is getting lower with the decrease in the size of the confinement, suggesting that the interactions are getting marginally weaker with the reduction in the size. This could be due to due to lesser space available for the systematic reorganization of acetone molecules inside smaller confinements. Additionally, dipole-dipole interactions between acetone-acetone molecules remained unaffected by the effect of confinement.[110]

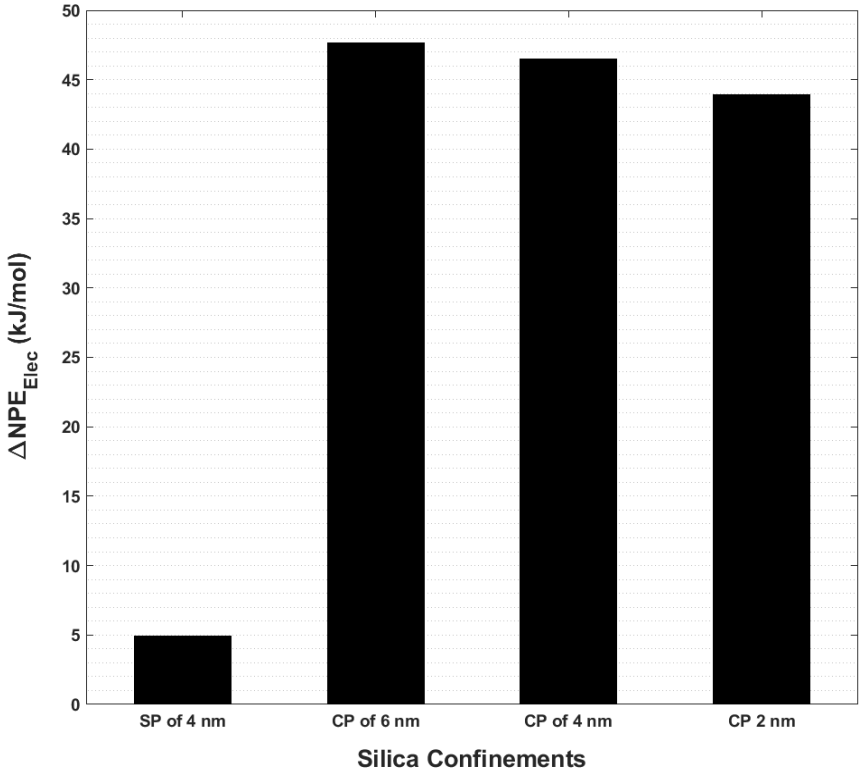

Figure 4.12: Computed values of change in potential energy (ΔNPE_{Elec}) of Acetone with the introduction of charges on silica atoms (Difference between the potential energy per molecule of acetone without charges and with charges).

The reported trends for ΔNPE_{Elec} and ΔPE_{Elec} for the cylindrical pores of 6,4 and 2 nm is not similar to heptane molecules. In the case of heptane, the intermolecular interactions became weaker with the reduction in the size of the confinement. Whereas, for acetone we observed that the intermolecular interactions between the acetone and silica molecules are getting stronger with the reduction of the size of the confinement. In addition, the acetone-acetone interactions remain unaltered inside the nanoconfinements.[110]

Looking at the results collectively for acetone, the reduction in intrapore diffusivities of acetone molecules with the reduction of size of the confinements could be attributed to the change in the entropy and intermolecular interactions of confined acetone. The increase in the loss in entropy of acetone molecules with the reduction in the size of the nanostructure lead to a reduction in the diffusivities. Additionally, reduction in the diffusivity of the acetone molecules could be attributed to strong acetone-silica interactions, unaltered acetone-acetone interactions and change in the pore volumes available for the molecular reorientation. To study further about local densities and pore volumes for acetone molecules inside the nanostructures, we calculated the radial density profiles and effective pore volumes available for the movement of the substrate molecules.

4.3.2.3 Density Profile and Effective Pore Volume

In this subsection, we study the local densities of the acetone molecules across the silica nanostructures by calculating the percentage of molecules residing in the first shell near the silica surface. We also look into the MD trajectory snapshots when the electrostatics on the silica atoms are switched on and off, to analyze the effective pore volumes available for the substrate molecules. The systems with zero charges on silica molecules is hypothetical, however it was used for the qualitative comparison of the substrate-surface distance between the substrate molecules. Figure 4.13 shows the snapshots of the MD simulations of the two systems mentioned above.

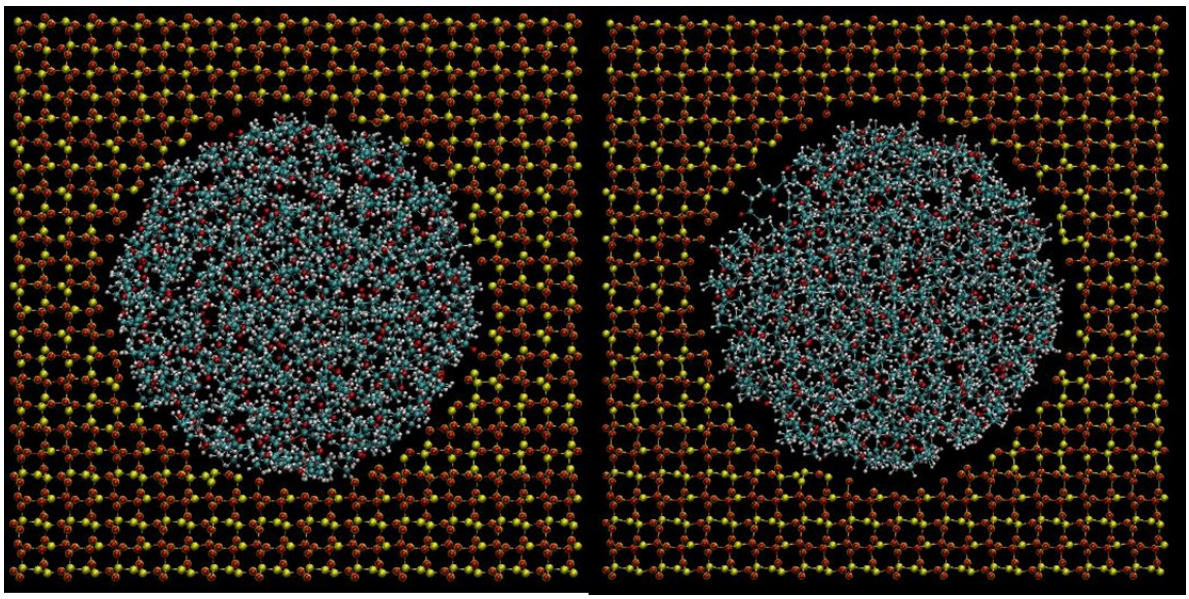

Figure 4.13: MD trajectory snapshots of the nanoconfined acetone molecules inside the silica nanopore of 4 nm with (right) and without (left) charges assigned on the silica atoms.

Looking at the effective pore volumes, the available volume for the mobility of acetone molecules reduces with the inclusion of charges on the silica atoms. In contrast, the heptane molecules didn't move closer to the silica surface when the charges were switched on. This observation shows that in the case of acetone, the molecules are much farther away (refer figure 4.13 with charges on silica) from the silica surface, suggesting a lower effective pore volume available for acetone molecules in comparison to heptane (refer figure 4.8). Furthermore, we observed that the local density of acetone molecules is higher near the centre of the confinement as opposed to near the confinement wall, for all the four confinements. This result was confirmed with the simulation studies, where they have reported higher local densities of acetone molecules near the surface in comparison to the centre of the pore.[110] To further validate this, we analyze the number density profile of the acetone molecules across the nanostructures. Table 4.2 shows the computed values of percentage of molecules of acetone present in the first solvation shell around the surface of the silica catalyst.

Table 4.2: Percentage of acetone molecules present near the silica surface as compared to the total number of substrate molecules confined inside the nanostructure.

Confinement	***Percentage of molecules in the first shell around the silica surface***
Slit pore 4 nm	10.64%
Cylindrical pore 6 nm	11.18%
Cylindrical pore 4 nm	13.72%
Cylindrical pore 2 nm	19.48%

We observed that the percentage of acetone molecules in the first shell is fairly low (<20%) in contrast to remainder of the molecules inside the confined space. The local density values (percentage) increase gradually with the increase in dimension (from slit pore of 4 nm to cylindrical pore of 4 nm) as well as with reduction in the confinement size. This result is in accordance with the previous claim of higher local density near the centre as opposed to near the surface, causing increased in the intermolecular interactions near the centre of the pore.[110] Based on these results, it can be stated that the increase in the local densities of acetone molecules near

the centre and lower effective volumes available for the mobility of molecules leads to a decrease in the intrapore diffusivities of the acetone molecules.

4.3.2.4 Summary for Acetone

Confinement effects on the intrapore dynamics of Acetone was studied using a combination of MD and GCMC simulations. The above results obtained for acetone are summarized in this subsection to provide an overview on the alteration of its dynamics inside a silica catalyst. The intrapore densities remain constant with the change in both the size and dimension of the silica nanostructure, except for 2 nm pore where we observed a much lower density. From the diffusivity calculations, we observed that the PFG interaction parameters varied with respect to both dimension and size of the confinement. Nanoconfined acetone molecules had lower entropy values in comparison to the bulk. The entropy loss was found to be a function of dimension and size. Specifically, 2 nm cylindrical pore showed a dramatic loss in the entropy in comparison to other confinements. This is due to the molecular size of acetone, restricting molecular reorientation of the acetone molecules around the silica surface. This result is in line with the published result on the perturbation of the molecular alignment of acetone inside small nanopores.[110,147] From the ΔPE_{Elec} and ΔPE calculations, the electrostatic interactions between acetone-silica molecules improves with decrease in the size of the confinement, whereas the vdW interactions were observed to get weaker between acetone and silica. This was also reported in literature that the vdW interactions between acetone-silica atoms are relatively weaker than the electrostatic attraction between these molecules.[110,148] Based on the ΔNPE_{Elec} calculations, as we go from slit pore to cylindrical pores, the strength of acetone-surface interactions increases due to better surface area to volume ratios. But within the pores, with the reduction in size of the confinement, the acetone-surface interactions remains almost constant. In addition, acetone showed lower effective pore volume with the inclusion of charges on the surface silica atoms, and increased local density near the centre of the confinements. In conclusion, the reduction in the diffusivities of acetone with the change in the geometry from slit to cylindrical pore and with the reduction in the size of the confinement is a combined effect of (a) entropy loss of inside the confinements (b) increase in the acetone-acetone interactions and (c) higher densities near the centre of the confinement and lower effective pore volumes available for the molecular mobility.

4.3.3 Water

Water has been widely used as a solvent in the condensed phase biomass conversion reactions in the presence of nanoporous catalysts, therefore understanding the confinement effects of nanoporous catalysts on the structure and dynamics of water is essential.[31,37] In addition, We are considering water in this study due to availability of extensive data on intrapore dynamics of water inside a silica catalyst, which allows us to benchmark our simulation methods throughout the process. It was reported in literature that water has exceptional ability to interact with the silica surface due to the presence of two hydrogens capable of forming hydrogen bonds with the silica oxygen. As mentioned earlier, the PFG interaction parameters for water were observed to remain constant and almost equal to bulk for slit pore of 4 nm and cylindrical pores of 4 and 6 nm. However, in the case of 2 nm cylindrical nanopore, we observed a drastic increase in the PFG interaction parameters, suggesting a drop in the diffusivities in comparison to the bulk (refer to figure 4.2). To explain the trend of diffusivities for water, we have provided results on the change in thermodynamic properties like potential energy and entropy, and analyzed the density profiles and intermolecular interactions in the following sections.

4.3.3.1 Potential Energy and Entropy

In this subsection, we present the change in entropy and potential energy as the water molecules go from bulk liquid to inside any confinement using the methodology given in Section 3.2.4.2. The computed values of the change in the entropy (ΔS) for water molecules inside the four nanostructures is reported in Figure 4.14. For these molecules, entropy is lost inside the confinement irrespective of the size or dimension. The computed change in entropy increases as we go from slit pore of 1D to cylindrical pores of 2D. We see negligible change in the ΔS within pores of 6 and 4 nm. This unique result for water in comparison to heptane and acetone, where we observed an increase in the entropy change (loss) with a reduction in the size from 6 to 4 nm. This could be due to the difference in the molecular sizes of water in comparison to bigger molecules like acetone and heptane in comparison to the size of the pore. On the contrary, a significantly higher loss in entropy was observed with the reduction in the size from 4 to 2 nm. This result for the 2 nm cylindrical pore in the entropy change is similar to the results obtained for heptane and acetone as reported in Section 4.3.1.1 and 4.3.2.1 respectively, and it could be due to change in the

molecular orientations of water, acetone and heptane molecules inside a critical cylindrical pore size of 2 nm (in comparison to size of the molecule).

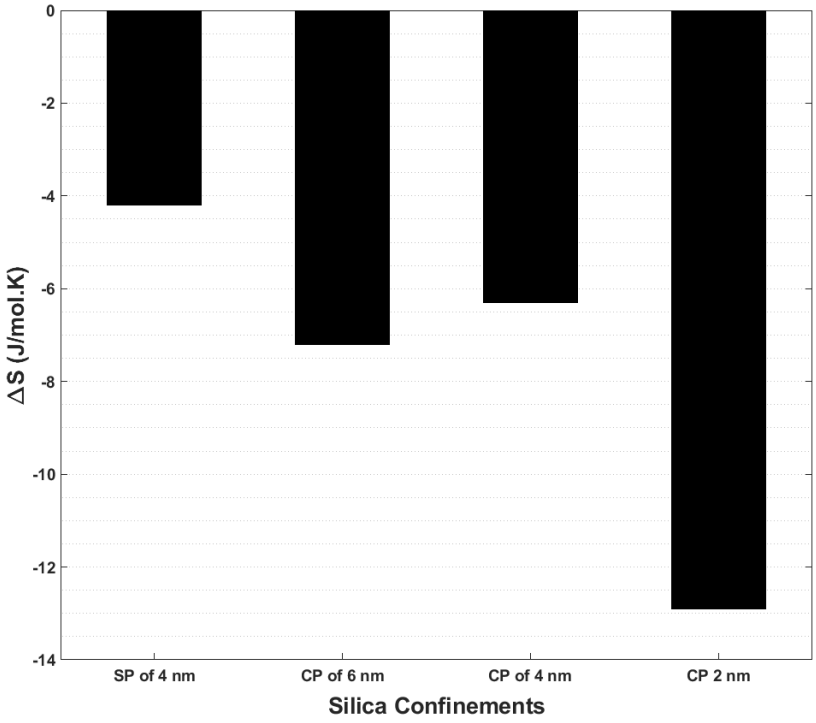

Figure 4.14: Computed values of change in entropy (ΔS) of water between the bulk substrate and confined substrates (Confinement – bulk) inside various silica nanostructures (CP is cylindrical pore and SP is slit pore).

Although, water is a relatively small molecule, it was reported that the rotational and translational mobilities of water molecules inside nanoporous catalysts were affected by the reduction of the pore size. For example, in a study conducted on confinement effects on water molecules in a layered saponite structure (with interlayer spacing of 0.8 nm and 1.4 nm, slit-pore), it was found that rotational motion remained largely unaffected, while the translational motion was significantly influenced.[149] On the other hand, an MD study conducted on water molecules in TiO_2 pores (of sizes 1.3 nm, 2.8 nm, and 5.1 nm) showed two varying regimes of rotational motion.[150] Farimani et al.[151] found that if the pore space is small enough, confinement effects altered rotational motion as well. They showed that while water in bulk phase exhibits stochastic rotational motion, a single water molecule sheathed in a buckyball (C60) displays harmonic motion. Milischuk and coworkers suggested that with the decrease in the size of the confinement, due to better surface

area to volume ratio and exceptional ability of water molecules to interact with the silica surface, the water molecules tend to form very strong H-bonding pattern inside the confinement leading to a reduced diffusivity inside small nanopores (2 nm cylindrical pore).[39] Based on these results, we could attribute the reduction in entropy of water molecules to arise from exceptional H-bonding structure of water inside the catalyst, and strong water-silica interactions.

As mentioned earlier, to overcome the loss in entropy, the molecules attempt to reorganize inside the nano-confinement, which could cause a corresponding loss in the potential energy per molecule of water with respect to the bulk liquid. The alteration in the molecular orientations can be caused by a change in the intermolecular interactions of the confined water molecules, leading to a change in the potential energy. To validate this hypothesis, we calculate the change in potential energy (ΔPE) reported in Figure 4.15.

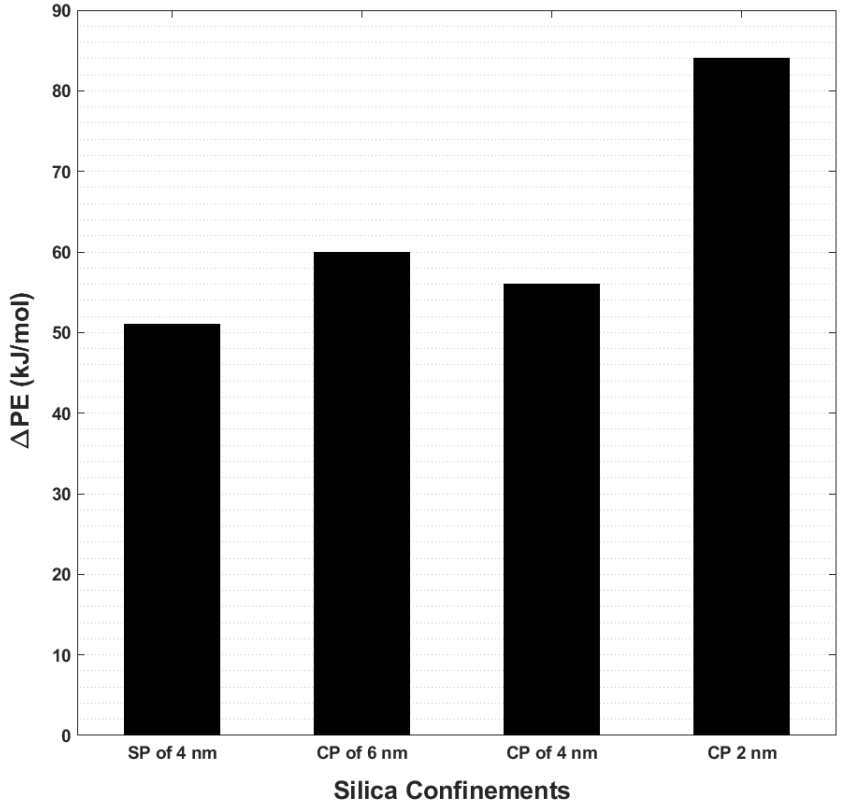

Figure 4.15: Computed values of change in potential energy (ΔPE) of water between the bulk substrate and confined substrates (Confinement – bulk) inside various silica nanostructures (CP is cylindrical pore and SP is slit pore).

In this figure, a positive value of ΔPE suggests less favourable intermolecular interactions of the substrate molecules inside the pore compared to the bulk liquid (refer to equation 3.3). The computed values of ΔPE for water does not vary significantly with the increase in the dimension of the confinement (slit to cylindrical pore). Within the 2D pores of varying size, the ΔPE remains similar for the 6 and 4 nm pores. But with the further reduction in the size of confinement to 2 nm, we see a huge spike in the values of the ΔPE with the reduction in the pore size from 4 to 2 nm. This is attributed to change in the water-water and water-silica interactions, although the extent of impact on the PE is still unclear. For the slit-pore of 4 nm and cylindrical pores of 6 and 4 nm, the potential energy remains almost constant suggesting that the formation of water-silica H-bonds would lead to a decrease in the water-water interactions, thereby maintaining the PE change to be constant inside nanopores of different sizes. For these confinements, the water behaves bulk-like due to relatively smaller molecular size in comparison to the pore size.[119] In comparison to heptane and acetone, we observed a unique result of spike in the ΔPE between cylindrical pore of 4 and 2 nm for water molecules. This could be a result of weakening of water-water interactions inside the 2 nm pore. Recent publications on the intrapore dynamics of water in nanopores have reported that water forms much stronger interactions with silica, leading to a breakage of less favourable water-water hydrogen bonds.[119,120,152] To validate this result, we analyzed the water-surface and water-water interactions in detail in the following subsection.

4.3.3.2 Intermolecular interactions between water-water and water-silica molecules

Intermolecular interactions of the substrate molecules with themselves and with the silica surface would affect the dynamics of the nanoconfined substrates. Applying the methodology reported in section 3.2.4.3, we calculate the change in potential energy (ΔPE_{Elec}) of the water molecules, as the electrostatics of the silica atoms are switched on (vdW and Electrostatic interactions) and off (only vdW interactions). Introduction of electrostatics on the silica atoms leads to alteration to the intermolecular interactions between water-surface and water-water molecules, due to the ability of water molecule to interact strongly with the surface atoms. By doing so, we have eliminated the effects due physical structure of the pore wall and van der Waals forces between water-surface and water-water atoms to a great extent; and the change in the PE observed here is purely for the electrostatic interactions between these molecules.

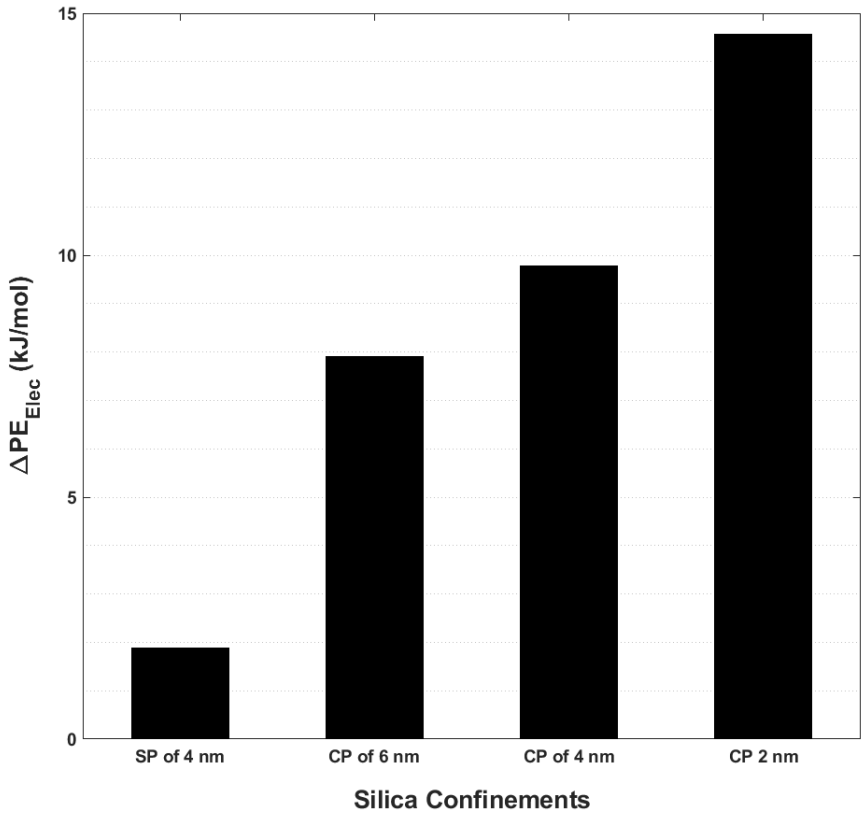

Figure 4.16: Computed values of change in potential energy (ΔPE_{Elec}) of water with the introduction of charges on silica atoms. (Without – with charges on silica atoms)

Figure 4.16 shows the computed values of ΔPE_{Elec} for water. Here, a positive value of ΔPE_{Elec} represents favourable interactions (refer equation 3.9). In this plot, we observed that the ΔPE_{Elec} increases drastically with the change in the dimension of the confinement (slit to cylindrical pore). This increase is a result of better surface area to volume ratio available for the molecules interacting with the silica surface. Within pores of different sizes, the computed ΔPE_{Elec} increases with the reduction in the size of the confinement from 6 to 4 nm, and increases significantly with further decrease in the size to 2 nm. The change in PE was witnessed to be a function of the surface area to volume ratio. Water forms very favourable H-bonds with the silica surface, however this leads to the change in the water-water H-bond network.[119,120,152] Although, the extent of impact is not yet conclusive as this PE corresponds to both substrate-surface and substrate-substrate interactions. This result is in accordance with published simulations, where they have reported that the strength of water-silica H-bonds get stronger with

the reduction in the size of the confinement.[85,104,119,131] Water has an exceptional ability to form water-water hydrogen bonds. But, with the inclusion of charges on the silica atoms, the water tends to form much stronger interactions with the silica surface. This would lead to a change in the water-water hydrogen bonds, affecting the overall potential energy change.

The trend of the ΔPE_{Elec} for water is similar to acetone for the slit pore of 4 nm and cylindrical pores of 4 and 6 nm, where we observed an increase in the ΔPE_{Elec} with the change in the geometry from slit to cylindrical pore, and also with the reduction in the size of the cylindrical pores. This is attributed to stronger surface-substrate interactions (strong hydrogen bonds) for water with an increase in the surface area to volume ratio in comparison to Acetone-silica interactions. However, the spike in the ΔPE_{Elec} for water from 4 to 2 nm cylindrical pore is comparatively lower than acetone. This could be a result of breakage of strong water-water hydrogen bonds occurring due to the formation of more favourable water-silica hydrogen bonds. To further understand this, we will normalize this potential energy with respect to the surface area to volume ratio, as suggested previously in Section 3.2.4.2. Upon normalizing the ΔPE_{Elec} with respect to the factor F (refer Section 3.2.4.2), the substrate-surface interactions per number of molecules interacting with the surface yields information about the strength of interactions and the change in the substrate-substrate interactions.

Figure 4.17 shows the computed values of normalized PE change (ΔNPE_{Elec}) for water molecules inside different silica confinements. We see that the ΔNPE_{Elec} of substrate-surface interactions due to the inclusion of charges on the silica atoms increases significantly with the change in the dimension (slit to cylindrical pores), suggesting that the intermolecular interactions are altered much drastically in the case of cylindrical pores as compared to the slit pore (due to better surface area to volume ratio). But within the cylindrical pores, we see that the ΔNPE_{Elec} is getting lower with the decrease in the size of the confinement, suggesting that the interactions are getting marginally weaker with the reduction in the size, specifically for the case of 2 nm pore.

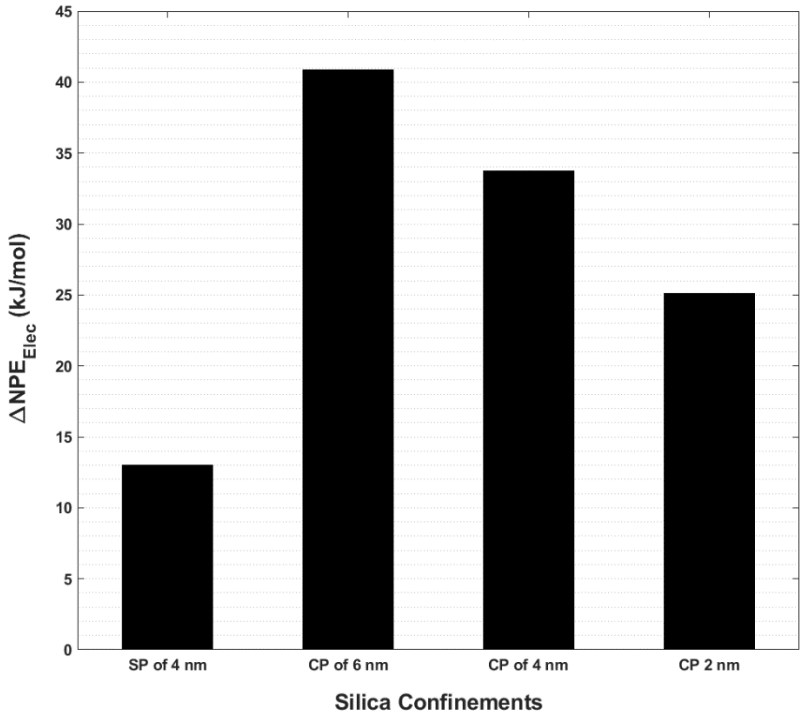

Figure 4.17: Computed values of change in potential energy (ΔNPE_{Elec}) of water with the introduction of charges on silica atoms. (Without – with charges on silica atoms)

The spike in the ΔNPE_{Elec} for water molecules as we go from a slit-pore of 4 nm to cylindrical pores is very similar to heptane and acetone, which was observed to be a result of stronger interactions of water molecules with the surface. For the cylindrical pores of 2,4 and 6 nm, water follows similar trend as acetone (refer Figure 4.12). This suggests that the water-water interactions gets weaker with the decrease in the size of the confinement from 4 to 2 nm, although the change is not significant. This is attributed to the breakage of H-bonds between the substrate molecules due to the formation of stronger water-silica interactions. To study the effect of confinement on the distribution of water molecules inside the nanostructures, we calculated the density profiles of the water molecules across the silica confinements to study the radial density and effective pore volumes available for the movement of the substrate molecules.

Looking at the results collectively for water, the negligible change in the intrapore diffusivities of water inside slit pore of 4 nm and cylindrical pores of 6 and 4 nm could be a result of formation of

water-silica H-bonds and subsequent reduction in the water-water interactions. It was reported that the total number of hydrogen bonds for water (water-water and water-silica) remained constant and equal to bulk inside a nanopore of 4 nm.[121] In addition, the diffusivity of water inside the confinement of 4 nm was equal to the bulk liquid. However, the reduction in intrapore diffusivities of water molecules with the reduction of size of the confinements from 4 to 2 nm could be attributed to the change in the entropy and intermolecular interactions of confined water. The increase in the loss of entropy of water molecules with the reduction in the size of the nanostructure (from 4 to 2 nm) lead to a reduction in the diffusivities. Additionally, reduction in the diffusivity of the water molecules inside smaller pores (2 nm cylindrical pore) could be attributed to strong water-silica interactions and change in the pore volumes available for the molecular reorientation. To study further about local densities and pore volumes for water molecules inside the nanostructures, we calculated the radial density profiles and effective pore volumes available for the movement of the substrate molecules.

4.3.3.3 Density Profile and Effective Pore Volume

In this subsection, we study the local densities of the water molecules across the silica nanostructures by calculating the percentage of molecules residing in the first shell near the silica surface. We also look into the MD trajectory snapshots when the electrostatics on the silica atoms are switched on and off, to analyze the effective pore volumes available for the substrate molecules. With higher effective pore volumes, the molecules tend to move faster causing an enhancement in the diffusivities.[110] Figure 4.18 shows the snapshots of the MD simulations of the two systems mentioned above. From the MD snapshots, we observed that the molecules tend to move towards the surface of the silica nanostructure when the charges on the silica atoms are assigned. This leads to an increase in the effective pore volume available for the mobility of the water molecules inside the confinements. The increase in the effective pore volumes is due to the formation of strong water-silica H-bonds.[110,119]

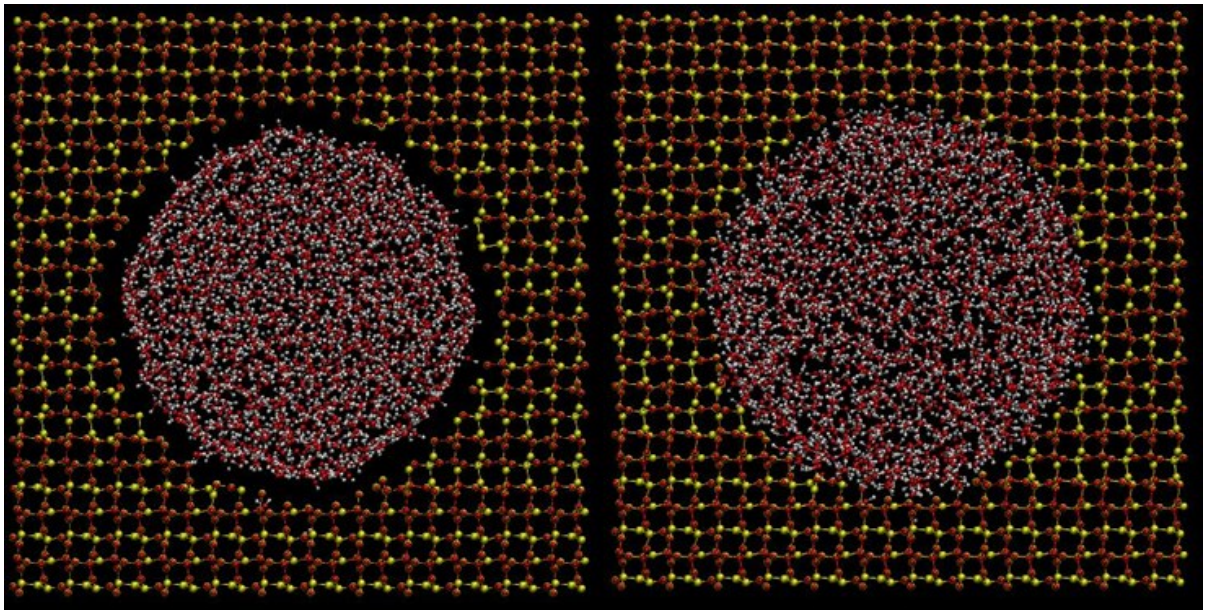

Figure 4.18: MD trajectory snapshots of the nanoconfined water molecules inside the silica nanopore of 4 nm with (right) and without (left) charges assigned on the silica atoms.

To further validate this, we analyze the number density profile of the water molecules across the nanostructure. Table 4.3 shows the computed values of percentage of molecules of water present in the first shell near the surface of the silica catalyst.

Table 4.3: Percentage of water molecules present near the silica surface as compared to the total number of substrate molecules confined inside the nanostructure.

Confinement	***Percentage of molecules in the first shell near the silica surface***
Slit pore 4 nm	12.04%
Cylindrical Pore 6 nm	13.02%
Cylindrical Pore 4 nm	24.80%
Cylindrical Pore 2 nm	38.61%

We see that the percentage of the water molecules near the surface remains the same as we go from a slit pore of 1D to 6 nm cylindrical pore of 2D. But within the pores, we see an increase in the percentage of molecules with the decrease in the size of the confinement with better surface area

to volume ratio. Especially for the case of 2 nm pore, around ~40% of the molecules was observed to reside close to the surface, suggesting much stronger interactions with the surface for 2 nm pore. In comparison to heptane and acetone (refer Table 4.1 and 4.2 respectively), water has much higher local densities near the silica surface in comparison to the centre of the confinement due to more favourable substrate-surface interactions. Due to very strong interactions with the surface and increased local density near the silica surface, we see a reduction in the diffusivity of the water molecules in the 2 nm pore. Due to formation of strong hydrogen bonds with the silica surface, the water-water hydrogen bonds could get altered leading to a change in the dynamics. The following analysis on the hydrogen bonding network provides a better perspective of the intermolecular interactions of the water molecules within itself and with the silica surface.

4.3.3.4 Hydrogen Bonding Analysis

Water has a remarkable ability to form hydrogen bonds with the surface as well as with the other water molecules. Introduction of an alien molecule to this system would lead to a change in the intermolecular interactions of water. The extent of impact of the confinement on the hydrogen bonding network of the water molecules is discussed in this subsection to provide an additional perspective to the alteration in the intrapore dynamics. Figure 4.19 presents the number of water-water and water-surface hydrogen bonds (H-bonds) per molecule of water.

In figure 4.19, the orange line depicts the water-surface H-bonds, blue line denoting the water-water H-bonds and the yellow line is the total number of hydrogen bonds in the system (substrate-substrate and substrate-surface). H-bonds between water-water molecules (blue) decreases with the increase in the confinement dimension (slit to cylindrical pores). However, it gradually increases with the reduction in the pore sizes from 6 to 2 nm. Secondly, the number of H-bonds between water and surface molecules (red) increases with only change in the dimension of the confinement (slit to cylindrical pores), but was found to be constant for pores of different sizes.

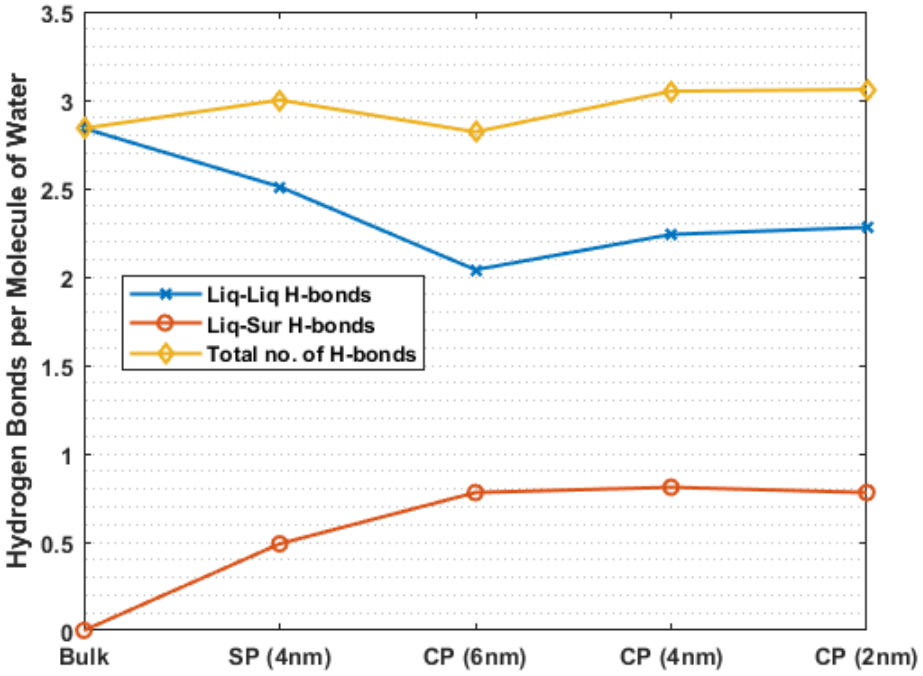

Figure 4.19: Hydrogen bonding analysis of water molecules confined inside various silica nanostructures.

An important observation here being, the total number of H-bonds inside all confinements remained nearly constant and equal to the bulk liquid. The average bond lengths of the water-surface H-bonds was observed to be shorter than the water-water H-bonds by 0.4 Å, suggesting that the surface interactions are stronger than the intermolecular water-water interactions. These results are in line with the published literature, where Milischuk and coworkers have reported a reduction in the water-water H-bonds and corresponding increase in the water-silica H-bonds; leading to a constant total number of H-bonds equal to the bulk liquid. They also reported that the water-silica H-bonds are stronger than the water-water H-bonds. [119] Additional analysis on the radial distribution of the intermolecular interactions (H-bonds), i.e., number density near the surface and near the centre of the confinement, and H-bond lengths for water-water and water-silica are reported in Section A4.1.1 of the appendix. In this analysis, we observed that the total number of H-bonds (per molecule of water) near the surface was higher than total number of H-bonds of near the centre of the pore for the slit pore of 4 nm and cylindrical pores of 4 and 6 nm. However, we observed a minor increase in the hydrogen bonds per molecule of water near the centre of the pore as we go from cylindrical pore of 4 nm to 2 nm, suggesting that water-water

interactions are higher in the case of 2 nm pore. This increase in the number of H-bonds would contribute to the reduction in the diffusivities of water molecules inside 2 nm pore.

4.3.3.5 Summary for Water

The results obtained based on the detailed analysis for water are summarized in this subsection to provide an overview of the alteration of its dynamics inside a silica catalyst. For the slit pore of 4 nm and cylindrical pores of 4 and 6 nm, the intrapore densities remained constant with the change in both the size and dimension of the silica nanostructure, and equal to the bulk liquid. However, for the 2 nm cylindrical pore we observed a reduction in the diffusivities of water in comparison to bulk. Nanoconfined water molecules had lower entropy values in comparison to the bulk. The entropy loss and PE change were found to vary with the dimension and size of the confinement, although it does not follow a particular trend. Specifically, 2 nm cylindrical pore showed a dramatic loss in the entropy in comparison to other confinements. Based on the results obtained for the ΔPE and ΔPE_{Elec}, it can be concluded that the water molecules form stable H-bonds with the surface, and this is compensated by the breakage of water-water H-bonds. Water-surface interactions were found to be stronger than the water-water interactions. Water shows higher effective pore volume and lower local density near the centre of the confinements. The total number of H-bonds remains constant for all of the confinements. These results are in accordance with previously published simulation results, where they have reported a constant total number of H-bonds.[119] Additionally, for the 2 nm pore, substrate-surface and substrate-substrate interactions are highly altered due to confinement effects. Water forms very strong interactions with the silica surface, however the water-water H-bonds remains almost the same, leading to a reduction in the diffusivity in the case of 2 nm cylindrical pore. In conclusion, the change in the diffusivities of nanoconfined water was only noted for pore sizes between 4 to 2 nm and lower, mainly due to very strong liquid-surface interactions, drastic drop in the entropy and much higher local density near the silica surface.

4.3.4 Glycerol

Glycerol is a commodity chemical with multitude of applications in pharmaceutical, food and cosmetic industries. We are considering glycerol in this study primarily due to the presence of three hydroxyl groups with the ability to interact strongly with the silica surface. Experimental results (as reported in Section 2.2) showed that nanoconfined glycerol molecules showed an anomalous enhancement in the diffusivities inside mesoporous materials. Here we begin with the results obtained from the molecular simulations to explain the phenomenon behind the enhanced diffusion rates of the glycerol molecules. We have also analyzed the hydrogen bonding network of glycerol molecules to assess the experimental hypothesis of breakage of H-bonds inside the mesoporous structures.[29] The understanding of these confinement effects on the dynamics of glycerol would broaden the research in the field of heterogeneous catalytic conversion of glycerol into value-added products, specifically glycerol oxidation reactions.[34,153,154] To explain the trend of diffusivities for glycerol, we have provided results on the change in thermodynamic properties like potential energy and entropy, and analyzed the density profiles and intermolecular interactions in the following sections.

4.3.4.1 Potential Energy and Entropy

In this subsection, we present the change in entropy and potential energy as the glycerol molecules go from bulk liquid to inside any confinement using the methodology given in Section 3.2.4.2. The computed values of the change in the entropy (ΔS) for glycerol molecules inside the four nanostructures is reported in Figure 4.20. For these molecules, entropy is lost inside the confinement irrespective of the size or dimension. The computed change in entropy increases drastically as we go from slit pore of 1D to cylindrical pore of 2D. We see a gradual increase in the ΔS within pores of 6 and 4 nm, and a slightly higher loss in entropy was observed with the reduction in the size from 4 to 2 nm. In comparison to water, acetone and heptane, the trend of ΔS for the cylindrical pores of 2, 4 and 6 nm is much different, specifically for the case of 2 nm cylindrical pore. The reduction in the entropy for glycerol is seen as a function of the dimension of the confinement, and it does not alter much with the reduction in the size of the nanostructures. This is a noteworthy observation contributing to an anomaly from the other molecules (water, acetone and heptane), where we observed a drastic drop in the entropy values for 2 nm cylindrical pores.

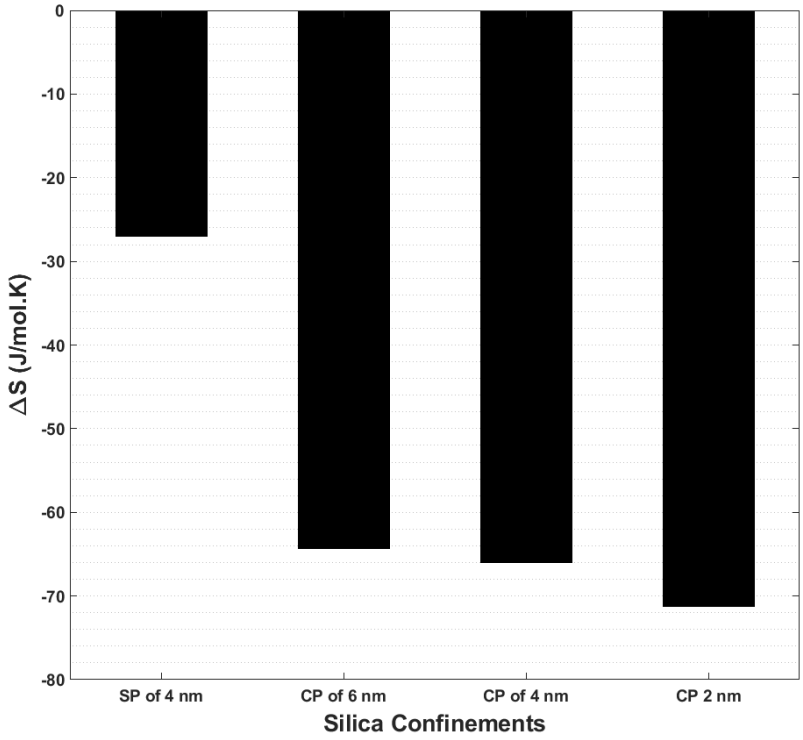

Figure 4.20: Computed values of change in entropy (ΔS) of glycerol between the bulk substrate and confined substrates (confinement – bulk) inside various silica nanostructures (CP is cylindrical pore and SP is slit pore).

As mentioned in Section 4.2, glycerol shows an increase in the PFG interactions with reduction in size of the confinement of the cylindrical pores, which suggests a slight reduction in the translational motion. Another possible explanation could be due to the molecular size of glycerol that restricts rotational motion of the confined molecules due to physical restrictions posed by the silica wall in the case of cylindrical pores in comparison to slit pores. However, it remains unchanged with the reduction in the size of the cylindrical pores.

In order to overcome the loss in entropy, the molecules attempt to reorganize inside the nano-confinement, which could cause a corresponding loss in the potential energy per molecule of glycerol with respect to the bulk liquid. The alteration in the molecular orientations can be caused by a change in the intermolecular interactions (hydrogen bonding) of the confined glycerol

molecules, leading to a change in the potential energy. To validate this hypothesis, we calculate the change in potential energy (ΔPE) reported in Figure 4.21. In this figure, a positive value of ΔPE suggests less favourable intermolecular interactions of the substrate molecules inside the pore compared to the bulk liquid (refer equation 3.3).

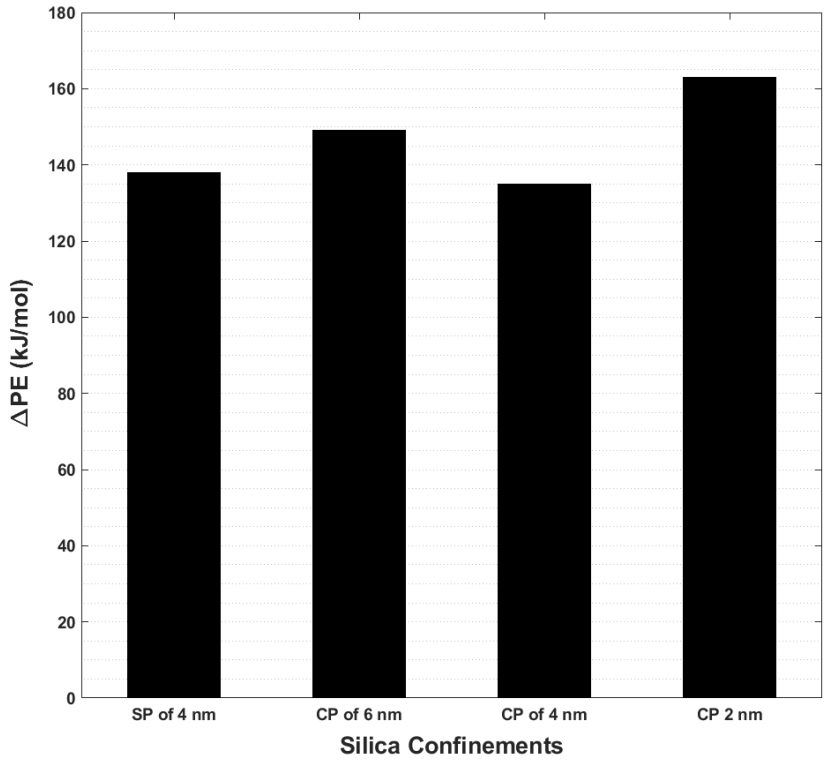

Figure 4.21: Computed values of change in potential energy (ΔPE) of glycerol between the bulk substrate and confined substrates (Confinement – bulk) inside various silica nanostructures (CP is cylindrical pore and SP is slit pore).

The computed values of ΔPE for glycerol does not vary significantly with the increase in the dimension of the confinement (slit to cylindrical pore). Within the 2D pores of varying size, the ΔPE reduced for the transition from 6 and 4 nm pores. But with the further reduction in the size of confinement to 2 nm, we see a small spike in the values of the ΔPE. The computed ΔPE remains almost constant inside the confinements, resulting in a need for further analysis of the intermolecular interactions of the glycerol-glycerol and glycerol-surface atoms. This is similar to the case of water, for the slit-pore of 4 nm and cylindrical pores of 6 and 4 nm, the potential energy remains almost constant suggesting that the formation of glycerol-silica H-bonds would lead to a

decrease in the glycerol-glycerol interactions, thereby maintaining the PE change to be constant. However, the drastic change in the ΔPE observed for confined water in 2 nm cylindrical pore is not observed for glycerol. This could be attributed to much stronger substrate-surface interactions for glycerol in comparison to water (due to the presence of more H atoms per molecule, with an ability to form H-bonds with silica) further lowering the PE (more favourable interactions) inside the 2 nm cylindrical pore. Based on these results, a combined effect of entropy loss (causing a decrease in the mobility) and reduction of glycerol-glycerol H-bonds (causing an increases in the mobility) could potentially lead to enhancement of diffusivities of the confined glycerol molecules. In the following subsection we study the intermolecular interactions between glycerol-glycerol and glycerol-surface in order to validate the aforementioned result and also to study the role of alteration in interactions on the intrapore mobilities of glycerol molecules.

4.3.4.2 Intermolecular interactions between glycerol-glycerol and glycerol-silica molecules

Intermolecular interactions of the substrate molecules with themselves and with the silica surface would affect the dynamics of the nanoconfined substrates. Specifically, for glycerol, the hydrogen bonding network of the glycerol-glycerol interactions may be subjected to alteration due to the introduction of the confinement effects posed by the silica nanostructures.[155] Applying the methodology reported in section 3.2.4.3, we calculate the change in potential energy (ΔPE_{Elec}) for glycerol molecules, as the electrostatics of the silica atoms are switched on (vdW and Electrostatic interactions) and off (only vdW interactions). Introduction of electrostatics on the silica atoms leads to alteration to the intermolecular interactions between glycerol-surface and glycerol-glycerol molecules, due to the ability of glycerol molecule to interact strongly with the surface atoms. By doing so, we have eliminated the effects due physical structure of the pore wall and van der Waals forces between glycerol-surface and glycerol-glycerol atoms by a great extent; and the change in the PE observed here is purely for the electrostatic interactions of the glycerol and silica molecules. Figure 4.22 shows the computed values of ΔPE_{Elec} for glycerol. In this figure, a positive value of ΔPE_{Elec} represents favourable interactions (refer equation 3.9).

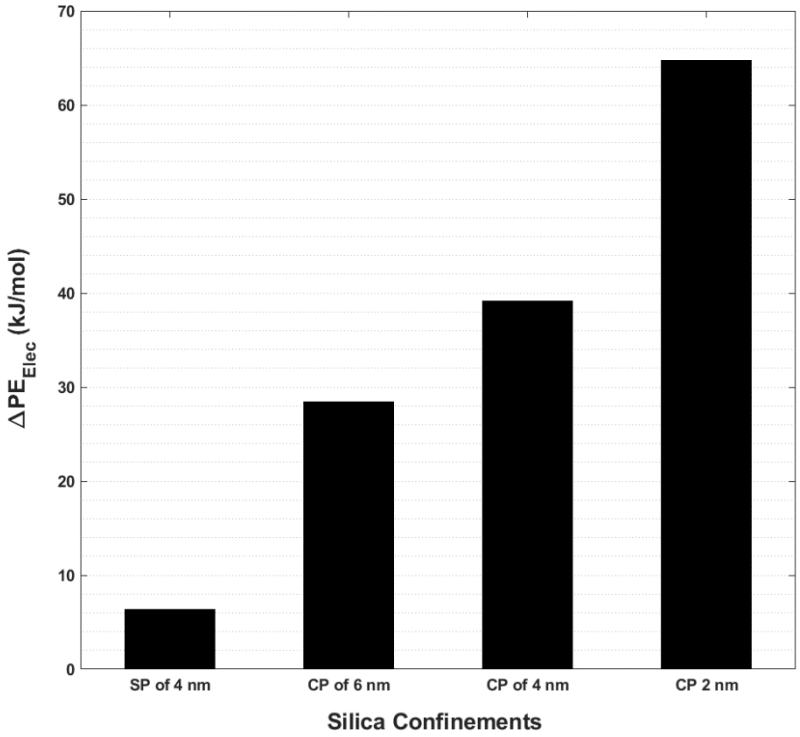

Figure 4.22: Computed values of change in potential energy (ΔPE_{Elec}) of glycerol with the introduction of charges on silica atoms. (Without – with charges on silica atoms)

In this plot, we observed that the ΔPE_{Elec} increases drastically with the change in the dimension of the confinement (slit pore to cylindrical pore). This increase is a result of better surface area to volume ratio available for the molecules interacting with the silica surface. Within pores of different sizes, the computed ΔPE_{Elec} increases with the reduction in the size of the confinement from 6 to 4 nm, and increases significantly with further decrease in the size to 2 nm. The change in PE was a function of the surface area to volume ratio. The trend in the ΔPE_{Elec} for glycerol is very similar to that of water. However, the ΔPE trend for the glycerol and water molecules are different. This could be due to much stronger interactions of glycerol molecules with silica surface in comparison to water (due to the presence of three hydrogens with the ability to interact well with silica in comparison to water with two hydrogens). Similar to water, glycerol has an exceptional ability to form H-bonds with themselves (three H-bonds). On the other hand, with the inclusion of charges on the silica atoms, the glycerol tends to form much stronger interactions with the silica surface. This would lead to a change in the glycerol-glycerol hydrogen bonds, affecting the overall potential energy change (ΔPE).[59,119] This effect was validated by normalizing the

potential energy change with respect to the surface area to volume ratio, as suggested previously in Section 3.2.4.2. This would standardize the effect due to glycerol-surface interactions and emphasize the glycerol-glycerol interactions.

Upon normalizing the ΔPE_{Elec} with respect to the factor F (refer Section 3.2.4.2), the substrate-surface interactions per number of molecules interacting with the surface yields information about the strength of interactions and the change in the substrate-substrate interactions, as the number of molecules interacting the surface remains constant.

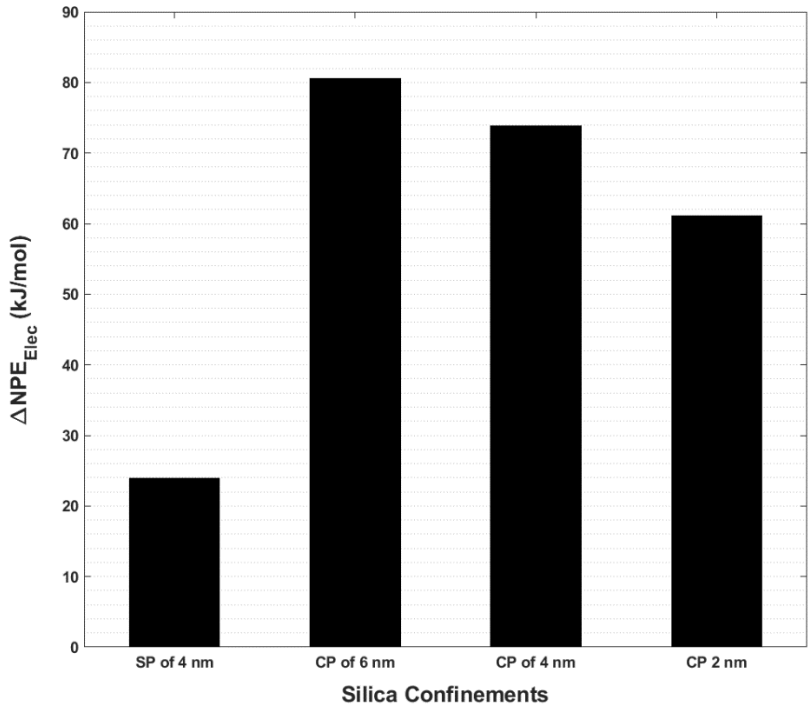

Figure 4.23: Computed values of change in potential energy (ΔNPE_{Elec}) of glycerol with the introduction of charges on silica atoms. (Without – with charges on silica atoms)

Figure 4.23 shows the computed values of normalized PE change (ΔNPE_{Elec}) for glycerol molecules inside different silica confinements. We see that the ΔNPE_{Elec} of substrate-surface and substrate-subtrate interactions due to the inclusion of charges on the silica atoms increases significantly with the change in the dimension (Slit to cylindrical pores), suggesting that the intermolecular interactions are altered much drastically in the case of cylindrical pores as compared to the slit pore (due to better surface area to volume ratio). But within the pores, we see

that the ΔNPE_{Elec} is getting lower with the decrease in the size of the confinement, suggesting that the interactions are getting marginally weaker with the reduction in the size, specifically for the case of 2 nm pore. In comparison to water and acetone, glycerol shows a steeper drop in the ΔNPE_{Elec} with the reduction in the size of the cylindrical pores. This suggests that the glycerol-glycerol interactions reduce with the decrease in the size of the confinement from 6 to 2 nm, which was not observed in the case water. This observation is in line with the experimental and simulation results obtained for the disruption of hydrogen bonding network inside the nanoporous structures.[29,38]

Looking at the results collectively for glycerol, the change in the intrapore diffusivities of glycerol inside slit pores could be attributed to the loss in the entropy of the molecules (reduction in the diffusivity) and reduction in the glycerol-glycerol interactions (enhancement in the diffusivities). To validate this claim, we have calculated the radial density profiles, effective pore volumes available for the movement of the substrate molecules and the hydrogen bonding network of glycerol in the subsequent sections.

4.3.4.3 Density Profiles and Effective Pore Volume

In this section, we study the local densities of the glycerol molecules across the silica nanostructures by calculating the percentage of molecules residing in the first shell near the silica surface. We also look into the MD trajectory snapshots when the electrostatics on the silica atoms are switched on and off, to analyze the effective pore volumes available for the substrate molecules. Figure 4.24 shows the snapshots of the MD simulations of the two systems mentioned above. Similar to water, we observed that the molecules tend to move towards the surface of the silica nanostructure when the charges on the silica atoms are assigned. Whereas, it follows the opposite trend of acetone, where we observed a molecular movement towards the centre of the silica pore. This leads to an increase in the effective pore volume available for the mobility of the glycerol molecules inside the confinements.[38,110,119]

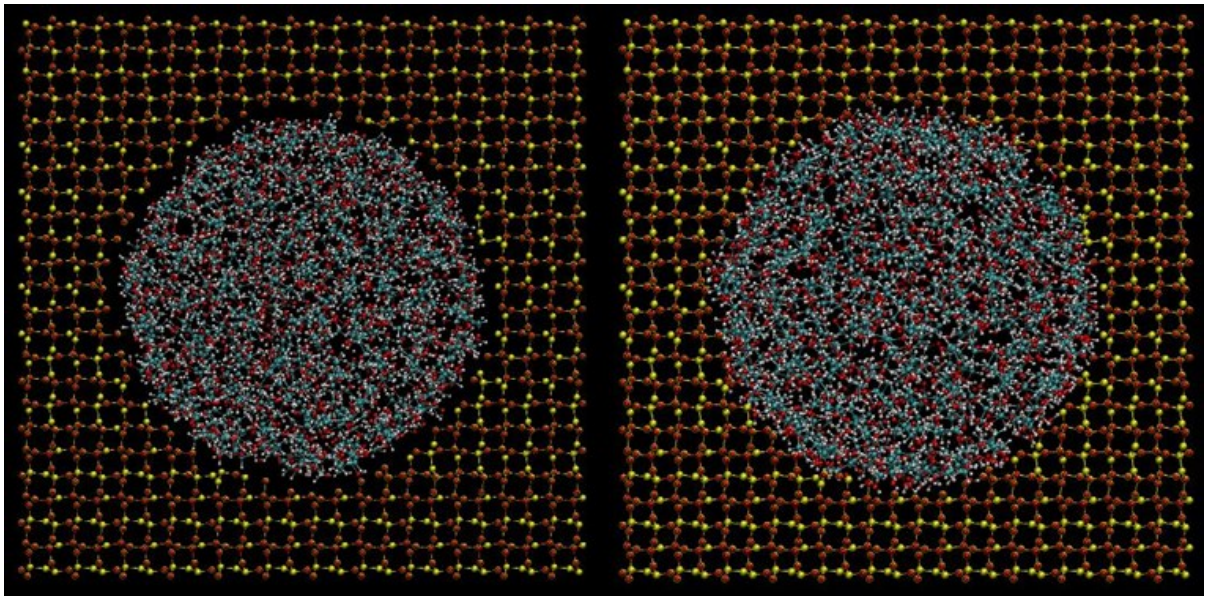

Figure 4.24: MD trajectory snapshots of the nanoconfined glycerol molecules inside the silica nanopore of 4 nm with (right) and without (left) charges assigned on the silica atoms.

To further validate this, we analyze the number density profile of the glycerol molecules across the nanostructure. Table 4.4 shows the computed values of percentage of molecules of water present in the first solvation shell around the surface of the silica catalyst.

Table 4.4: Percentage of glycerol molecules present near the silica surface as compared to the total number of substrate molecules confined inside the nanostructure.

Confinement	***Percentage of molecules in the first shell near the silica surface***
Slit Pore 4 nm	14.30%
Cylindrical Pore 6 nm	14.22%
Cylindrical Pore 4 nm	26.08%
Cylindrical Pore 2 nm	31.37%

We see that the percentage remains the same as we go from a slit pore of 1D to 6 nm cylindrical pore of 2D. But within the pores, we see an increase in the percentage of molecules with the decrease in the size of the confinement. Especially for the case of 2 nm pore, around ~30% of the

molecules was observed to reside close to the surface, suggesting much stronger interactions with the surface for 2 nm pore. In comparison to heptane and acetone (refer Table 4.1 and 4.2 respectively), glycerol has much higher local densities near the silica surface in comparison to the centre of the confinement due to more favourable substrate-surface interactions. Whereas, the trend in the local densities near the surface for glycerol is very similar to water (refer Table 4.3), wherein we observed much higher local densities for 2 nm cylindrical pore (>30%). Due to very strong interactions with the surface and increased local density near the silica surface, we see a reduction in the diffusivity of the glycerol molecules in the 2 nm pore. In addition to this, the formation of strong hydrogen bonds with the silica surface could potentially lead to a breakage of the glycerol-glycerol hydrogen bonds. The following analysis on the hydrogen bonding network provides a better perspective of the intermolecular interactions of the glycerol molecules within itself and with the silica surface.

4.3.4.4 Hydrogen Bonding analysis

As mentioned earlier, glycerol has a remarkable ability to form hydrogen bonds with the surface as well as with the other glycerol molecules. Introduction of silica molecules to this system to lead to a change in the intermolecular interactions of glycerol. The extent of impact of the confinement on the hydrogen bonding network of the glycerol molecules is discussed in this subsection to provide an additional perspective to the alteration in the intrapore dynamics. Figure 4.25 presents the number of glycerol-glycerol and glycerol-surface hydrogen bonds (H-bonds) per molecule of glycerol.

In this figure, the orange line depicts the glycerol-surface H-bonds, blue line denoting the glycerol-glycerol H-bonds and the yellow line is the total number of hydrogen bonds in the system (substrate-substrate and substrate-surface). H-bonds between glycerol-glycerol molecules (blue) decreases with the increase in the confinement dimension (slit to cylindrical pores). A further reduction in the substrate-substrate H-bonds was observed with the change in the size of the porous structures from 6 to 2 nm. On the contrary, the number of H-bonds between glycerol and surface molecules (orange) increases with change in the dimension and size of the confinement. Within the pores, the substrate-surface interactions were observed to increase with the reduction in the size of the confinement. Additionally, the total number of H-bonds inside all confinements reduced

with the reduction in the size of the confinements. The average bond lengths of the glycerol-surface H-bonds was recorded to be shorter than the glycerol-glycerol H-bonds by 0.3 Å, suggesting that the surface interactions are stronger than the intermolecular glycerol-glycerol interactions (refer section A4.1.2).

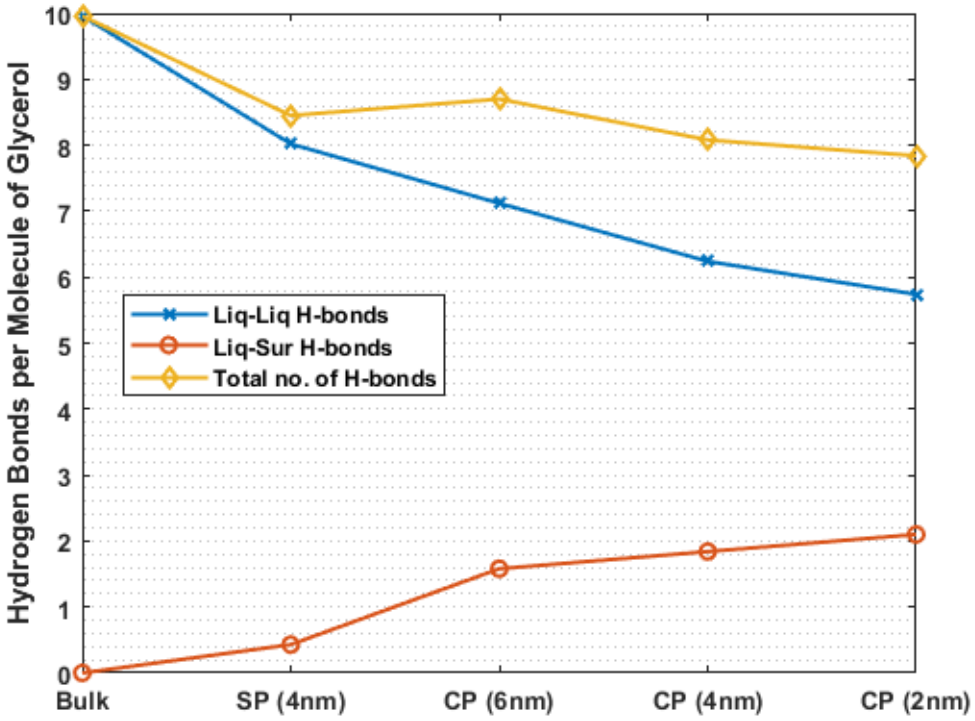

Figure 4.25: Hydrogen bonding analysis of glycerol molecules confined inside various silica nanostructures.

In comparison to water, glycerol follows a different trend for the substrate-surface and substrate-substrate interactions. For water, the substrate-substrate and substrate-substrate interactions remained constant within the cylindrical pores of 2, 4 and 6 nm. However, we observe a systematic decrease in the substrate-substrate interactions and an increase in the substrate-surface interactions with the reduction of pore size. The reduction in the total number of hydrogen bonds decreases for glycerol, whereas it remains constant for water. This leads to an enhancement in the diffusivities of nanoconfined glycerol inside slit pore of 4 nm and cylindrical pores of 4 and 6 nm. This result is in agreement with the experimental hypothesis of the breakage of hydrogen bonding network inside mesoporous catalysts.[29] These results are in complete agreement with the simulation study on the disruption of hydrogen bonding network inside various alumina slit pores.[38]

Whereas for 2 nm cylindrical pore, glycerol forms much stronger interactions with the silica surface (as shown in section 4.3.4.2), and due to increased local densities near the surface (from the local density calculations), the overall diffusivity of glycerol is reduced inside the 2 nm pore. This unique result is similar to the reduction in the diffusivity of water molecule inside the 2 nm pore due to much stronger water-silica interactions and increased local density near the silica surface (increased percentage of molecules near the surface in comparison to the centre of the pores).

4.3.4.5 Summary for Glycerol

The results obtained based on the detailed analysis of the molecular simulations for glycerol are summarized in this subsection to provide an overview of the change in the intrapore dynamics inside silica catalysts. The intrapore densities remained constant with the change in both the size and dimension of the silica nanostructure, and equal to the bulk liquid. From the diffusivity calculations, we observed that the PFG interaction parameters were observed to be a function of the dimension and size of the confinement. For the slit pore of 4 nm and cylindrical pores of 4 and 6 nm, the results on the enhanced diffusivity of glycerol (in comparison alkanes) is in accordance with the experimental results.[29] However, we observed a reduction in the diffusivity with a decrease in the size of the confinement from 4 to 2 nm. The entropy loss and PE change were found to vary with the dimension and size of the confinement, although it does not follow a particular trend. Nanoconfined glycerol molecules had lower entropy values in comparison to the bulk. Specifically, cylindrical pores showed a greater loss in the entropy in comparison to other confinements. This is attributed to change in the molecular orientation of the confined glycerol molecules. Based on the results obtained for the ΔPE and ΔPE_{Elec}, it can be concluded that the glycerol molecules form stable H-bonds with the surface, and this is compensated by the breakage of glycerol-glycerol H-bonds. The glycerol-surface interactions were found to be stronger than the glycerol-glycerol interactions. Similar to water, glycerol shows higher effective pore volume and lower local density near the centre of the confinements. The total number of H-bonds reduced inside the confinements with the reduction in the size. This result is in complete agreement with the simulation study on the disruption of hydrogen bonds inside alumina catalysts, leading to anomalous enhancement in the diffusivities of glycerol.[38] However this anomaly is not followed with the reduction of pore size between 4 to 2 nm. For the 2 nm pore, the formation of stronger

glycerol-silica interactions and increased local densities (31%) near the silica surface causes a decrease in the diffusivities of glycerol molecules residing near the surface. This consequently lead to a reduction in the diffusivities of glycerol inside the 2 nm cylindrical pore. In conclusion, the enhancement in diffusivities of glycerol inside slit pore of 4 nm and cylindrical pores of 4 and 6 nm is attributed to a combined effect of reduction of the glycerol-glycerol H-bonds and high effective pore volumes and lower local densities near the centre of the confinement. Whereas, for 2 nm pore, the stronger substrate-surface interactions and higher local densities (higher percentage of glycerol molecules) near the silica surface lead to a reduction in the self-diffusivities of the glycerol molecules.

5 Summary, Conclusions & Perspectives

5.1 Summary & Conclusions

In this thesis, we provide a detailed overview on the effect of confinement imposed by the silica nanostructures (Slit pore of 4 nm, and cylindrical pores of 2, 4 and 6 nm) on the dynamic properties of the water, glycerol, acetone and heptane molecules, using a combination of MD and GCMC simulations. We studied the effect of the size and geometry of the nanostructures on the intermolecular interactions, dynamic and thermodynamic properties (change in entropy and potential energy) of the confined substrates. We analyzed both physical, i.e. Hydrogen bonding, density profiles, intermolecular interactions, effective pore volumes, and thermodynamic properties, such as potential energy and entropy of the system; on the intrapore diffusivities of the functionalized molecules. For this study, heptane was taken as a reference for the comparison of the intrapore diffusivities of the functionalized molecules water, acetone and glycerol. In addition to slit-pore configurations used in previously published computational results used to evaluate the influence of intermolecular interactions on the dynamic properties, we also consider two dimensional confinements (cylindrical pores) of varying sizes to address the knowledge gaps pertaining to the effect of confinement size and geometry on the diffusivities of nanoconfined substrates. We calculated the entropy change to provide an additional perspective on the entropic effects on the molecular orientations of the substrate molecules occurring due to confinements. We observed that the entropy is lost (w.r.t bulk liquid) for water, acetone, glycerol and heptane inside all the silica confinements. This result was used in conjunction with the change in the potential energy of the confined substrate molecules in comparison to the bulk liquid to study the size and geometric effects of the silica confinement. We further looked into the intermolecular interactions arising due to the introduction of charges on the silica atoms, to study the effect of confinement on the intermolecular interactions of the confined substrates. Furthermore, we studied the effective pore volumes available for the mobility of the substrate molecules and the local density profiles across the nanostructures for these substrates. Finally, we performed hydrogen bonding network analysis for water and glycerol in bulk and inside all the confinements. Table 5.1 summarizes the effect of confinement size and geometry on the intermolecular interactions, change in the entropy, radial density profiles, effective pore volumes and intrapore diffusivities of the confined heptane, acetone, water and glycerol.

Table 5.1: Summary of confinement effects imposed by silica nanostructures of varying sizes and geometries on the change in entropy, intermolecular interactions, local densities, effective pore volumes and intrapore diffusivities of confined substrate molecules. (Geometry corresponds to slit to cylindrical pores and Size corresponds to decrease in the size of the cylindrical confinement from 6 to 2 nm).

Properties	Confinement (Size/Geometry)	Substrate			
		Heptane	**Acetone**	**Water**	**Glycerol**
Entropy	Geometry	Decreases	Decreases	Constant	Decreases
	Size	Decreases	Decreases	Decreases (2 nm CP)	Decreases
Substrate-Surface	Geometry	Increases (weak)	Increases	Increases	Increases
	Size	Constant (weak)	Increases	Increases (Strong)	Increases (Strong)
Substrate-Substrate	Geometry	Increases	Increases	Increases	Increases
	Size	Decreases	Increases	Decreases	Decreases
Local density near pore	Geometry	Low	Low	High	High
	Size	Low	Low	Very High (2 nm CP)	High
Effective Pore Volume	Geometry	Constant	Low	High	High
	Size	Constant	Low	High	High
Intrapore Diffusivities	**Geometry**	**Constant**	**Reduced**	**Constant (Bulk-like)**	**Reduced**
	Size	**Constant**	**Reduced**	**Reduced (2 nm CP)**	**Enhanced for CP of 4, 6 nm; Reduced for 2 nm CP**

In conclusion, the modifications in the intrapore diffusivities (reported in Table 5.1) of heptane, acetone, water and glycerol inside confinements of varying geometries and sizes are summarized as follows:

- For heptane, the negligible change in the diffusivities was observed to be a combined effect of entropy loss (reduction in the diffusivity) and weakening of the intermolecular interactions (enhancement in the diffusivity).
- The reduction in the diffusivities of acetone inside the silica confinements is due to increased acetone-surface interactions, unaltered acetone-acetone interactions, higher densities of acetone molecules near the centre of the pore and lower effective pore volume available for the molecular mobility.
- Diffusivities of water was observed to change for pore sizes between 4 to 2 nm and lower, mainly due to very strong water-surface interactions and much higher local density (percentage of molecules) near the silica surface.
- Enhancement in the diffusivities of Glycerol is due to the reduction in substrate-substrate interactions (hydrogen-bonding), lower local densities near the centre of the pore and high effective pore volumes, for the slit pore of 4 nm and cylindrical pores of 4 and 6 nm. Whereas, for 2 nm pore, the stronger substrate-surface interactions and high local density near the surface lead to a reduction in the self-diffusivities of the glycerol molecules.

Based on the aforementioned findings, we validated the experimental hypothesis of increased diffusivities of polyols like glycerol arising due to the disruption of the hydrogen bonding network inside the nanostructures. Glycerol showed anomalous enhanced diffusivities inside the slit pore of 4 nm, and cylindrical pores of 6 and 4 nm in comparison to acetone and heptane due to a reduction in the glycerol-glycerol hydrogen bonds, high effective pore volumes and low local densities (percentage of molecules) near the center of the confinement. Reduction in the total number of hydrogen bonds was observed for glycerol inside all the confinements, confirming the experimental hypothesis. However, this anomaly for glycerol was not obeyed for the 2 nm cylindrical pore where we observed reduced diffusivities in the cylindrical pore of 2 nm, due to stronger interactions with the cylindrical pore surface and much higher local densities of glycerol near the pore surface. This unique result suggests that the intrapore dynamics of functionalized substrates is a function of the size and geometry of the confinement, in addition to the change in

the intrapore densities, intermolecular interactions and thermodynamic properties like entropy and potential energy.

5.2 Future prospects

The following potential avenues have been identified for future work in the field of heterogeneous catalysis using nanopores based on the work done in this thesis.

- **Confinement effects on dynamics and intermolecular interactions of solvent-reactant mixtures inside nanoporous catalysts:** In this thesis, we have investigated the confinement effects on the intrapore dynamics and intermolecular interactions of pure substrate systems. In practice, however, conversion reactions of bio-derived substrates like glycerol is often conducted in the presence of solvents like water, methanol etc.,[153] and the change in intrapore dynamics and intermolecular interactions would lead to a change in the selectivity and conversion of the chemical reactions. Therefore, the study of confinement effects on intrapore dynamics and intermolecular interactions of such solvent-reactant systems is a potential future prospect.

- **Confinement effects on adsorption kinetics of solvent-reactant mixtures inside nanoporous catalysts:** In addition to physical interactions studied in this thesis, it is important to additionally assess the adsorption kinetics of the pure substrates or reactant-solvent systems inside nanopores. This will potentially take chemisorption into consideration, which is beyond the scope of this thesis. The effect of confinement on the relative adsorption of reactant and solvent molecules have been accessed using NMR-relaxometry studies in the past and first principles based modeling techniques could be employed to explain the experimental observations on the change in reaction selectivities and conversion of the heterogeneous catalytic reactions inside nanopores of varying sizes and geometries.[34]

- **Confinement effects on intrinsic reaction kinetics and thermodynamics:** In this thesis, we concluded that the effect of the confinement on the intermolecular interactions and intrapore dynamics of pure substrates are a function of the pore size and geometry. Similarly, for a

reaction systems inside a confinement, the results obtained from this thesis and the adsorption studies (as mentioned above) in conjunction with AIMD or DFT studies could potentially explain the change in intrinsic reactions kinetics and thermodynamic properties of the chemical reactions inside nanopores of different sizes and geometries. Detailed understanding of this would additionally yield us information on the critical pore size or geometry of the confinement for obtaining targeted conversion rates and selectivities, specifically for condensed phase polyol conversion reactions reported in Section 2.2.2.[37,98]

Bibliography

[1] F. Ma, M.A. Hanna, Biodiesel production: A review, Bioresour. Technol. 70 (1999) 1–15. doi:10.1016/S0960-8524(99)00025-5.

[2] P.T.V. Ae, M. Briggs, Biodiesel production-current state of the art and challenges, (n.d.). doi:10.1007/s10295-008-0312-2.

[3] A. Abbaszaadeh, B. Ghobadian, M.R. Omidkhah, G. Najafi, Current biodiesel production technologies: A comparative review, in: Energy Convers. Manag., Pergamon, 2012: pp. 138–148. doi:10.1016/j.enconman.2012.02.027.

[4] W.A. Khanday, P.U. Okoye, B.H. Hameed, Biodiesel byproduct glycerol upgrading to glycerol carbonate over lithium-oil palm ash zeolite, (2017). doi:10.1016/j.enconman.2017.08.091.

[5] S.N. Gebremariam, J.M. Marchetti, Economics of biodiesel production: Review, Energy Convers. Manag. 168 (2018) 74–84. doi:10.1016/j.enconman.2018.05.002.

[6] M.J. Haas, A.J. McAloon, W.C. Yee, T.A. Foglia, A process model to estimate biodiesel production costs, Bioresour. Technol. 97 (2006) 671–678. doi:10.1016/j.biortech.2005.03.039.

[7] G.A. Somorjai, A.S. Mujumdar, Introduction to surface chemistry and catalysis, Dry. Technol. 13 (1995) 507–508. doi:10.1080/07373939508916972.

[8] N.V. Orupattur, S.H. Mushrif, V. Prasad, Catalytic materials and chemistry development using a synergistic combination of machine learning and ab initio methods, Comput. Mater. Sci. 174 (2020) 109474. doi:10.1016/j.commatsci.2019.109474.

[9] T.U.S.C. Industry, Technology Vision 2020 Chemical Industry, Sci. News. 150 (1996) 202. doi:10.2307/3980385.

[10] J. Gong, R. Luque, Catalysis for production of renewable energy, Chem. Soc. Rev. 43 (2014) 7466–7468. doi:10.1039/c4cs90084g.

[11] G.H. Gu, J. Noh, I. Kim, Y. Jung, Machine learning for renewable energy materials, J. Mater. Chem. A. 7 (2019). doi:10.1039/c9ta02356a.

[12] S.T. Sie, Past, Present and Future Role of Microporous Catalysts in the Petroleum Industry, Stud. Surf. Sci. Catal. 85 (1994) 587–631. doi:10.1016/S0167-2991(08)60779-X.

[13] R.M. Heck, R.J. Farrauto, S.T. Gulati, Catalytic air pollution control : commercial technology, John Wiley, 2009.

[14] A.K. Ray, Development of a New Photocatalytic Reactor for Water Purification, Catalysis Today 40 (1) (1998) pp.73., 40 (1998) 73–83.

[15] P.L. Mills, R. V. Chaudhari, Multiphase catalytic reactor engineering and design for pharmaceuticals and fine chemicals, Catal. Today. 37 (1997) 367–404. doi:10.1016/S0920-5861(97)00028-X.

[16] A. Corma, S. Iborra, A. Velty, Chemical Routes for the Transformation of Biomass into Chemicals, (2007). doi:10.1021/cr050989d.

[17] G.W. Huber, S. Iborra, A. Corma, Synthesis of Transportation Fuels from Biomass: Chemistry, Catalysts, and Engineering, (2006). doi:10.1021/cr068360d.

[18] D.G. Vlachos, J.G. Chen, R.J. Gorte, G.W. Huber, M. Tsapatsis, Catalysis center for energy innovation for biomass processing: Research strategies and goals, Catal. Letters. 140 (2010) 77–84. doi:10.1007/s10562-010-0455-4.

[19] A.T. Bell, B.C. Gates, D. Ray, A Primer on Chemical Reactions and Catalysis, n.d.

[20] C. Sievers, Y. Noda, L. Qi, E.M. Albuquerque, R.M. Rioux, S.L. Scott, Phenomena Affecting Catalytic Reactions at Solid−Liquid Interfaces, (2016). doi:10.1021/acscatal.6b02532.

[21] B.F.G. Johnson, Nanoparticles in catalysis, Top. Catal. 24 (2003) 147–159. doi:10.1023/B:TOCA.0000003086.83434.b6.

[22] A. Corma, From Microporous to Mesoporous Molecular Sieve Materials and Their Use in Catalysis, 1997. https://pubs.acs.org/sharingguidelines (accessed February 8, 2021).

[23] B.Z. Zhan, M.A. White, M. Lumsden, J. Mueller-Neuhaus, K.N. Robertson, T.S. Cameron, M. Gharghouri, Control of particle size and surface properties of crystals of NaX zeolite, Chem. Mater. 14 (2002) 3636–3642. doi:10.1021/cm011635f.

[24] B.A. Holmberg, H. Wang, J.M. Norbeck, Y. Yan, Controlling size and yield of zeolite Y nanocrystals using tetramethylammonium bromide, Microporous Mesoporous Mater. 59 (2003) 13–28. doi:10.1016/S1387-1811(03)00271-3.

[25] C.C. Freyhardt, M. Tsapatsis, R.F. Lobo, K.J. Balkus, M.E. Davis, A high-silica zeolite with a 14-tetrahedral-atom pore opening, Nature. 381 (1996) 295–298. doi:10.1038/381295a0.

[26] Y. Tao, H. Kanoh, L. Abrams, K. Kaneko, Mesopore-Modified Zeolites: Preparation,

Characterization, and Applications, (2006). doi:10.1021/cr040204o.

[27] J.M. Martínez De La Hoz, P.B. Balbuena, Geometric and electronic confinement effects on catalysis, J. Phys. Chem. C. 115 (2011) 21324–21333. doi:10.1021/jp207548k.

[28] J. Kärger, R. Valiullin, Mass transfer in mesoporous materials: The benefit of microscopic diffusion measurement, Chem. Soc. Rev. 42 (2013) 4172–4197. doi:10.1039/c3cs35326e.

[29] C.D.' Agostino, J. Mitchell, L.F. Gladden, M.D. Mantle, Hydrogen Bonding Network Disruption in Mesoporous Catalyst Supports Probed by PFG-NMR Diffusometry and NMR Relaxometry, (2012). doi:10.1021/jp2123295.

[30] C. D'Agostino, T. Kotionova, J. Mitchell, P.J. Miedziak, D.W. Knight, S.H. Taylor, G.J. Hutchings, L.F. Gladden, M.D. Mantle, Solvent Effect and Reactivity Trend in the Aerobic Oxidation of 1,3-Propanediols over Gold Supported on Titania: NMR Diffusion and Relaxation Studies, Chem. - A Eur. J. 19 (2013) 11725–11732. doi:10.1002/chem.201300502.

[31] C.D. Agostino, T. Kotionova, J. Mitchell, P.J. Miedziak, D.W. Knight, S.H. Taylor, G.J. Hutchings, L.F. Gladden, M.D. Mantle, Solvent Effect and Reactivity Trend in the Aerobic Oxidation of 1,3-Propanediols over Gold Supported on Titania: NMR Diffusion and Relaxation Studies, (2013) 11725–11732. doi:10.1002/chem.201300502.

[32] M.D. Mantle, D.I. Enache, E. Nowicka, S.P. Davies, J.K. Edwards, C. D'Agostino, D.P. Mascarenhas, L. Durham, M. Sankar, D.W. Knight, L.F. Gladden, S.H. Taylor, G.J. Hutchings, Pulsed-Field Gradient NMR Spectroscopic Studies of Alcohols in Supported Gold Catalysts, J. Phys. Chem. C. 115 (2011) 1073–1079. doi:10.1021/jp105946q.

[33] C.D. Agostino, G.L. Brett, P.J. Miedziak, D.W. Knight, G.J. Hutchings, L.F. Gladden, M.D. Mantle, Understanding the Solvent Effect on the Catalytic Oxidation of 1 , 4- Butanediol in Methanol over Au / TiO 2 Catalyst : NMR Diffusion and Relaxation Studies, (2012) 14426–14433. doi:10.1002/chem.201201922.

[34] J.J. Varghese, L. Cao, C. Robertson, Y. Yang, L.F. Gladden, A.A. Lapkin, S.H. Mushrif, Synergistic Contribution of the Acidic Metal Oxide−Metal Couple and Solvent Environment in the Selective Hydrogenolysis of Glycerol: A Combined Experimental and Computational Study Using ReO x −Ir as the Catalyst, (2018). doi:10.1021/acscatal.8b03079.

[35] P.H. Hintermeier, S. Eckstein, D. Mei, M. V. Olarte, D.M. Camaioni, E. Baráth, J.A.

Lercher, Hydronium-Ion-Catalyzed Elimination Pathways of Substituted Cyclohexanols in Zeolite H-ZSM5, ACS Catal. 7 (2017) 7822–7829. doi:10.1021/acscatal.7b01582.

[36] P.T. Vasudevan, M. Briggs, Biodiesel production - Current state of the art and challenges, J. Ind. Microbiol. Biotechnol. 35 (2008) 421–430. doi:10.1007/s10295-008-0312-2.

[37] J.J. Varghese, S.H. Mushrif, Origins of Complex Solvent Effects on Chemical Reactivity and Computational Tools to Investigate Them: A Review The Cambridge Centre for Carbon Reduction in Chemical Technology (C4T)-IRP1 (2013) 1–3. doi:10.1039/C8RE00226F.

[38] G. Campos-Villalobos, F.R. Siperstein, C. D'Agostino, L. Forster, A. Patti, Self-diffusion of glycerol in γ-alumina nanopores. The neglected role of pore saturation in the dynamics of confined polyalcohols, Appl. Surf. Sci. 516 (2020) 146089. doi:10.1016/j.apsusc.2020.146089.

[39] A.A. Milischuk, B.M. Ladanyi, Structure and dynamics of water confined in silica nanopores, J. Chem. Phys. 135 (2011). doi:10.1063/1.3657408.

[40] C.M. Friend, B. Xu, Heterogeneous catalysis: A central science for a sustainable future, Acc. Chem. Res. 50 (2017) 517–521. doi:10.1021/acs.accounts.6b00510.

[41] D. Khemakhem Riyadh, The Outlook for Energy: A View to 2040, 2013. www.exxonmobil.com. (accessed March 16, 2021).

[42] A. Vojvodic, J.K. Nørskov, New design paradigm for heterogeneous catalysts, 2015. https://academic.oup.com/nsr/article/2/2/140/2097907 (accessed March 16, 2021).

[43] D.Y. Murzin, I.L. Simakova, Catalysis in biomass processing, Catal. Ind. 3 (2011) 218–249. doi:10.1134/S207005041103007X.

[44] P. Sudarsanam, R. Zhong, … S.V. den B.-C.S., undefined 2018, Functionalised heterogeneous catalysts for sustainable biomass valorisation, Pubs.Rsc.Org. (n.d.). https://pubs.rsc.org/fa/content/articlehtml/2018/cs/c8cs00410b (accessed March 16, 2021).

[45] A.M. Molenbroek, A.E. Stig, H. Ae, H. Topsøe, A.E. Bjerne, S. Clausen, Nano-Particles in Heterogeneous Catalysis, Springer. (n.d.). doi:10.1007/s11244-009-9314-1.

[46] L. Wang, F.S. Xiao, Nanoporous catalysts for biomass conversion, Green Chem. 17 (2015) 24–39. doi:10.1039/c4gc01622j.

[47] M. Pagliaro, R. Ciriminna, H. Kimura, M. Rossi, C. Della Pina, From Glycerol to Value-Added Products, Angew. Chemie Int. Ed. 46 (2007) 4434–4440. doi:10.1002/anie.200604694.

[48] P. Guerrero-Urbaneja, Glycerol valorization by etherification to polyglycerols by using metal oxides derived from MgFe hydrotalcites, Elsevier. (2014).

[49] A. Galadima, A review on glycerol valorization to acrolein over solid acid catalysts, Elsevier. (2016).

[50] R. Varma, Glycerol valorization under continuous flow conditions-recent advances, Elsevier. (2019).

[51] G. Yadav, A green process for glycerol valorization to glycerol carbonate over heterogeneous hydrotalcite catalyst, Elsevier. (2014).

[52] A. Cornejo, I. Barrio, Oxygenated fuel additives from glycerol valorization. Main production pathways and effects on fuel properties and engine performance: A critical review, Elsevier. (2017).

[53] C. Crotti, E. Farnetti, N. Guidolin, Alternative intermediates for glycerol valorization: iridium-catalyzed formation of acetals and ketals †, Pubs.Rsc.Org. (2010). doi:10.1039/c0gc00096e.

[54] C.L. Gargalo, P. Cheali, J.A. Posada, K. V Gernaey, G. Rkan Sin, Economic Risk Assessment of Early Stage Designs for Glycerol Valorization in Biorefinery Concepts, ACS Publ. 55 (2016) 6801–6814. doi:10.1021/acs.iecr.5b04593.

[55] P. Amaral, T. Ferreira, Glycerol valorization: new biotechnological routes, Elsevier. (2009).

[56] E. Farnetti, J. Kašpar, C. Crotti, A novel glycerol valorization route: chemoselective dehydrogenation catalyzed by iridium derivatives, Pubs.Rsc.Org. (2009). doi:10.1039/b819870e.

[57] L. Liu, S. Kawakami, Y. Nakagawa, M. Tamura, K. Tomishige, Highly active iridium–rhenium catalyst condensed on silica support for hydrogenolysis of glycerol to 1,3-propanediol, Appl. Catal. B Environ. 256 (2019) 117775. doi:10.1016/j.apcatb.2019.117775.

[58] J. Chaminand, L.A. Djakovitch, P. Gallezot, P. Marion, C. Pinel, C. Rosier, Glycerol hydrogenolysis on heterogeneous catalysts, Green Chem. 6 (2004) 359–361. doi:10.1039/b407378a.

[59] A.D. da Silva Ruy, R.M. de Brito Alves, T.L. Reis Hewer, D. de Aguiar Pontes, L.S. Gomes Teixeira, L.A. Magalhães Pontes, Catalysts for glycerol hydrogenolysis to 1,3-propanediol: A review of chemical routes and market, Catal. Today. (2020).

doi:10.1016/j.cattod.2020.06.035.

[60] K. Tomishige, Y. Nakagawa, M. Tamura, Taming heterogeneous rhenium catalysis for the production of biomass-derived chemicals, Chinese Chem. Lett. 31 (2020) 1071–1077. doi:10.1016/j.cclet.2019.07.014.

[61] L. Liu, T. Asano, Y. Nakagawa, M. Tamura, K. Tomishige, One-pot synthesis of 1,3-butanediol by 1,4-anhydroerythritol hydrogenolysis over a tungsten-modified platinum on silica catalyst, Green Chem. 22 (2020) 2375–2380. doi:10.1039/d0gc00244e.

[62] K. Tomishige, Y. Nakagawa, M. Tamura, Design of supported metal catalysts modified with metal oxides for hydrodeoxygenation of biomass-related molecules, Curr. Opin. Green Sustain. Chem. 22 (2020) 13–21. doi:10.1016/j.cogsc.2019.11.003.

[63] J.J. Varghese, Computational design of catalysts for bio-waste upgrading, Curr. Opin. Chem. Eng. 26 (2019) 20–27. doi:10.1016/j.coche.2019.08.002.

[64] A. Imran, E.A. Bramer, K. Seshan, G. Brem, An overview of catalysts in biomass pyrolysis for production of biofuels, Biofuel Res. J. 5 (2018) 872–885. doi:10.18331/BRJ2018.5.4.2.

[65] P. Mäki-Arvela, B. Holmbom, T. Salmi, D.Y. Murzin, Recent progress in synthesis of fine and specialty chemicals from wood and other biomass by heterogeneous catalytic processes, Catal. Rev. - Sci. Eng. 49 (2007) 197–340. doi:10.1080/01614940701313127.

[66] C. Mondelli, G. Gözaydin, N. Yan, J. Pérez-Ramírez, Biomass valorisation over metal-based solid catalysts from nanoparticles to single atoms, Chem. Soc. Rev. 49 (2020) 3764–3782. doi:10.1039/d0cs00130a.

[67] E.G. Rodrigues, M.F.R. Pereira, X. Chen, J.J. Delgado, J.J.M. Órfão, Influence of activated carbon surface chemistry on the activity of Au/AC catalysts in glycerol oxidation, J. Catal. 281 (2011) 119–127. doi:10.1016/j.jcat.2011.04.008.

[68] C.D. Agostino, M.R. Feaviour, G.L. Brett, J. Mitchell, A.P.E. York, G.J. Hutchings, D. Mantle, L.F. Gladden, Solvent inhibition in the liquid-phase catalytic oxidation of 1,4-butanediol: understanding the catalyst behaviour from NMR relaxation time measurements†, (2016) 7896–7901. doi:10.1039/c6cy01458e.

[69] V. Mouarrawis, R. Plessius, J.I. van der Vlugt, J.N.H. Reek, Confinement effects in catalysis using well-defined materials and cages, Front. Chem. 6 (2018). doi:10.3389/fchem.2018.00623.

[70] P. Serp, Catalysis in carbon nanotubes, Wiley Online Libr. (2010).

[71] S. Leenders, Transition metal catalysis in confined spaces, Pubs.Rsc.Org. (2015).

[72] V. Mouarrawis, R. Plessius, Confinement effects in catalysis using well-defined materials and cages, Frontiersin.Org. (2018).

[73] Javier.M. de la. Geometric and electronic confinement effects on catalysis, ACS Publ. (2011).

[74] S. Wu, X. Yang, Confinement Effects in Zeolite-Confined Noble Metals, Wiley Online Libr. (2019).

[75] S.C. Reyes, E. Iglesia, Effective diffusivities in catalyst pellets: new model porous structures and transport simulation techniques, J. Catal. 129 (1991) 457–472. doi:10.1016/0021-9517(91)90049-A.

[76] X. Pan, X. Bao, The effects of confinement inside carbon nanotubes on catalysis, Acc. Chem. Res. 44 (2011) 553–562. doi:10.1021/ar100160t.

[77] J. Xiao, X. Pan, S. Guo, P. Ren, X. Bao, Toward fundamentals of confined catalysis in carbon nanotubes, J. Am. Chem. Soc. 137 (2015) 477–482. doi:10.1021/ja511498s.

[78] H. Li, J. Xiao, Q. Fu, X. Bao, Confined catalysis under two-dimensional materials, Natl. Acad Sci. 114 (2017). doi:10.1073/pnas.1701280114.

[79] J. Xiao, X. Pan, S. Guo, P. Ren, Toward fundamentals of confined catalysis in carbon nanotubes, ACS Publ. (2015).

[80] X. Pan, The effects of confinement inside carbon nanotubes on catalysis, ACS Publ. (2011).

[81] S.M. Wu, X.Y. Yang, C. Janiak, Confinement Effects in Zeolite-Confined Noble Metals, Angew. Chemie - Int. Ed. 58 (2019) 12340–12354. doi:10.1002/anie.201900013.

[82] P. Serp, E. Castillejos, Catalysis in carbon nanotubes, ChemCatChem. 2 (2010) 41–47. doi:10.1002/cctc.200900283.

[83] F. Yang, D. Deng, X. Pan, Q. Fu, X.B.-N.S. Review, undefined 2015, Understanding nano effects in catalysis, Academic.Oup.Com. (n.d.). https://academic.oup.com/nsr/article-abstract/2/2/183/2097938 (accessed February 9, 2021).

[84] M.D. Mantle, D.I. Enache, E. Nowicka, S.P. Davies, J.K. Edwards, C.D.' Agostino, D.P. Mascarenhas, L. Durham, M. Sankar, D.W. Knight, L.F. Gladden, S.H. Taylor, G.J. Hutchings, Pulsed-Field Gradient NMR Spectroscopic Studies of Alcohols in Supported Gold Catalysts †, (n.d.). doi:10.1021/jp105946q.

[85] F. D'Orazio, S. Bhattacharja, W.P. Halperin, R. Gerhardt, Fluid transport in partially filled

porous sol-gel silica glass, Phys. Rev. B. 42 (1990) 6503–6508. doi:10.1103/PhysRevB.42.6503.

[86] R.R. Valiullin, V.D. Skirda, S. Stapf, R. Kimmich, Molecular exchange processes in partially filled porous glass as seen with NMR diffusometry, Phys. Rev. E - Stat. Physics, Plasmas, Fluids, Relat. Interdiscip. Top. 55 (1997) 2664–2671. doi:10.1103/PhysRevE.55.2664.

[87] P.T. Callaghan, A. Coy, D. MacGowan, K.J. Packer, F.O. Zelaya, Diffraction-like effects in NMR diffusion studies of fluids in porous solids, Nature. 351 (1991) 467–469. doi:10.1038/351467a0.

[88] K. Kidena, Anisotropic diffusion of water in perfluorosulfonic acid membrane and hydrocarbon membranes, J. Memb. Sci. 323 (2008) 201–206. doi:10.1016/j.memsci.2008.06.037.

[89] C. D'Agostino, R.C. Harris, A.P. Abbott, L.F. Gladden, M.D. Mantle, Molecular motion and ion diffusion in choline chloride based deep eutectic solvents studied by 1H pulsed field gradient NMR spectroscopy, Phys. Chem. Chem. Phys. 13 (2011) 21383–21391. doi:10.1039/c1cp22554e.

[90] M.P. Hollewand, L.F. Gladden, Transport heterogeneity in porous pellets-I. PGSE NMR studies, Chem. Eng. Sci. 50 (1995) 309–326. doi:10.1016/0009-2509(94)00218-G.

[91] R. Evans, U. Marini Bettolo Marconi, P. Tarazona, Fluids in narrow pores: Adsorption, capillary condensation, and critical points, J. Chem. Phys. 84 (1985) 2376–2399. doi:10.1063/1.450352.

[92] R. Evans, U. Marini Bettolo Marconi, P. Tarazona, Fluids in narrow pores: Adsorption, capillary condensation, and critical points, J. Chem. Phys. 84 (1985) 2376–2399. doi:10.1063/1.450352.

[93] M. Dijkstra, Confined thin films of linear and branched alkanes, J. Chem. Phys. 107 (1997) 3277–3288. doi:10.1063/1.474678.

[94] M. Shetty, H. Wang, F. Chen, N. Jaegers, Y. Liu, D.M. Camaioni, O.Y. Gutiérrez, J.A. Lercher, Directing the Rate-Enhancement for Hydronium Ion Catalyzed Dehydration via Organization of Alkanols in Nanoscopic Confinements, Angew. Chemie. 133 (2021) 2334–2341. doi:10.1002/ange.202009835.

[95] C. D'Agostino, T. Kotionova, J. Mitchell, P.J. Miedziak, D.W. Knight, S.H. Taylor, G.J.

Hutchings, L.F. Gladden, M.D. Mantle, Solvent effect and reactivity trend in the aerobic oxidation of 1,3-propanediols over gold supported on titania: Nmr diffusion and relaxation studies, Chem. - A Eur. J. 19 (2013) 11725–11732. doi:10.1002/chem.201300502.

[96] L.F. Gladden, M.D. Mantle, A.J. Sederman, Magnetic Resonance Imaging of Catalysts and Catalytic Processes, Adv. Catal. 50 (2006) 1–75. doi:10.1016/S0360-0564(06)50001-X.

[97] C. D'Agostino, G.L. Brett, P.J. Miedziak, D.W. Knight, G.J. Hutchings, L.F. Gladden, M.D. Mantle, Understanding the Solvent Effect on the Catalytic Oxidation of 1,4-Butanediol in Methanol over Au/TiO_2 Catalyst: NMR Diffusion and Relaxation Studies, Chem. - A Eur. J. 18 (2012) 14426–14433. doi:10.1002/chem.201201922.

[98] J.J. Varghese, L. Cao, C. Robertson, Y. Yang, L.F. Gladden, A.A. Lapkin, S.H. Mushrif, Synergistic Contribution of the Acidic Metal Oxide−Metal Couple and Solvent Environment in the Selective Hydrogenolysis of Glycerol: A Combined Experimental and Computational Study Using ReO x −Ir as the Catalyst, (2018). doi:10.1021/acscatal.8b03079.

[99] P.H. Hintermeier, S. Eckstein, D. Mei, M. V Olarte, D.M. Camaioni, E.B. Baráth, J.A. Lercher, Hydronium-Ion-Catalyzed Elimination Pathways of Substituted Cyclohexanols in Zeolite H-ZSM5, ACS Publ. 7 (2017) 7822–7829. doi:10.1021/acscatal.7b01582.

[100] J. Jae, G.A. Tompsett, A.J. Foster, K.D. Hammond, S.M. Auerbach, R.F. Lobo, G.W. Huber, Investigation into the shape selectivity of zeolite catalysts for biomass conversion, J. Catal. 279 (2011) 257–268. doi:10.1016/j.jcat.2011.01.019.

[101] A.A. Milischuk, B.M. Ladanyi, Structure and dynamics of water confined in silica nanopores, J. Chem. Phys. 135 (2011) 174709. doi:10.1063/1.3657408.

[102] R. Busselez, R. Lefort, Q. Ji, F. Affouard, D. Morineau, Molecular dynamics simulation of nanoconfined glycerol, Phys. Chem. Chem. Phys. 11 (2009) 11127–11133. doi:10.1039/b911859d.

[103] A. Brodka, T.W. Zerda, Molecular dynamics of SF6 in porous silica, J. Chem. Phys. 95 (1991) 3710–3718. doi:10.1063/1.461778.

[104] A. Striolo, A.A. Chialvo, K.E. Gubbins, P.T. Cummings, Water in carbon nanotubes: Adsorption isotherms and thermodynamic properties from molecular simulation, J. Chem. Phys. 122 (2005) 234712. doi:10.1063/1.1924697.

[105] T. Le, A. Striolo, D.R. Cole, CO2-C4H10 Mixtures Simulated in Silica Slit Pores: Relation

between Structure and Dynamics, J. Phys. Chem. C. 119 (2015) 15274–15284. doi:10.1021/acs.jpcc.5b03160.

[106] S.B. Badmos, A. Striolo, D.R. Cole, Aqueous Hydrogen Sulfide in Slit-Shaped Silica Nanopores: Confinement Effects on Solubility, Structural, and Dynamical Properties, J. Phys. Chem. C. 122 (2018) 14744–14755. doi:10.1021/acs.jpcc.8b04527.

[107] P. Pissis, D. Daoukaki-Diamanti, L. Apekis, C. Christodoulides, The glass transition in confined liquids, J. Phys. Condens. Matter. 6 (1994) L325. doi:10.1088/0953-8984/6/21/008.

[108] R.J. Mashl, S. Joseph, N.R. Aluru, E. Jakobsson, Anomalously immobilized water: A new water phase induced by confinement in nanotubes, Nano Lett. 3 (2003) 589–592. doi:10.1021/nl0340226.

[109] M. Matsumoto, S. Saito, Molecular dynamics simulation of the ice nucleation and growth process leading to water freezing, Nature.Com. (2002).

[110] A. Bródka, T.W. Zerda, Properties of liquid acetone in silica pores: Molecular dynamics simulation, J. Chem. Phys. 104 (1996) 6319. doi:10.1063/1.471292.

[111] R. Iftimie, P. Minary, M.E. Tuckerman, Ab initio molecular dynamics: Concepts, recent developments, and future trends, Proc. Natl. Acad. Sci. U. S. A. 102 (2005) 6654–6659. doi:10.1073/pnas.0500193102.

[112] J. Marx, D., & Hutter, Ab initio molecular dynamics: basic theory and advanced methods., in: Cambridge University Press, 2009.

[113] W.L. Jorgensen, D.S. Maxwell, J. Tirado-Rives, Development and Testing of the OPLS All-Atom Force Field on Conformational Energetics and Properties of Organic Liquids, J. Am. Chem. Soc. 118 (1996) 11225–11236. doi:10.1021/ja9621760.

[114] W.L. Jorgensen, J.D. Madura, C.J. Swenson, Optimized Intermolecular Potential Functions for Liquid Hydrocarbons, J. Am. Chem. Soc. 106 (1984) 6638–6646. doi:10.1021/ja00334a030.

[115] B. Kirchner, J. Vrabec, Multiscale molecular methods in applied chemistry, 2012.

[116] Y. Guo, Z. Zeng, L. Li, C. Su, R. Chen, C. Wang, K. Zhou, X. Xu, H. Li, Competitive Adsorption of Methanol-Acetone on Surface Functionalization (-COOH, -OH, -NH2, and -SO3H): Grand Canonical Monte Carlo and Density Functional Theory Simulations, ACS Appl. Mater. Interfaces. 11 (2019) 34241–34250. doi:10.1021/acsami.9b10804.

[117] X. Lu, M. Wang, G. Luo, S. Zhou, J. Wang, H. Xin, Z. Wang, S. Liu, S. Wei, High-efficiency CO2 capture and separation over N2 in penta-graphene pores: insights from GCMC and DFT simulations, J. Mater. Sci. 55 (2020) 16603–16611. doi:10.1007/s10853-020-05251-9.

[118] D.D. Do, H.D. Do, Pore characterization of carbonaceous materials by DFT and GCMC simulations: A review, Adsorpt. Sci. Technol. 21 (2003) 389–424. doi:10.1260/026361703769645753.

[119] A.A. Milischuk, B.M. Ladanyi, Structure and dynamics of water confined in silica nanopores, J. Chem. Phys. 135 (2011) 174709. doi:10.1063/1.3657408.

[120] M. Rovere, M.A. Ricci, D. Vellati, F. Bruni, A molecular dynamics simulation of water confined in a cylindrical SiO2 pore, J. Chem. Phys. 108 (1998) 9859–9867. doi:10.1063/1.476424.

[121] E. Spohr, C. Hartnig, P. Gallo, M. Rovere, Water in porous glasses. A computer simulation study, J. Mol. Liq. 80 (1999) 165–178. doi:10.1016/S0167-7322(99)80006-3.

[122] A. Smolyanitsky, A.F. Kazakov, T.J. Bruno, M.L. Huber, Mass diffusion of organic fluids: a molecular dynamics perspective, n.d. doi:10.6028/NIST.TN.1805.

[123] A. V Egorov, A.P. Lyubartsev, A. Laaksonen, Molecular Dynamics Simulation Study of Glycerol-Water Liquid Mixtures, J. Phys. Chem. B. 115 (2011) 14572–14581. doi:10.1021/jp208758r.

[124] G. Kaminski, W.L. Jorgensen, Performance of the AMBER94, MMFF94, and OPLS-AA Force Fields for Modeling Organic Liquids, 1996. https://pubs.acs.org/sharingguidelines (accessed March 12, 2021).

[125] W.L. Jorgensen, D.S. Maxwell, J. Tirado-Rives, Development and Testing of the OPLS All-Atom Force Field on Conformational Energetics and Properties of Organic Liquids, 1996. https://pubs.acs.org/sharingguidelines (accessed March 12, 2021).

[126] G.C. Boulougouris, I.G. Economou, D.N. Theodorou, Engineering a Molecular Model for Water Phase Equilibrium over a Wide Temperature Range, J. Phys. Chem. B. 102 (1998) 1029–1035. doi:10.1021/jp9725821.

[127] T.S. Gulmen, W. Thompson, Model silica pores with controllable surface chemistry for molecular dynamics simulatinos, MRS Proc. 899 (2005) 0899-N06-05. doi:10.1557/PROC-0899-N06-05.

[128] H.B. Schlegel, Geometry optimization, WIREs Comput. Mol. Sci. 1 (2011) 790–809. doi:10.1002/wcms.34.

[129] D.J. Evans, B.L. Holian, The Nose-Hoover thermostat, J. Chem. Phys. 83 (1985) 4069–4074. doi:10.1063/1.449071.

[130] Estimation of absolute and relative entropies of macromolecules using the covariance matrix, Elsevier. (1993).

[131] C. Hartnig, W. Witschel, E. Spohr, P. Gallo, M.A. Ricci, M. Rovere, Modifications of the hydrogen bond network of liquid water in a cylindrical SiO2 pore, J. Mol. Liq. 85 (2000) 127–137. doi:10.1016/S0167-7322(99)00169-5.

[132] P. Gallo, M. Rovere, E. Spohr, Glass transition and layering effects in confined water: A computer simulation study, J. Chem. Phys. 113 (2000) 11324–11335. doi:10.1063/1.1328073.

[133] R. Mancinelli, S. Imberti, A.K. Soper, K.H. Liu, C.Y. Mou, F. Bruni, M.A. Ricci, Multiscale approach to the structural study of water confined in MCM41, J. Phys. Chem. B. 113 (2009) 16169–16177. doi:10.1021/jp9062109.

[134] G. Rother, A.G. Stack, S. Gautam, T. Liu, D.R. Cole, A. Busch, Water Uptake by Silica Nanopores: Impacts of Surface Hydrophilicity and Pore Size, J. Phys. Chem. C. 124 (2020) 29. doi:10.1021/acs.jpcc.0c02595.

[135] V. Kocherbitov, Properties of water confined in an amphiphilic nanopore, J. Phys. Chem. C. 112 (2008) 16893–16897. doi:10.1021/jp805247b.

[136] V. Crupi, S. Magazù, D. Majolino, P. Migliardo, V. Venuti, M.C. Bellissent-Funel, Confinement influence in liquid water studied by Raman and neutron scattering, J. Phys. Condens. Matter. 12 (2000) 3625–3630. doi:10.1088/0953-8984/12/15/311.

[137] M.C. Bellissent-Funel, S.H. Chen, J.M. Zanotti, Single-particle dynamics of water molecules in confined space, Phys. Rev. E. 51 (1995) 4558–4569. doi:10.1103/PhysRevE.51.4558.

[138] E. Walther Hansen, R. Schmidt, M. Stöcker, D. Akporiaye, Self-diffusion coefficient of water confined in mesoporous MCM-41 materials determined by 1H nuclear magnetic resonance spin-echo measurements, Microporous Mater. 5 (1995) 143–150. doi:10.1016/0927-6513(95)00053-C.

[139] Zhimei Du, G. Manos, T.J.H. Vlugt, B. Smit, Molecular simulation of adsorption of short

linear alkanes and their mixtures in silicalite, AIChE J. 44 (1998) 1756–1764. doi:10.1002/aic.690440807.

[140] J. Talbot, Analysis of adsorption selectivity in a one-dimensional model system, AIChE J. 43 (1997) 2471–2478. doi:10.1002/aic.690431010.

[141] A. Torres-Knoop, J. Heinen, R. Krishna, D. Dubbeldam, Entropic Separation of Styrene/Ethylbenzene Mixtures by Exploitation of Subtle Differences in Molecular Configurations in Ordered Crystalline Nanoporous Adsorbents, (2015). doi:10.1021/acs.langmuir.5b00363.

[142] S. Deng, D. Wang, X. Wang, Y. Wei, Effect of nanopore confinement on the thermal and structural properties of heneicosan, Elsevier. (2018).

[143] F. Eder, J.A. Lercher, Alkane Sorption on Siliceous and Aluminophosphate Molecular Sieves. A Comparative Study, 1996.

[144] J. Sui, S.Q. Zhang, M. Zhai, F. Tian, J. Zhang, X.Z. Lan, Polymorphism of a hexadecane-heptadecane binary system in nanopores, RSC Adv. 7 (2017) 10737–10747. doi:10.1039/c6ra28210e.

[145] S. Yin, C. Wang, X. Qiu, B. Xu, C. Bai, Theoretical study of the effects of intermolecular interactions in self-assembled long-chain alkanes adsorbed on graphite surface, Surf. Interface Anal. 32 (2001) 248–252. doi:10.1002/sia.1047.

[146] I. Dhiman, D. Bhowmik, U. Shrestha, Effect of molecular shape on rotation under severe confinement, Elsevier. (2018).

[147] A. Brodka, T.W. Zerda, Molecular dynamics of SF6 in porous silica, J. Chem. Phys. 95 (1991) 3710–3718. doi:10.1063/1.461778.

[148] B. Boekfa, P. Pantu, M. Probst, J. Limtrakul, Adsorption and Tautomerization Reaction of Acetone on Acidic Zeolites: The Confinement Effect in Different Types of Zeolites, (n.d.). doi:10.1021/jp1058947.

[149] S. Gautam, T. Liu, S. Patankar, D. Tomasko, D. Cole, Location dependent orientational structure and dynamics of Ethane in ZSM5, 2016.

[150] M.I. Velasco, M.B. Franzoni, E.A. Franceschini, E. Gonzalez Solveyra, D. Scherlis, R.H. Acosta, G.J.A.A. Soler-Illia, Water Confined in Mesoporous TiO2 Aerosols: Insights from NMR Experiments and Molecular Dynamics Simulations, J. Phys. Chem. C. 121 (2017) 7533–7541. doi:10.1021/acs.jpcc.6b12511.

[151] A. Farimani, Y. Wu, Rotational motion of a single water molecule in a buckyball, Pubs.Rsc.Org. (2013).

[152] P. Gallo, M. Rapinesi, M. Rovere, Confined water in the low hydration regime, J. Chem. Phys. 117 (2002) 369–375. doi:10.1063/1.1480860.

[153] C.D. Agostino, G. Brett, G. Divitini, C. Ducati, G.J. Hutchings, M.D. Mantle, L.F. Gladden, Increased Affinity of Small Gold Particles for Glycerol Oxidation over Au/TiO 2 Probed by NMR Relaxation Methods, (2017). doi:10.1021/acscatal.7b01255.

[154] J.J. Varghese, S.H. Mushrif, Origins of complex solvent effects on chemical reactivity and computational tools to investigate them: a review, 4 (n.d.) 153–448. doi:10.1039/c8re00226f.

[155] G. Campos-Villalobos, F.R. Siperstein, C.D.' Agostino, L. Forster, A. Patti, Self-diffusion of glycerol in γ-alumina nanopores. The neglected role of pore saturation in the dynamics of confined polyalcohols, (2020). doi:10.1016/j.apsusc.2020.146089.

[156] M. Bender, Economic feasibility review for community-scale farmer cooperatives for biodiesel, Bioresour. Technol. 70 (1999) 81–87. doi:10.1016/S0960-8524(99)00009-7.

[157] J. Esteban, E. Domínguez, M. Ladero, F. Garcia-Ochoa, Kinetics of the production of glycerol carbonate by transesterification of glycerol with dimethyl and ethylene carbonate using potassium methoxide, a highly active catalyst, Fuel Process. Technol. 138 (2015) 243–251. doi:10.1016/j.fuproc.2015.06.012.

[158] L.C. Meher, D. Vidya Sagar, S.N. Naik, Technical aspects of biodiesel production by transesterification - A review, Renew. Sustain. Energy Rev. 10 (2006) 248–268. doi:10.1016/j.rser.2004.09.002.

[159] J.M. Marchetti, V.U. Miguel, A.F. Errazu, Possible methods for biodiesel production, Renew. Sustain. Energy Rev. 11 (2007) 1300–1311. doi:10.1016/j.rser.2005.08.006.

[160] E.F. Aransiola, T. V Ojumu, O.O. Oyekola, T.F. Madzimbamuto, D.I.O. Ikhu-Omoregbe, A review of current technology for biodiesel production: State of the art. doi:10.1016/j.biombioe.2013.11.014.

[161] Yusuf, S.K. Kamarudin, Z. Yaakub, Overview on the current trends in biodiesel production, Energy Convers. Manag. 52 (2011) 2741–2751. doi:10.1016/j.enconman.2010.12.004.

[162] M. Pagliaro, R. Ciriminna, H. Kimura, M. Rossi, C. Della Pina, Recent advances in the conversion of bioglycerol into value-added products, Eur. J. Lipid Sci. Technol. 111 (2009)

788–799. doi:10.1002/ejlt.200800210.

[163] A. Corma, G. Huber, L. Sauvanaud, Biomass to chemicals: catalytic conversion of glycerol/water mixtures into acrolein, reaction network, Elsevier. (2008).

[164] T. Miyazawa, Y. Kusunoki, K. Kunimori, Glycerol conversion in the aqueous solution under hydrogen over Ru/C+ an ion-exchange resin and its reaction mechanism, Elsevier. (2006).

[165] D. Roy, B. Subramaniam, Cu-based catalysts show low temperature activity for glycerol conversion to lactic acid, ACS Publ. (2011).

[166] C. da Silva, V. Gonçalves, Water-tolerant zeolite catalyst for the acetalisation of glycerol, Pubs.Rsc.Org. (2009).

[167] M. Aresta, A. Dibenedetto, F. Nocito, A study on the carboxylation of glycerol to glycerol carbonate with carbon dioxide: the role of the catalyst, solvent and reaction conditions, Elsevier. (2006).

[168] N. Razali, Production of lactic acid from glycerol via chemical conversion using solid catalyst: A review, Elsevier. (2017).

[169] D. Roy, B. Subramaniam, R. V. Chaudhari, Cu-based catalysts show low temperature activity for glycerol conversion to lactic acid, ACS Catal. 1 (2011) 548–551. doi:10.1021/cs200080j.

[170] R. Karinen, New biocomponents from glycerol, Elsevier. (2006).

[171] M. Dasari, P. Kiatsimkul, Low-pressure hydrogenolysis of glycerol to propylene glycol, Elsevier. (2005).

[172] F. Héroguel, B. Rozmysłowicz, J.S. Luterbacher, Improving heterogeneous catalyst stability for liquid-phase biomass conversion and reforming, Chimia (Aarau). 69 (2015) 582–591. doi:10.2533/chimia.2015.582.

[173] S. Hu, X. Luo, C. Wan, Y. Li, Characterization of Crude Glycerol from Biodiesel Plants, ACS Publ. 60 (2012) 5915–5921. doi:10.1021/jf3008629.

[174] A. Villa, N. Dimitratos, C.E. Chan-Thaw, C. Hammond, L. Prati, G.J. Hutchings, Glycerol Oxidation Using Gold-Containing Catalysts, (2015). doi:10.1021/ar500426g.

[175] A.E. Dıáz-A ´ Lvarez, J. Francos, B. Lastra-Barreira, P. Crochet, V. Cadierno, Glycerol and derived solvents: new sustainable reaction media for organic synthesis, This J. Is Cite This Chem. Commun. 47 (2011) 6208–6227. doi:10.1039/c1cc10620a.

[176] P.D. Vaidya, A.E. Rodrigues, Glycerol Reforming for Hydrogen Production: A Review, Chem. Eng. Technol. 32 (2009) 1463–1469. doi:10.1002/ceat.200900120.

[177] Y. Gu, F. Jérôme, Glycerol as a sustainable solvent for green chemistry, Green Chem. 12 (2010) 1127–1138. doi:10.1039/c001628d.

[178] N. Ueda, Y. Nakagawa, K. Tomishige, Conversion of Glycerol to Ethylene Glycol over Pt-modified Ni Catalyst, Chem. Lett. 39 (2010) 506–507. doi:10.1246/cl.2010.506.

[179] B. Katryniok, H. Kimura, E. Skrzyńska, J.S. Girardon, P. Fongarland, M. Capron, R. Ducoulombier, N. Mimura, S. Paul, F. Dumeignil, Selective catalytic oxidation of glycerol: Perspectives for high value chemicals, Green Chem. 13 (2011) 1960–1979. doi:10.1039/c1gc15320j.

[180] C.H. Zhou, J.N. Beltramini, G.Q. Lu, Chemoselective catalytic conversion of glycerol as a biorenewable source to valuable commodity chemicals, Chem. Soc. Rev. 37 (2008) 527–549. doi:10.1039/b707343g.

[181] S. Carrettin, P. McMorn, P. Johnston, K. Griffin, G.J. Hutchings, Selective oxidation of glycerol to glyceric acid using a gold catalyst in aqueous sodium hydroxide, Chem. Commun. 7 (2002) 696–697. doi:10.1039/b201112n.

[182] S. Carrettin, P. McMorn, P. Johnston, K. Griffin, C.J. Kiely, G.J. Hutchings, Oxidation of glycerol using supported Pt, Pd and Au catalysts, Phys. Chem. Chem. Phys. 5 (2003) 1329–1336. doi:10.1039/b212047j.

[183] S. Carrettin, P. McMorn, P. Johnston, K. Griffin, C.J. Kiely, G.A. Attard, G.J. Hutchings, Oxidation of glycerol using supported gold catalysts, Top. Catal. 27 (2004) 131–136. doi:10.1023/B:TOCA.0000013547.35106.0d.

[184] A. Villa, N. Dimitratos, C.E. Chan-Thaw, C. Hammond, L. Prati, G.J. Hutchings, Glycerol Oxidation Using Gold-Containing Catalysts, ACS Publ. 48 (2015) 1403–1412. doi:10.1021/ar500426g.

[185] M.S. Ide, R.J. Davis, The important role of hydroxyl on oxidation catalysis by gold nanoparticles, Acc. Chem. Res. 47 (2014) 825–833. doi:10.1021/ar4001907.

[186] S. Carrettin, P. McMorn, P. Johnston, K. Griffin, C.J. Kiely, G.A. Attard, G.J. Hutchings, Oxidation of glycerol using supported gold catalysts, Top. Catal. 27 (2004) 131–136. doi:10.1023/B:TOCA.0000013547.35106.0d.

[187] S. Demirel-Gülen, M. Lucas, Liquid phase oxidation of glycerol over carbon supported gold

catalysts, Elsevier. (2005).

[188] A. Villa, G. Veith, Selective oxidation of glycerol under acidic conditions using gold catalysts, Wiley Online Libr. (2010).

[189] I. Sobczak, K. Jagodzinska, Glycerol oxidation on gold catalysts supported on group five metal oxides—A comparative study with other metal oxides and carbon based catalysts, Elsevier. (2010).

[190] E. Taarning, A. Madsen, J. Marchetti, Oxidation of glycerol and propanediols in methanol over heterogeneous gold catalysts, Pubs.Rsc.Org. (2008).

[191] I. Sobczak, K. Jagodzinska, M. Ziolek, Glycerol oxidation on gold catalysts supported on group five metal oxides - A comparative study with other metal oxides and carbon based catalysts, in: Catal. Today, Elsevier, 2010: pp. 121–129. doi:10.1016/j.cattod.2010.04.022.

[192] C. D'agostino, G. Brett, G. Divitini, C. Ducati, G.J. Hutchings, M.D. Mantle, L.F. Gladden, Increased Affinity of Small Gold Particles for Glycerol Oxidation over Au/TiO 2 Probed by NMR Relaxation Methods, ACS Publ. 7 (2017) 4235–4241. doi:10.1021/acscatal.7b01255.

[193] P. Bauer, P. Horlacher, P. Claus, Direct isomerization of linoleic acid to conjugated linoleic acids (CLA) using gold catalysts, Chem. Eng. Technol. 32 (2009) 2005–2010. doi:10.1002/ceat.200900384.

[194] S. Demirel, K. Lehnert, M. Lucas, Use of renewables for the production of chemicals: Glycerol oxidation over carbon supported gold catalysts, Elsevier. (2007).

[195] S. Demirel, P. Kern, M. Lucas, Oxidation of mono-and polyalcohols with gold: Comparison of carbon and ceria supported catalysts, Elsevier. (2007).

[196] L. Prati, Gold on carbon as a new catalyst for selective liquid phase oxidation of diols, Elsevier. (1998).

[197] L.A. Rowley, D. Nicholson, N.G. Parsonage, Monte Carlo Grand Canonical Ensemble Calculation in a Gas-Liquid Transition Region for 12-6 Argon, 1975.

[198] G. E. Norman; V. S. Filinov, "Investigations of Phase transitions by a Monte-Carlo method, High Temp. (1969) 216–222.

Appendices

A1 Appendix to Chapter 2

In the following section, we discuss the theory behind the Pulse-Field Gradient Nuclear Magnetic Resonance (PFG-NMR) experimental method used to measure the intrapore molecular diffusion of the substrate molecules confined inside a mesoporous catalyst (Section A1.1 and A1.2). We have also reported the importance of studying the condensed phase effects in glycerol valorization reactions in Section A1.3.

A1.1 NMR fundamentals

In the porous space of interest, a direct access is provided to the fluid behavior's key data by the Nuclear Magnetic Resonance (NMR). Most notably, it is able to probe their dynamical properties and phase-state related quantities. Therefore, in a sample of a porous solid as a function of the external gas pressure, one can measure the respective adsorption isotherm. In the pores, the adsorption isotherm serves as an indicator of the phase state. Under the same conditions and in the same sample, a number of additional quantities can be measured simultaneously. For example, molecular diffusion. Therefore, NMR proves to be a self-consistent tool for correlating the phase state of the pore fluid with its transport properties. It allows monitoring molecular ensembles as they are without creating any external disturbances owing to their intrinsically non-perturbative and non-invasive properties. The classic understanding of nuclear magnetism can be suitably used to rationalize the principles of NMR at a sufficient level in the context of this contribution. According to it, nuclear spins with a magnetic field of intensity B_0 was used to produce a precessional motion in the direction of B_0 with an angular frequency,

$$\omega_0 = \gamma B_0 \tag{A1.1}$$

where γ is the nuclear gyromagnetic ratio. There will be a tiny difference (10^{-3}%) between the numbers of spins owing to their interaction with the external magnetic field thus resulting in projections along and opposite to B_0 (Zeeman splitting in terms of quantum-mechanical description), provided by the Boltzmann statistics. A net equilibrium magnetization along B_0 is

produced due to this difference. Therefore, in comparison to other spectroscopic techniques, NMR must operate with fairly large nuclear ensembles for providing a measurable signal. Nevertheless, the downside of having to ensure the presence of large numbers of nuclei that may be typically of the order of 10^{18}, is, essentially, complemented by the advantage of acquiring well-averaged quantities.

Over a well-defined brief interval of time (the so-called 90^{o} or $\pi/2$ pulse), when an additional radio-frequency field of the resonance frequency ω_0 is applied, the direction of the net magnetization can be turned from that of the magnetic field into the plane perpendicular to it. Under this condition, it can simply be measured by using a coil with an axis positioned perpendicular to B_0. A voltage referred to as the NMR signal or, more accurately, the NMR free induction decay (FID) signal is induced by the rotating net magnetization in this coil. Clearly, the intensity of the FID signal is proportional to the number of nuclei and, consequently, to the number of molecules in the sample. By tracking the FID signal intensity as a function of the given gas pressure, this gives a simple way to measure the adsorption isotherm. The thus-measured NMR signal can be assigned to be essentially proportional to the amount adsorbed particularly owing to the substantial differences between the densities of the adsorbed and gaseous phases.

Finally, the nuclear magnetic relaxation rates are strongly dependent on the physical state of matter. Thus, due to rapid translational and rotational motion, the inter- and intramolecular dipolar interactions in liquids are susceptible to a strong averaging. This leads to relatively long nuclear magnetic relaxation times. Consequently, this leads to longer time spans, normally of the order of seconds over which an NMR signal may be observed. In solid state, on the other hand, very rapid nuclear magnetic relaxation times, on a time scale of a few up to tens of microseconds are caused by these interactions. This massive difference in the relaxation rates may be exploited for separating the NMR signals stemming, respectively, from the liquid and frozen phases and, therefore, for studying liquid–solid phase transition phenomena in pore spaces by applying suitable relaxation ‘filters’.[28]

A1.2 Pulse-Field Gradient Nuclear Magnetic Resonance (PFG-NMR)

PFG-NMR is considered a well-established tool for examining diffusion properties of molecules in a broad range of applications, for example, ionic liquids, heterogeneous catalysts , and molecular sieves.[29] Perhaps, one of the few fields that fully exploits the ability and potential of NMR techniques is 'measuring transport properties in porous media'. The reason being, they are able to probe diffusion in complex systems with a chemically selective and a non-invasive approach, all the while monitoring molecular displacements over a wide range of length scales. One can exploit the impact of a purposefully created inhomogeneity of the magnetic field on the Larmor frequency ω of the nuclear spins which is, in general, applied over intermittently, as the so-called field gradient pulses in order to measure the translational mobility. A scheme of the experimental realization of this approach, particularly useful for the investigation of porous materials, is shown in Fig. A.1.

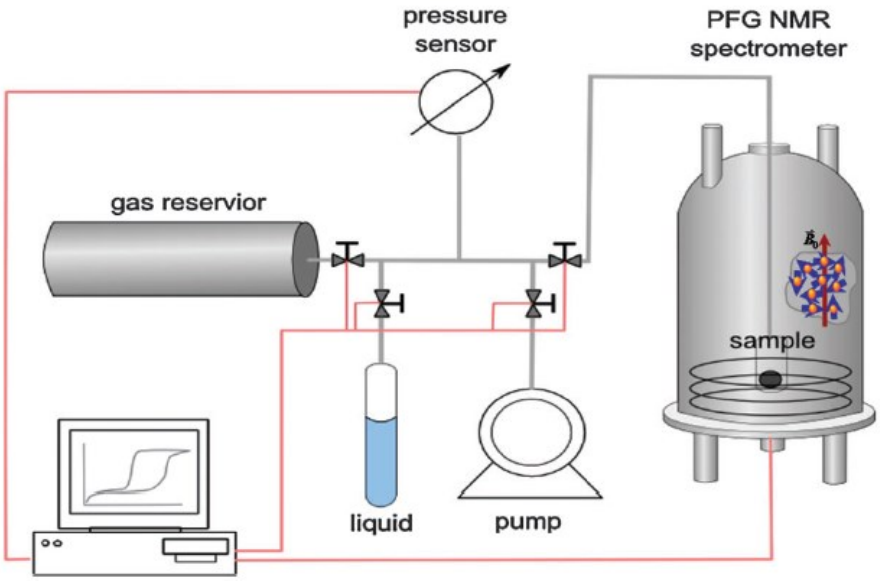

Figure A.1: Schematic representation of the PFG-NMR experimental setup. Reproduced with permission from [28].

Molecular diffusion and phase equilibria may be probed using a setup shown in Fig. A1.1 by incorporating the following procedure. Firstly, a reservoir is connected to a flask containing the liquid under study or to a turbo-molecular pump. This helps set the pressure in the reservoir to a desired value. It should also be noted that the volume of the reservoir should substantially exceed that of the NMR sample. Subsequently, until equilibrium is established, the reservoir is brought

into contact with the NMR tube comprising the porous material under study. For monitoring the equilibration process, the NMR free induction decay (FID) signal is recorded. Then, by the application of the PFG NMR pulse sequence, guest self-diffusivities are measured. In Addition, sometimes the loaded PFG NMR sample tubes are fused to facilitate diffusion measurements at different temperatures. Such a procedure provides an easy way to measure the temperature dependence of diffusion for a given loading provided the total amount of guest molecules in the free space of the sample tube remains insignificantly small in contrast to the amount in the pore space.[28]

A1.3 Condensed phase catalytic reactions for Glycerol valorization

The conventional diesel derived from non-renewable sources such as fossil fuels vastly contribute to global warming. Biodiesel (BD) on the other hand, is an alternative and sustainable energy resource that is produced from biomass feedstock.[1–3] According to the United States Department of Energy, the average cost per gallon of 100% BD in clean cities is approximately USD 0.89 (CAD 1.16) higher than that of fossil diesel fuel.[4] Therefore, in order to make BD production more feasible and marketable, the price difference between the fossil fuel and BD must be waived or further reduced.[5,6] A widely studied and industrially applied synthesis pathway for the production of BD is the Triglyceride transesterification (refer to figure A.2) of fatty acid containing feedstock, such as vegetable oils, animal fats and non-edible seed oil.[2,3] This process comprises methanol molecules reacting with triglycerides in the presence of a base or an acid catalyst, and one or multi-phase reaction systems at ambient conditions, or high temperatures and pressures to produce BD.[156] Additionally, glycerol forms as the primary by-product accounting for 10% (w/w) of the total BD produced worldwide.[4,157]

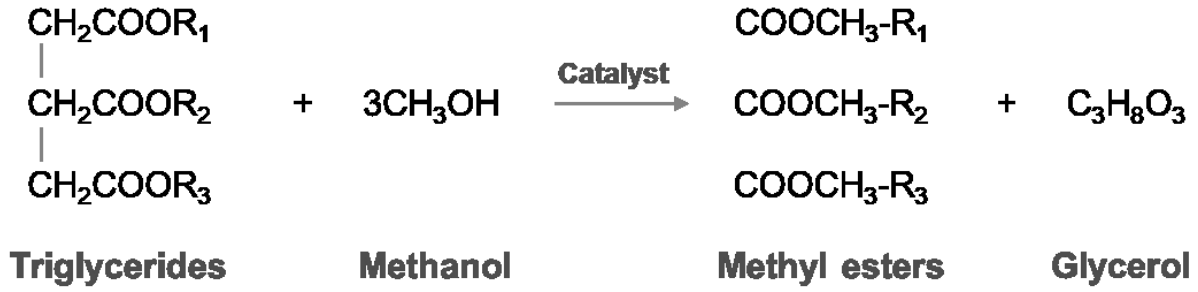

Figure A.2: Transesterification reaction pathway for Biodiesel production.

The rising need for alternative fuels like biodiesel has led to abundance of glycerol. However, it is important to consider that the purity of glycerol obtained from this process is fairly low due to the impurities present such as unused catalysts, soaps, salts and esters formed as by-products of the reaction. Therefore, purification of bio-glycerol as well as its utilization to produce valuable chemicals has attained garnering interest in recent years due to the dramatic growth of biodiesel industry.[2,158–161]

One of the major factors that will contribute to the boost in the economy of biodiesel production is the effective utilization of glycerol, which is one of the main by-products (accounting to 10% w/w) obtained during the production of biodiesel.[4,6,159,161,162] Due to Glycerol's efficient conversion into several value-added products transpire in increased production and utilization of this alternative bio renewable fuel resource. Thus, for the increased biodiesel production in the future, probing into new technological avenues for the utilization of glycerol will prove beneficial.[47] In the foreseeable future, Glycerol has the usefulness to become one of the major renewable building block chemicals as comparable to others from the petrochemical industry such as methane, methanol, ethylene etc.[163–171] A majority of biomass-derived oxygenate compounds, such as glycerol, containing at least two functional groups, exhibit insignificant vapor pressure. As a result, most conversion reactions pertaining to such compounds are performed in their liquid-phase, wherein the reactant is dissolved in a suitable solvent, the presence of which may affect the reaction. Hereof, we will now focus on Glycerol's catalytic reactions using supported metal nanoparticles, in condensed phase.[1,163,172]

Glycerol is an organic compound and it has the chemical formula $C_3H_8O_3$. It is a polyalcohol that consists of three-carbon chain with a hydroxyl group attached to each carbon. The multi-functionality of this compound is due to its molecular structure and physicochemical properties. Physically, glycerol is a clear, colourless, odourless, hygroscopic, vicious and sweet tasting liquid. Virtually, it is known to be nontoxic to both humans and the environment in general. The boiling point of glycerol is 290 °C. At room temperature and atmospheric pressure, glycerol has a density of 1261 kg/m^3, molecular weight of 92.09 g/mol, and a viscosity of 1.5 Pa.s.[173] Glycerol has a high boiling point and viscosity owing to the extensive intermolecular hydrogen bonding. It is a highly reactive molecule that can undergo a greater number of reactions due to the presence of

primary and secondary alcoholic groups that can be substituted with other chemical groups.[4,174–178]

From the industrial standpoint, one of the most efficacious and desirable avenues to produce glycerol derivatives is the heterogeneous catalytic oxidation of glycerol with molecular oxygen. The selective oxidation of glycerol into fine chemicals using monometallic and bimetallic catalysts, such as Au, Pt, Pd, Rh, Co, and Bi, supported on carbon, graphite or metal oxides among others has been investigated in several works.[47,174,179,179–183] However, the above discussed process poses the following challenges: (i) the control of selectivity to the desired products, (ii) high activity and resistance to oxygen poisoning, and (iii) reducing the usage of alkaline conditions. Therefore, in order to tackle these challenges, the most common catalysts used for the oxidation of glycerol are centered on supported metal nanoparticles. Figure A.3 depicts an overview of various catalytic conversion reactions of glycerol into value-added products.

As suggested by recent studies on polyol oxidations over Au/TiO_2, there exists a rather strong dependency of the catalyst activity upon the adsorption strength of the reactant. Besides, by changing the solvent composition and the type of polyols, the adsorption properties of various polyols were observed to differ greatly. This resultantly revealed that the molecular structure of the polyols can considerably affect their adsorption over the catalyst surface.[184–190] As compared to platinum-based catalysts, this gold-based catalyst has a strong resistance to oxygen poisoning thus, paving way for the use of high oxygen partial pressures. Additionally, using gold-based catalysts contribute to improvement of the catalyst lifetime, stability and reusability that are vital factors for prospective commercialization.[182]

In gold catalysis with respect to glycerol oxidation reactions, there is a major degree of emphasis on the effect of gold particle size upon catalyst activity and reactant selectivity. Deposition of smaller gold particles over the surface has indicated to improve catalytic activity in glycerol oxidation reactions and thus confirms that the effect of gold loading on catalytic activity can be related to particle size.[191] Theoretical and computational studies have suggested that smaller Au particles favor the formation of stronger bonds with adsorbates such as glycerol. Regardless, such

conclusions are still built on theoretical results, and in the hindsight, it is not entirely clear as to how these smaller gold particles promote higher activity.[192]

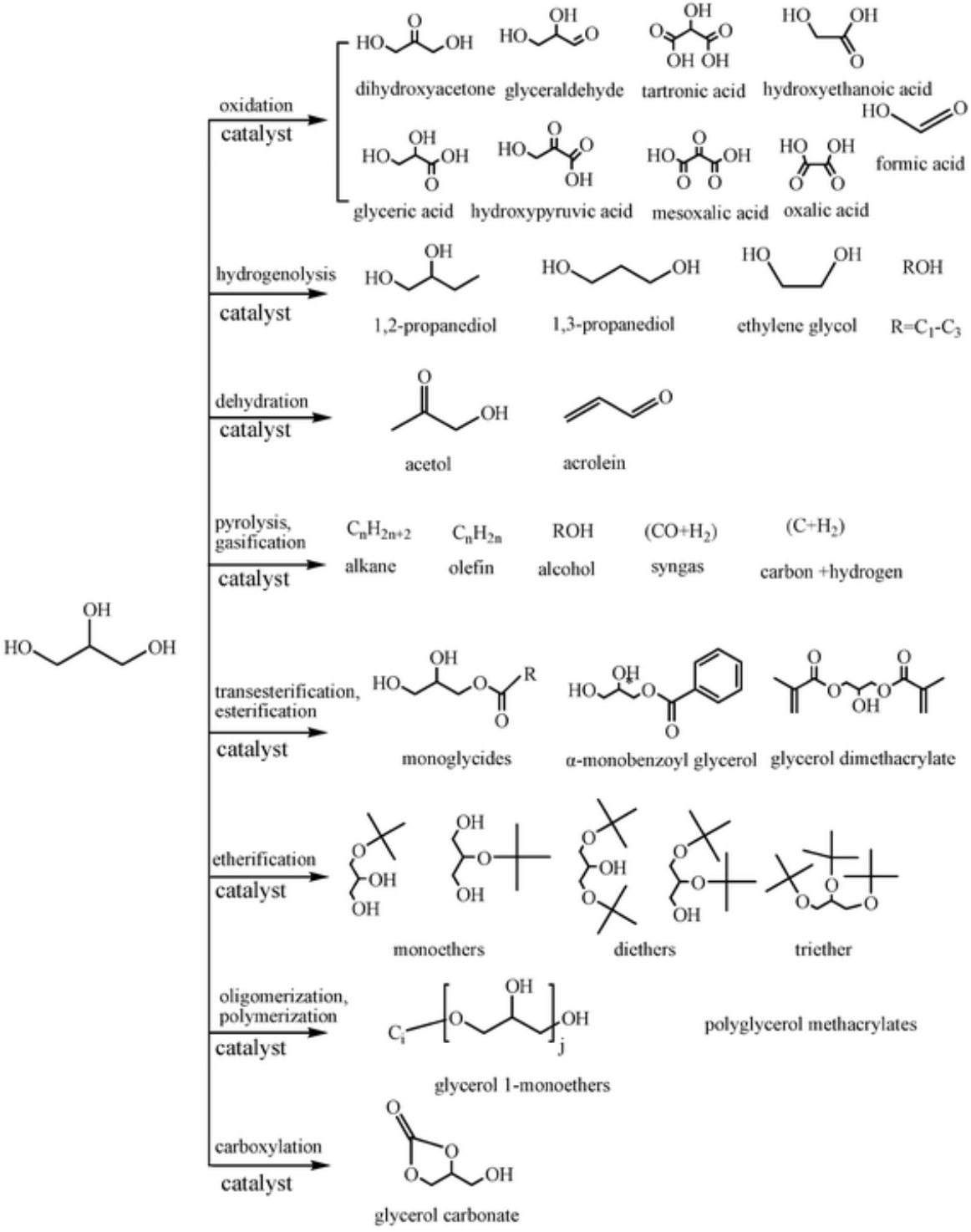

Figure A.3: Processes of catalytic conversion of glycerol into useful chemicals. Reproduced with permission from [180].

In addition, besides particles size, the activity of gold catalysts is also affected by the nature of support. Nano-sized gold particles supported on different carbon materials (e.g., carbon black, activated carbon, and graphite) and oxides (TiO_2, SiO_2, and Al_2O_3) are active for the oxidation of glycerol but show very different performances, being carbon supported gold catalysts more active than most oxides-supported catalysts.[193–196] However, the role of the support is rather complex to comprehend due to the great variation in the textural and chemical properties of different carbon materials on comparison. Moreover, despite its well-known influence on the catalyst activity, there is ambiguity in the confinement effects imposed by the support on the mechanism of glycerol oxidation.[67] In conclusion, the understanding of these effects provides a vantage point on the influence of support in conjunction with the adsorption kinetics of the substrate on the Au catalyst, for analyzing the alteration in nanoconfined catalytic reaction kinetics.

A2 Appendix to Chapter 3

In this section, we begin with the discussion about the physics behind the molecular simulations explained in Chapter 2 of the thesis. In section A2.1, we explain the theory behind the Molecular Dynamics simulation method used in the thesis. In section A2.2, we report the molecular simulation parameters used in the molecular simulations discussed in section 3.2.

A2.1 Classical Molecular Dynamics (Force-field method)

Molecular mechanics, also known as force-field based methods, are a collection of empirical methods that use fitted parameters (derived empirically or from ab initio calculations) to describe the potential energy of system under consideration. In these methods, the system is typically described using a ball (atom) and spring (bond) type model. The potential energy of the system for a particular atomic configuration is taken to be the sum of energies due to bonded (bond stretching, bond bending and torsional motion) and non-bonded (van der Waals and electrostatic) interactions, as shown in the equation below:

$$E_{MM} = E_{stretch} + E_{bend} + E_{torsion} + E_{vdW} + E_{electrostatic} \quad \text{(A.1)}$$

where, $E_{stretch}$ is the energy for stretching a bond between two atoms, E_{bend} is the energy for bending an angle formed by three bonded atoms, $E_{torsion}$ is the energy for twisting around a bond and E_{vdw} and $E_{electrostatic}$ are the energies accounting for electrostatic interaction between two atoms and van der Waals interaction. Figure A.4 illustrates the basic terms implicated in calculating the force field energy.

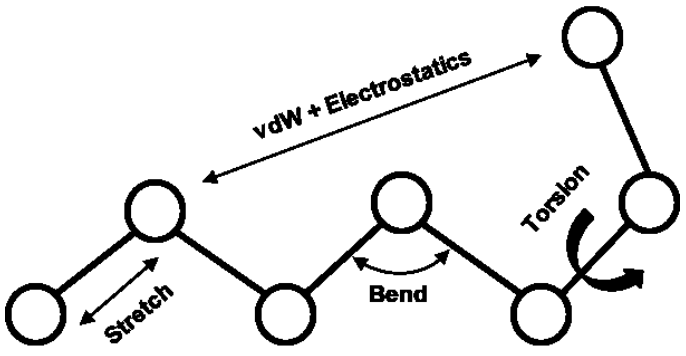

Figure A.4: Pictorial representation of the bonded (stretch, bend and torsion) and non-bonded interactions (vdW and Electrostatics).

Bonded and non-bonded interactions are calculated using the following equations provided. When written as a Taylor Expansion at the length of the equilibrium bond, the stretching energy between two bonded atoms 1 and 2 is given as:

$$E_{stretch}^{12} = E_0 + \frac{dE}{dl}\Big|(l^{12} - l^0) + \frac{1}{2!}\frac{d^2E}{dl^2}\Big|(l^{12} - l^0)^2 + \cdots \quad \text{(A.2)}$$

Since, E_0 is a zero point in the energy scale, it is usually set at zero. Similarly, the first derivative at l^0 is zero. Hence, the equation can also be written as:

$$E_{stretch}^{12} = \frac{1}{2!}\frac{d^2E}{dl^2}\Big|(l^{12} - l^0)^2 = K_{stretch}(l^{12} - l^0)^2 \quad \text{(A.3)}$$

Where, $K_{stretch}$ is the force constant. This equation takes the form of a harmonic oscillator. A similar equation for angle bending can be given as:

$$E_{bend}^{123} = K_{bend}(\theta^{123} - \theta^0)^2 \quad \text{(A.4)}$$

The functional form of bending and stretching can be extended in order to include higher order terms. Instead of using a Taylor series expansion as in the previous equations, it makes use of a Morse Potential type function. This is mainly done because although, the harmonic form of stretching and bending is quite simple, it is not entirely sufficient. The morse potential type function is given below:

$$E_{morse}^{12} = E_{diss}\left(1 - e^{-\alpha\{l^{12} - l^0\}}\right) \quad \text{(A.5)}$$

Where, α is related to the force constant and E_{diss} is the dissociation energy.

Let us consider a four-atom sequence 1-2-3-4 where, 1-2, 2-3 and 3-4 are all bonded atoms. The torsion energy associated with the twisting around bond 2-3 is different in physical terms as compared to the stretching and bending energy due to the following reasons:

i. Both, bonded and non-bonded interactions contribute to the rotation along the bond.

ii. The torsion energy must return to the same value after rotating along the bond for 360 degrees. In other words, it is needs to be periodic. Taking into account this periodicity, the torsion energy is usually given as:

$$E_{torsion}^{1234} = K_{torsion}(1 - \cos(n\omega)) \quad \text{(A.6)}$$

Where, n determines the periodicity, ω is the angle of rotation and $K_{torsion}$ is the constant.

The van der Waals energy due to the attraction and repulsion between the two non-bonded atoms is generally given in the form of the popular Lennard-Jones potential as follows:

$$E_{VdW}^{12} = 4E_{min}^{L-J}\left[\left(\frac{R^0}{R^{12}}\right)^{12} - \left(\frac{R^0}{R^{12}}\right)^{6}\right] \quad \text{(A.7)}$$

Where E_{min}^{L-J} is the depth of the minimum in the potential and R^0 is the distance at which the potential is zero. Finally, the electrostatic energy between two atoms is given by the Coulomb potential as:

$$E_{electrostatic}^{12} = \frac{Q^1 Q^2}{\varepsilon_{dielec} R^{12}} \quad \text{(A.8)}$$

Where, ε_{dielec} is the dielectric constant and Q^1 and Q^2 are the atomic charges.

Here, the minimum in the energy conforming to the most stable configuration can be calculated by minimizing E_{MM} as a function of atomic coordinates since the energy is a function of atomic coordinates.

It must be noted that an arbitrarily chosen nuclear (or atomic configuration in the case of MM methods) configuration may not be the most stable (low energy) one and hence, the energy of the system must be minimized with respect to nuclear configuration. Local optimization methods aid in finding the nearest stationary point in which the system lies. Such optimization is termed as geometry optimization (GO) and takes the system to the local minimum. However, the most stable configuration of the system corresponds to the global minimum in energy, which serves to

determine equilibrium structures. A non-stochastic method to obtain the global minimum in molecular simulations is Molecular Dynamics (MD).

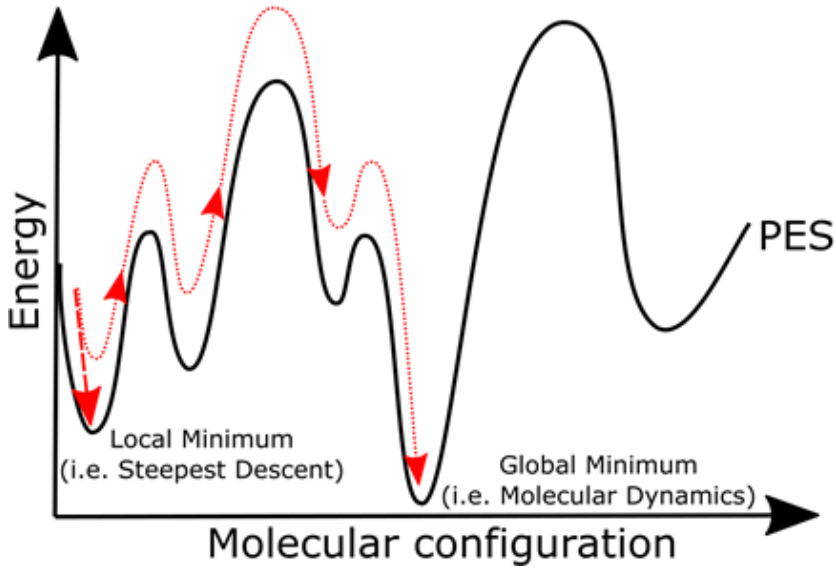

Figure A.5: Exploration of the Potential Energy Surface (PES) using Molecular dynamics.

The simulation technique used to study the interaction and motion of a certain number of molecules or atoms is called Molecular Dynamics. From a reference initial position, at finite temperatures, molecular dynamics simulations trace the time evolution of atoms and molecules by the integration of Newton's equations of motion along with the forces on atoms that are derived from an interaction potential. In molecular dynamics, the system examines the potential energy surface (as shown in Figure A.5) part with the energies lower than the kinetic energy of the system. Figure A.6 shows a basic scheme of molecular dynamics simulations.

Considering the majority of the systems are at some finite temperature and the temperature dependent dynamics observed in this method serve as the real dynamics of the system, Molecular Dynamics is a better representation of the physical state of the system. The kinetic energy and the potential energy (the energy calculated using force field methods) of the system during the molecular dynamics run at each configuration aid in the calculation of the forces acting on every atom of the system. This calculation of the force on each atom is used to determine the velocities of each atoms in the system and the time evolution of the particle positions.

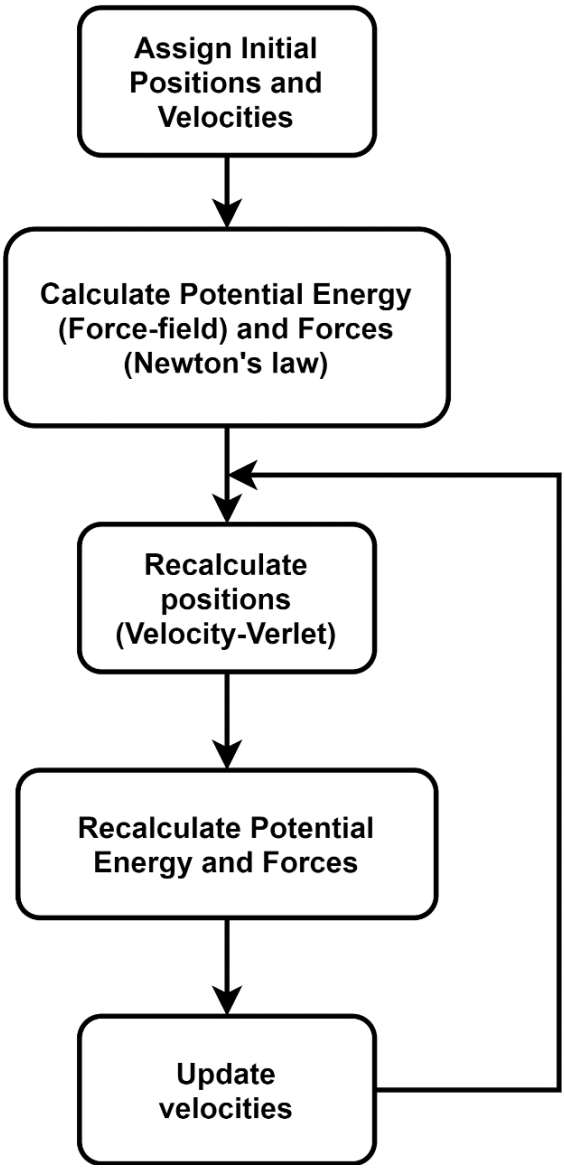

Figure A.6: Overview of the MD simulation using Velocity Verlet integration algorithm.

In such wise, a sequence of points in phase space evolving in time is generated by MD simulation. In a conservative forcefield, forces can be taken as the gradient of the potential energy of the system. Hence, the resulting equation of motion can be expressed as,

$$m_i \frac{d^2 r_i}{dt^2} = -\frac{dV}{dr_i} \tag{A.9}$$

Where r is the position of the atoms, V is the potential energy, m is the mass and t is the time. To integrate the equations of motion, various algorithms have been proposed and the frequently utilized algorithms described below.

A2.1.1 Integration Algorithms

A2.1.1.1 Verlet Algorithm

Here, in order to calculate new positions at t + Δt, the positions from t - Δt and accelerations and positions at time t are used. This algorithm does not use Explicit Velocities. The algorithm is advantageous in that it requires minimal and economical storage requirements. The drawback of Verlet Algorithm is that the velocities are computed from the positions hence rendering the algorithm of moderate precision. It is represented by the following two equations for velocity and position, respectively.

$$r(t + \Delta t) = 2r(t) - r(t - \Delta t) + \frac{f(t)}{m}\Delta t^2 \quad \text{(A.10)}$$

$$v(t) = \frac{r(t+\Delta t) - r(t-\Delta t)}{2\Delta t} \quad \text{(A.11)}$$

where, $r(t)$ is position of the particle at time t, Δt is the time step for molecular dynamics scheme, $f(t)$ is the force on the particle, m is the mass of particle and $v(t)$ is the velocity of the particle at time t.

A2.1.1.2 Leap-frog Algorithm

In this algorithm, the velocities calculated at time $t + \frac{1}{2}\Delta t$ are used to calculate r, the positions at time $t + \Delta t$. In such wise, the velocities and positions leap over each other. This algorithm, unlike Verlet Algorithm, has an advantage in that, velocities are calculated explicitly. However, the velocities are not calculated at the same time as the positions, making it hard to gauge the total energy at any point in time. The leapfrog algorithm is represented by,

$$r(t + \Delta t) = r(t) + v(t + \tfrac{1}{2}\Delta t)\Delta t \quad \text{(A.12)}$$

$$v\left(t + \tfrac{1}{2}\Delta t\right) = v\left(t - \tfrac{1}{2}\Delta t\right) + \frac{f(t)}{m}\Delta t \quad \text{(A.13)}$$

where $r(t)$ is position of the particle at time t, Δt is the time step for molecular dynamics scheme, $f(t)$ is the force on the particle, m is the mass of particle and $v(t)$ is the velocity of the particle at time t.

A2.1.1.3 Velocity-verlet Algorithm

In this algorithm, in order to calculate the position at time $t + \Delta t$, position and velocity at time t are used. the average of acceleration at time t and $t + \Delta t$ is used to calculate the velocity at $t + \Delta t$.

$$r(t + \Delta t) = r(t) + v(t)\Delta t + \frac{1}{2m} f(t)\Delta t^2 \quad \text{(A.14)}$$

$$v(t + \Delta t) = v(t) + \frac{1}{2m}[f(t) + f(t + \Delta t)]\Delta t \quad \text{(A.15)}$$

where, $r(t)$ is position of the particle at time t, Δt is the time step for molecular dynamics scheme, $f(t)$ is the force on the particle, m is the mass of particle and $v(t)$ is the velocity of the particle at time t.

As indicated above, the molecular dynamics algorithm discussed in the aforementioned section conserves the total energy. Therefore, the system naturally pertains to the micro canonical ensemble wherein, the system's volume, the total number of atoms, and its total energy are all collectively conserved. In the system, the difference between the constant total energy and the potential energy that is changing with atomic positions gives us the kinetic energy. Hence, the kinetic energy may differ significantly during the molecular dynamics run, thus causing variations in temperature. Although, it is more apt to execute the simulations at a constant temperature, especially when the goal of any simulation study is to validate/support/predict the experimental data. Integrating the system with a heat bath is one of the most common ways to execute molecular dynamics simulations at a constant temperature. In order to keep the system at a constant temperature, there is an occurrence of heat transfer between the system and the heat bath. Nose and Hoover provided the mathematical formulation for such a heat bath and therefore, it is commonly known as Nose-Hoover thermostat. The idea is to consider the heat bath as an essential part of the system by adding an artificial variable, associated with velocity as well as a hypothetical

mass (> 0). The coupling between the real system and the reservoir is determined by the magnitude of mass which therefore, influences the temperature fluctuations. [129]

A2.1.2 Molecular Dynamics simulations

A compilation of all the microstates of a system, which is consistent with the constraints using which a system is characterized macroscopically is better known as an ensemble in statistical mechanics. Ensemble averages form the basis for calculation of all the properties. To study the average behavior of a system comprising N particles by computing the system's time evolution and taking the average of the quantities over a considerable amount of time shapes the perception behind the molecular dynamics simulation. In the following subsections, we will discuss about the various steps involved in performing an MD simulation.

A2.1.2.1 Selection of the Interaction potential model

The functional parameter sets, and form used to calculate the potential energy of a system of atoms or particles in a molecular modeling is called a force field. Force fields are categorized into three types: i) United-atom where, every atom's parameters barring hydrogen are provided, ii) All-atom, in which every type of atom's parameters are provided, iii) Coarse-grained, every so often utilized in long-time simulations of macromolecules wherein, numerous atoms are congregated into larger beads with suitable interactions between the beads. In this thesis, an all-atom force field, the OPLS-AA (Optimized potential for liquid simulations - all atom) force field was employed.

A2.1.2.2 Boundary Conditions

In this study, in order to minimize edge effects, periodic boundary conditions (PBC) are applied in all directions. A unit cell is employed for approximating a large system by these applying boundary conditions for all the substrate molecules inside the silica nanostructures.

A2.1.2.3 Choice of Ensemble

In MD simulations, an ensemble is generally selected on the basis of the properties and the system we are keen on, such as N (number of particles), E (energy of the system), V (Volume of the system), P (Pressure of the system) and μ (Chemical potential of the system) that are kept constant

according to respective ensembles. In that regard, Ensembles are classified into the following four basic types: a) Microcanonical Ensemble (NVE) in which N, V and E are fixed, b) Canonical Ensemble (NVT) in which N, V and T are fixed, c) Isothermal-Isobaric Ensemble (NPT) in which N, V and P is kept constant, d) Grand Canonical Ensemble (μVT) in which μ, V and T is fixed. In this thesis, MD simulations pertaining to confined substrates are performed in Canonical ensemble. For pure substrates, NPT ensemble was used to calculate the density of the molecules. In order to determine the intrapore density of the substrate molecules, Grand Canonical Ensemble was applied to bulk as well as the confinements. Grand Canonical Monte Carlo techniques were used to match the chemical potential of the bulk with the confined substrates (which are in equilibrium) to accurately calculate the intrapore densities of the substrate molecules, without the need for molecular dynamics inside the porous media. It is computationally cheaper in comparison to MD simulations, making it an ideal tool obtaining accurate intrapore densities.

A2.1.2.4 Choice of Integrator, Thermostat, and Barostat

In MD Simulations, three types of integration algorithms are generally employed. Velocity-verlet integration algorithm was utilized in this system of study. As per our discussion in the previous subsection, the temperature of the system needs to be fixed in order to perform the MD simulations in the canonical ensemble (*NVT*). Hence, to achieve constant temperature during the simulation, a thermostat is used. It is responsible to make sure that the average temperature is kept close to a certain value. It is generally executed by getting the system to be in contact with a heat bath (reservoir) that is maintained at the desired temperature. Several methods such as Berendsen, Nosé-Hoover are developed to attain realistic conditions. Similarly, Berendsen, Parrinello – Rehman are employed to maintain the average pressure close to the preferred value in NPT ensemble. To run the simulation, several parameters such as volume, timestep, density, cut-off radius, temperature need to be set. The details of the simulations are reported in the methodology chapter (Section 3.1).

A2.1.2.5 Equilibration Run

Equilibration run is basically executed to ensure that there aren't any sizable fluctuations in the energy of the system. Furthermore, it aids in attaining the desired temperature whilst maintaining

equilibrium with the heat bath (velocity-rescaling). For this step, number of molecules, temperature and volume of the simulation box was kept constant. The temperature was maintained constant at 298 K with the use of velocity-rescaling algorithms. The cut-off radius for the vdW and columbic interactions was set at 1.0 nm each.

A2.1.2.6 Production Run

The system is well-equilibrated at the given volume and temperature after the equilibration. The number of molecules, temperature and volume of the systems was kept constant for this simulation run. Temperature was maintained at 298 K with the use of Nosé-Hoover thermostat. The cut-off radius for the vdW and columbic interactions was set at 1.0 nm each. During the production run, data is collected for every atom or molecule in the system. Several properties are calculated based on this data, like potential energy, entropy, intermolecular interactions and diffusivities.

A2.2 Grand Canonical Monte Carlo

The impact that Monte Carlo (MC) methods have made in the area of molecular and atomic modeling is difficult to overstate. With the advent of fast computers, Monte Carlo simulations have become a progressively more widespread method used to examine the behavior of adsorbates on a surface. The average thermodynamic properties of a system are calculated by evaluating the integrals of the form.

$$(\emptyset) = \int d^{3N}x \, \emptyset \, (x^N) f(x^N) \tag{A.16}$$

In the above equation, N is the number of particles, x is the position coordinate, x^N is the set of position coordinates, $f(x^N)$ is the normalized probability distribution such that $f(x^N) \geq 0$ and $\int d^{3N}x \, f(x^N) = 1$.

These integrals are evaluated by executing trial moves on the particles using the Monte Carlo Method. To generate an ensemble of representative configurations under specific thermodynamics conditions for a complex macromolecular system is the purpose of a Monte Carlo (MC) simulation. To generate these configurations, random perturbations may be applied. These perturbations need

to be energetically feasible, sufficiently large, and highly probable in order to properly sample the representative space. No information about time evolution is provided by Monte Carlo simulations. Instead, what they provide are an ensemble of representative configurations, and, subsequently, conformations from which relevant thermodynamic observables and probabilities, such as the free energy, may be calculated. Apart from being important on their own right, Monte Carlo simulations also play a vital role when designing hybrid and complex molecular dynamic (MD) algorithms.

The trial moves include different attempts at rotations, creation of particles, box volume changes or translations. According to the distribution $f(x^N)$, these trial moves may be accepted or rejected. For instance, if the system is in state x^N, the trial moves may be accepted or rejected in regard to the following algorithm:

1. A trial move that takes the system from the state x^N to state y^N is attempted.
2. Calculations are performed for the distributions f (x^N) and f (y^N).
3. The probability for acceptance of the trial move is:
   $A(x^N|y^N) = \min\ [1, \mathrm{f}\,(x^N)/\ \mathrm{f}\,(y^N)]$.

Until convergence is achieved, this process is held on. In this thesis, the convergence is achieved when the number of molecules inside the confinement remains constant after consecutive insertion attempts (when the chemical potential of the bulk is equal to the intrapore substrates).

To investigate liquid-surface interactions in the field of catalysis, grand canonical Monte Carlo simulations are widely employed. In order to make the insertion of molecules feasible, it is indicated that configurational-bias Monte Carlo technique can be used in a grand canonical Monte Carlo simulation.[197,198] In the grand canonical MC simulations of filling, the silica pore is fixed in space and the substrate molecules are allowed to be inserted or deleted. The coupled-decoupled configurational bias MC algorithm was used for the insertion and deletion moves. This approach increases the efficiency of insertion moves by "growing" the molecule an atom at a time into the liquid in which it is being inserted. To determine the density of a substrate in a confined space, grand canonical Monte Carlo (GCMC) simulations was conducted using the simulation package TOWHEE version 6.2.11. Two-box Gibbs ensemble MC simulations were performed. The first

box was originally an empty silica pore that was fixed in space and the second box included the bulk reservoir (both the systems are in equilibrium) of the substrate molecules at T = 298 K. Detailed description of the methodology for the GCMC simulations in Section 3.2.2.

A2.3 Factors for normalization (K and F)

In this subsection, we report the values of K (obtained using RDFs) and calculated values of F (factor for normalization), as reported in section 3.3.2, for water, acetone, glycerol and heptane inside different Silica nanostructures used in our study. Table A.1 provides the computed values of F and K for the aforementioned molecules.

Table A.1: Factor for normalization (F) and atomic distances (K) of water, acetone, glycerol and heptane inside silica nanostructures implemented in this study.

		F (factor for normalization)			
	K (nm)	Slit pore of 4 nm	Cylindrical Pore of 2 nm	Cylindrical Pore of 4 nm	Cylindrical Pore of 6 nm
Water	0.29	0.15	0.58	0.29	0.19
Acetone	0.64	0.32	1.28	0.64	0.43
Glycerol	0.53	0.27	1.06	0.53	0.35
Heptane	0.71	0.36	1.42	0.71	0.47

A3 Benchmarking report

For pure components, including water, glycerol, acetone and heptane were simulated at 25℃. In NPT simulations, the compressibility of pure components were obtained from speed of sound using:

$$\beta = -\frac{1}{V}\frac{\partial V}{\partial p} = \frac{1}{\rho c^2}$$

The speed of sound and calculated compressibility of pure components are shown in Table A.2.

Table A.2: Speed of sound and compressibility of pure components.

Components	***Speed of Sound (m/s)***	***Compressibility (bar^{-1})***
Water	1481	4.55526E-05
Glycerol	1920	2.15107E-05
Acetone	1192	8.88E-05
Heptane	1173	1.06E-04

Densities and diffusivities were used for benchmarking. Literature and simulated densities, as well as the relative errors for pure components are shown in Table A.3.

Table A.3: Literature and simulated densities, as well as the relative errors for pure components.

Components	***Literature Density (kg/m^3)***	***Simulated Density (kg/m^3)***	***Percentage error***
Water	997.07	994	0.3%
Glycerol	1258.02	1225	2.6%
Acetone	792.24	795	0.3%
Heptane	685.75	670	2.3%

A3.1 Glycerol

Glycerol is simulated with 1732 molecules at 25°C and 1 bar. The simulated and literature densities were found to be 1225 kg/m^3 and 1258.02 kg/m^3, respectively. The relative error was found to be 2.6%. Pure glycerol system was also simulated at different temperatures and the densities and diffusivities were calculated and shown in Table A.4. A comparison of simulated and literature diffusivity at different temperatures is shown in Figure A.7.

Table A.4. Densities and diffusivities of pure glycerol at different temperatures.

Temperature (K)	*1000/T (K^{-1})*	*Density (kg/m^3)*	*Diffusivity* $(10^{-5} cm^2/s)$
298	3.36	1225	2.20E-08
348	2.87	1180	5.46E-07
398	2.51	1140	3.57E-06
448	2.23	1100	6.74E-06
498	2.01	1060	1.63E-05
548	1.82	1020	2.73E-05

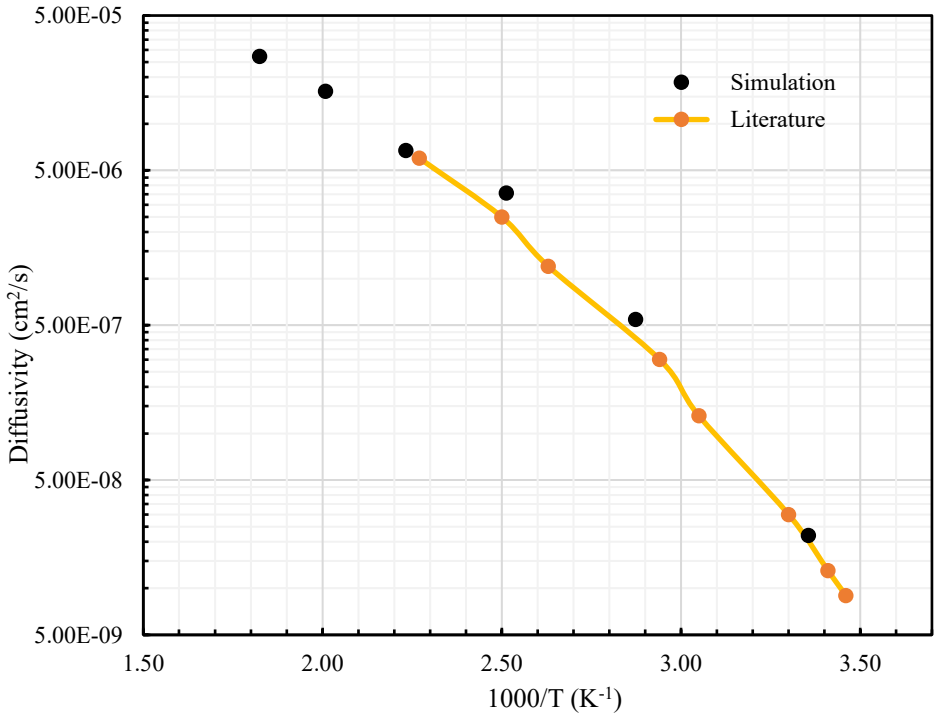

Figure A.7: A comparison of simulated and literature diffusivity at different temperatures.

A4 Appendix to Chapter 4

A4.1 Hydrogen Bonding Network of Water and Glycerol

In this section, we present the detailed results on hydrogen bonding network (number of H-bonds and H-bond lengths) of water and glycerol molecules inside the four silica nanostructures.

A4.1.1 Hydrogen Bonding Analysis of Water-Water and Water-Silica

Figure A.8 shows the computed values of total number of hydrogen bonds (near the surface and near the centre of the nanostructure), substrate-substrate H-bonds and substrate-surface H-bonds for water molecules inside the four nanostructures.

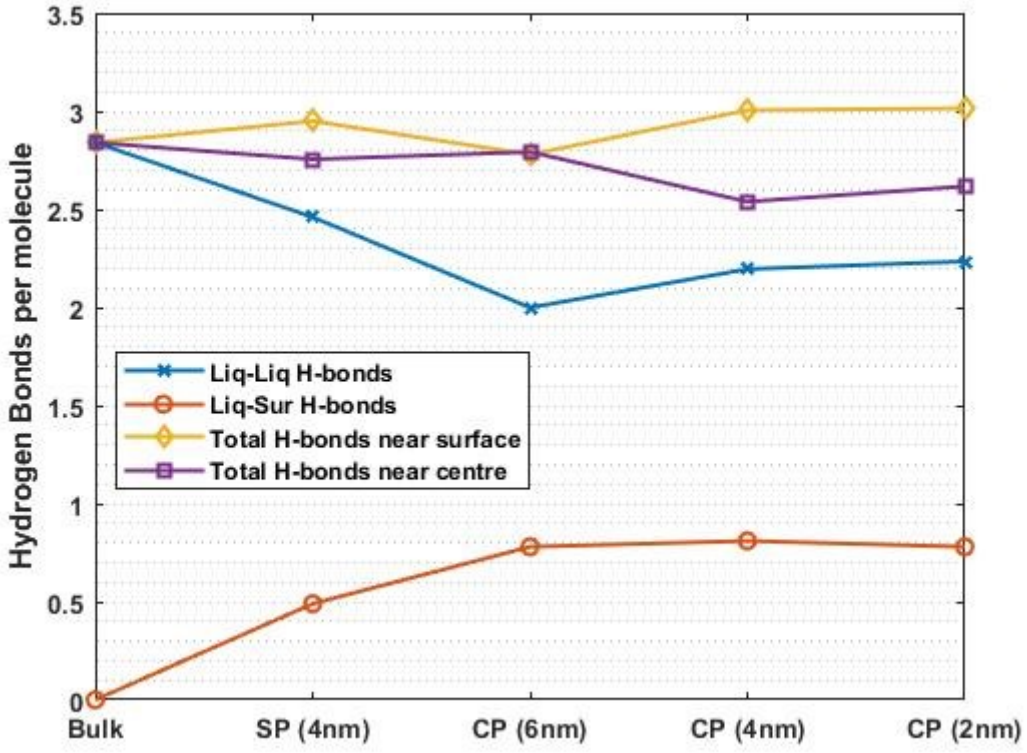

Figure A.8: Number of hydrogen bonds per molecule of water, confined inside various silica nanostructures (SP = slit pore and CP = cylindrical pore)

In this figure, the orange line depicts the water-surface H-bonds, blue line denoting the water-water H-bonds, yellow and violet line are the total number of hydrogen bonds in the system (substrate-substrate and substrate-surface) near the surface and centre of the porous structure,

respectively. H-bonds between water-water molecules (blue) decreases with the increase in the confinement dimension (slit to cylindrical pore). However, it gradually increases with the reduction in the pore sizes from 6 to 2 nm. Secondly, the number of H-bonds between water and surface molecules (orange) increases with only change in the dimension of the confinement (slit to cylindrical pore), but was found to be constant for pores of different sizes. An important observation here being, the total number of H-bonds near the surface inside all confinements remained constant and equal to the bulk liquid. However, near the centre of the confinement, the H-bonds remains constant and bulk-like for slit-pore of 4 nm and cylindrical pore of 6 nm, whereas it decreases (in comparison to bulk) with the reduction in the size of the cylindrical pores from 6 to 2 nm.

The possible explanation for the reduction in the H-bonds near the centre of the pore with decrease in the size would be due to the reduction in the local density of water near the centre as shown in Section 4.3.3.3. The reduction in the H-bonds near the centre of the silica pores enhances the mobility of water molecules residing at the centre of the pore, in comparison to the molecules near the silica surface. The strengths of Silica-water and water-water H-bonds were determined based on the respective bond lengths. Table A.5 presents the computed values of silica-water and water-water H-bonds; wherein the silica-water bond lengths were calculated using the RDFs between silica oxygen atoms (reference) and H atoms of water molecules, and water-water bond lengths were calculated using the RDFs between oxygen atoms (reference) and H atoms of water molecules.

Table A.5: Computed bond lengths of water-silica and water-water H-bonds.

	Average Bond Length (nm)			
Hydrogen Bond Type	***SP of 4 nm***	***CP of 6 nm***	***CP of 4 nm***	***CP of 2 nm***
Silica-Water	0.265	0.266	0.261	0.254
Water-Water	0.294	0.302	0.287	0.288

The average bond lengths of the water-surface H-bonds was observed to be shorter than the water-water H-bonds by 0.3-0.4 Å, suggesting that the surface interactions are stronger than the intermolecular water-water interactions.

A4.1.2 Hydrogen Bonding Analysis of Glycerol-Glycerol and Glycerol-Silica

Figure A.9 shows the computed values of total number of hydrogen bonds (near the surface and near the centre of the nanostructure), substrate-substrate H-bonds and substrate-surface H-bonds for glycerol molecules inside the four nanostructures.

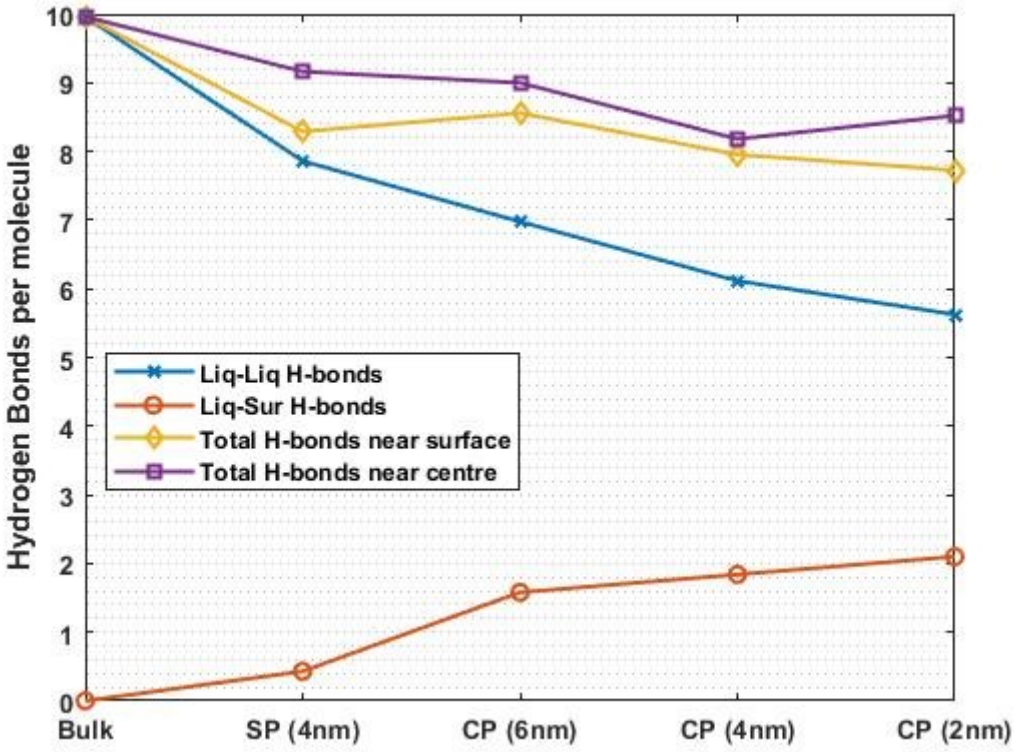

Figure A.9: Number of hydrogen bonds per molecule of glycerol, confined inside various silica nanostructures (SP = slit pore and CP = cylindrical pore)

In this figure, the orange line depicts the glycerol-surface H-bonds, blue line denoting the glycerol-glycerol H-bonds and the yellow line is the total number of hydrogen bonds in the system (substrate-substrate and substrate-surface). H-bonds between glycerol-glycerol molecules (blue) decreases with the increase in the confinement dimension (slit to cylindrical pore). A further reduction in the substrate-substrate H-bonds was observed with the change in the size of the porous structures from 6 to 2 nm. On the contrary, the number of H-bonds between glycerol and surface molecules (orange) increases with change in the dimension and size of the confinement. Within the pores, the substrate-surface interactions were observed to increase with the reduction in the

size of the confinement. Additionally, the total number of H-bonds inside all confinements reduced with the reduction in the size of the confinements, both near the centre and near the surface of the silica confinements. This result is in agreement with the experimental hypothesis of the breakage of hydrogen bonding network inside mesoporous catalysts.[29]

The strengths of Silica-glycerol and glycerol-glycerol H-bonds were determined based on the respective bond lengths. Table A.6 presents the computed values of Silica-glycerol and glycerol-glycerol H-bonds; wherein the silica-glycerol bond lengths were calculated using the RDFs between silica oxygen atoms (reference) and H atoms of glycerol molecules, and glycerol-glycerol bond lengths were calculated using the RDFs between oxygen atoms (reference) and H atoms of glycerol molecules.

Table A.6: Computed bond lengths of glycerol-silica and glycerol-glycerol H-bonds.

	Average Bond Length (nm)			
Hydrogen Bond Type	***SP of 4 nm***	***CP of 6 nm***	***CP of 4 nm***	***CP of 2 nm***
Silica-Glycerol	*0.258*	*0.256*	*0.251*	*0.243*
Glycerol-Glycerol	0.278	0.276	0.279	0.269

The average bond lengths of the glycerol-surface H-bonds was recorded to be shorter than the glycerol-glycerol H-bonds by 0.2-0.3 Å, suggesting that the surface interactions are stronger than the intermolecular glycerol-glycerol interactions. These results are in complete agreement with the simulation study on the disruption of hydrogen bonding network inside various alumina slit pores.[38]